



**HAL**  
open science

# Physicochemical characterisation of organic materials of interest for astrobiology: Titan's aerosols analogues

Jing He

► **To cite this version:**

Jing He. Physicochemical characterisation of organic materials of interest for astrobiology: Titan's aerosols analogues. Other. Ecole Centrale Paris, 2013. English. NNT: 2013ECAP0054. tel-01000229

**HAL Id: tel-01000229**

**<https://theses.hal.science/tel-01000229v1>**

Submitted on 4 Jun 2014

**HAL** is a multi-disciplinary open access archive for the deposit and dissemination of scientific research documents, whether they are published or not. The documents may come from teaching and research institutions in France or abroad, or from public or private research centers.

L'archive ouverte pluridisciplinaire **HAL**, est destinée au dépôt et à la diffusion de documents scientifiques de niveau recherche, publiés ou non, émanant des établissements d'enseignement et de recherche français ou étrangers, des laboratoires publics ou privés.



**ÉCOLE CENTRALE PARIS**

**THÈSE**

Présentée par

**Jing HE**

Pour l'obtention du

**GRADE DE DOCTEUR**

Spécialité : Chimie Analytique

Laboratoire d'accueil : **Laboratoire de Génie des Procédés et Matériaux**

SUJET:

**Physicochemical characterization of organic  
materials of interest for astrobiology: Titan's  
aerosols analogues**

Thèse soutenue au 8 Octobre 2013 devant la commission d'examen :

<b>Eric Quirico</b>	<b>Professeur, Univ. Grenoble 1</b>	<b>Rapporteur</b>
<b>François Raulin</b>	<b>Professeur, Univ. Paris 12</b>	<b>Rapporteur</b>
<b>Cornelia Meinert</b>	<b>Chargé de recherche, Univ. Nice-Sophia Antipolis</b>	<b>Examineur</b>
<b>Nathalie Carrasco</b>	<b>Maître de conférences, Latmos</b>	<b>Examineur</b>
<b>Cyril Szopa</b>	<b>Maître de conférences, Université Paris 6</b>	<b>Président du jury</b>
<b>Arnaud Buch</b>	<b>Maître de conférences, ECP</b>	<b>Directeur de thèse</b>



## Acknowledgement

This dissertation would not have been possible complete without the guidance and the help of several individuals who in one way or another contributed and extended their valuable assistance in the preparation and completion of this study.

First and foremost, I would like to express my sincere gratitude to my advisors: Arnaud Buch, Nathalie Carrasco, Cyril Szopa, for the continuous support of my Ph.D study and research, for their patience, motivation, enthusiasm, and immense knowledge. Their guidance and advices helped me in all the time of research and writing of this thesis.

Besides my advisors, I would like to thank my fellow labmates in Laboratoire de Génie des Procédés et Matériaux (LGPM): Amaury Brault and Carole Garnier for their help and advices when I have the trouble in use of the apparatus, they are always nice and patient. Of course, the others people in the laboratory are also very nice. When I first came to the laboratory and they gave me a lot of help which can let me quickly adapt to the laboratory environment and learning life. It's very important for me to continue my study in the future. I have a great time with them for these three years.

I want to also thank the rest of my colleagues worked in the labo LATMOS (Laboratoire Atmosphère, Milieux, Observation Spatiales) the members of RAMPRE team Thomas Gautier, Guy Cernogora, Ahmed Mahjoub for their support of sample, encouragement, insightful comments, and the advices for the content of my thesis. And Gilles BOEMARE, thanks for his help to carry out the TG-MS experiment.

I am very grateful for Monsieur. François Raulin and Monsieur. Éric Quirico could be as the rapporteurs and Madame Cornelia Meinert could be as the examiner in the jury of this thesis. I am so honored that they would like to be the defense committee members to participate my thesis defense (a very important day in my life). Thanks for they can evaluate my Ph.D thesis and propose their valuable suggestions, these will be very useful and helpful for my further study.

Furthermore, I would like to thank the CSC (China scholarship council) for my finance and the teachers who work in the Service de l'éducation Ambassade de la République Populaire de Chine en République Française care about my daily life and learning.

In addition, I wish to thank my Chinese friends who also study in France, we usually have a good time in the weekend and holiday, thank you for the pleasure they have brought to me when I live abroad. Especially I want to mention Zhaohuan MAI, I am so glad that we can study in the same laboratory even in the same office. Thank you for her accompany during the past three years and the help for my daily life. In addition, I want to thank Si CHEN, Pin LV, Yaqin YANG, Wenjun ZHANG, Wei AI, I am so glad I have this chance to work with them in the same lab and thanks for their help and advices in my daily life.

Last but not the least, I would like to thank my family: my parents for giving birth to me at the first place and supporting me spiritually throughout my life.

***Thank you!***

## Table of Contents

<b>General introduction</b> .....	<b>1</b>
<b>Chapter1. Introduction</b> .....	<b>5</b>
1.1 Titan versus Earth.....	6
1.2 The observation of Titan and in-situ data acquisition .....	8
1.2.1 The instruments for observation in situ on Cassini -Huygens.....	9
1.2.2 Surface composition from in situ observation .....	11
1.2.3 Aerosols in Titan’s atmosphere from in situ observation.....	13
1.3 Titan’s analogue: Tholins.....	21
1.3.1 The process of “Tholins” formation .....	21
1.3.2 Laboratory simulation of Titan’s aerosol (Tholins) .....	22
1.3.3 The PAMPRE method .....	25
1.3.4 Previous analysis of PAMPRE tholins .....	32
1.4 Conclusion.....	38
<b>Chapter 2. Determination of the chemical composition of Titan’s aerosols analogue (Tholins)</b> .....	<b>41</b>
2.1 Introduction .....	42
2.1.1 ACP experiment.....	42
2.1.2 Previous analysis of tholins using Pyr-GC-MS method .....	45
2.2 Experimental Section .....	48
2.2.1 Instruments .....	48
2.2.2 Experimental method and procedure .....	50
2.3 Results of the Pyr-GC-MS experiment .....	52
2.3.1 The results for sample 5pc .....	52
2.3.2 The results for sample 10pc .....	57
2.4 Discussion .....	61
2.4.1 Compared with two-dimensional gas chromatography-time-of-flight mass spectrometry .....	62

2.4.2	Comparison to the results obtained by the ACP experiment.....	64
2.5	Conclusion.....	66
<b>Chapter 3. The thermal degradation behavior of Tholins .....</b>		<b>67</b>
3.1	Research methods.....	68
3.1.1	Thermogravimetry analysis .....	68
3.1.2	Infrared absorption and Raman spectroscopy.....	69
3.1.3	Elemental analysis .....	73
3.1.4	TG-MS (thermogravimetry-mass spectrometry) .....	75
3.2	Samples and Experimental conditions .....	76
3.2.1	Samples.....	76
3.2.2	Experimental conditions .....	76
3.3	Results for TG-DSC and TG-MS analysis .....	76
3.3.1	Repeatability of the TG-DSC measurement .....	77
3.3.2	Analysis of TG-DSC results .....	78
3.3.3	TG-MS results .....	84
3.4	The analysis of sample heating residues .....	90
3.4.1	The result of Infrared Spectroscopy .....	90
3.4.2	The result of Raman spectroscopy.....	93
3.4.3	Elemental analysis .....	98
3.5	Discussion .....	100
3.5.1	Thermal stability of tholins.....	100
3.5.2	Evolution of elemental and chemical compositions of tholins.....	102
3.5.3	Changes in the structure of the carbon skeleton of tholins.....	102
3.6	Conclusion.....	103
<b>Chapter 4. The possible chemical evolution of the aerosols on the surface of Titan .....</b>		<b>105</b>
4.1	The fate of aerosols at the surface of Titan .....	106
4.1.1	Previous work on the chemical reaction in contact with liquid water: acidic hydrolysis by tholins .....	107
4.1.2	Organic macromolecules tholins in cold aqueous solutions.....	109

4.1.3	Low temperature hydrolysis of laboratory tholins in ammonia-water solutions ....	109
4.1.4	Formation of amino acids via low-temperature hydrolysis of tholins .....	110
4.1.5	Interaction of aerosols with aqueous ammonia on Titan .....	110
4.1.6	Production yields of organics of astrobiological interest from H <sub>2</sub> O-NH <sub>3</sub> hydrolysis of Titan's tholins.....	110
4.2	Experimental method and procedures .....	111
4.2.1	The sample synthesis and prepare the sample before GC-MS analysis.....	111
4.2.2	GC-MS analysis (Gas chromatography and Mass spectrometry).....	114
4.3	The results of different sample treatment method.....	116
4.3.1	The direct derivatization for non-hydrolyzed samples .....	117
4.3.2	Tholins hydrolysis in a neutral environment H <sub>2</sub> O .....	120
4.3.3	Tholins hydrolysis in acid environment HCl .....	123
4.4	The products of chemical evolution of Titan's tholins and how they may form .....	126
4.5	Conclusion.....	135
	<b>Conclusions and perspectives .....</b>	<b>137</b>
	<b>References .....</b>	<b>141</b>
	<b>Appendix .....</b>	<b>141</b>
	<b>List of Figures .....</b>	<b>141</b>
	<b>List of Tables.....</b>	<b>167</b>





## General introduction

Titan is one of the most studied objects in our solar system. This satellite of Saturn has a dense atmosphere which has analogies with the prebiotic Earth's atmosphere: has a similar majority gaseous components ( $\text{CH}_4$ ,  $\text{N}_2$ ), a methane cycle similar to the water cycle on Earth. In addition, the atmosphere of Titan has some gas molecules, for example hydrocyanic acid (HCN). These molecules are key molecules in the formation of first bricks of life. Finally, energetic particles, from different sources, to reach the atmosphere, and interact with the nitrogen and methane are the origin of many chemical reactions. This chemistry occurring in an atmosphere subjected to a low temperature makes Titan become a planetary laboratory. Some chemical reactions occurring in Titan's atmosphere lead to the formation of solids suspended in the atmosphere that aerosols ultimately settle on the surface of Titan.

Since the achievement of the first results from the Cassini Huygens (2004-2007) mission, aerosols of the atmosphere of Titan are now considered as an important element in the climate cycle of the satellite, mainly because they control the radiative transfer in the atmosphere, they adsorb nitriles in large quantities, and they sediment to the surface. These aerosols are composed of solid organic molecules coming from the atmospheric chemistry where the main constituents are  $\text{N}_2$  and  $\text{CH}_4$ . This natural chemical, process that involves converting gas into organic solids is rare in the solar system. It could have occurred on the early Earth and have generated a source for apparition of the first biomolecules. The compounds formed in the upper atmosphere eventually fall down to the surface, where the dunes, lakes cryovolcanism and craters can impact them and react with these aerosols. The direct exploration of the surface of Titan is very useful for us to understand the prebiotic chemistry, and perhaps ultimately to an understanding of how life arose on Earth. So it is necessary and important to well understand the physicochemical properties of aerosols of Titan, and correlate them with their production methods to better describe the atmosphere of the satellite, and evaluate the prebiotic chemistry that could occur.

The objective of this thesis is to study the physicochemical nature of aerosols of Titan. In order to achieve this object, there are three complementary approaches provide access to the chemical nature: observation, the modeling simulation, and experimental laboratory. Many studies have been carried out according to the last two approaches:

Numerical modeling showed that aerosols of Titan consist of a refractory core on which are condensed hydrocarbons having up to 4 carbon atoms, and low molecular weight nitriles. The core of these refractory aerosols would be composed of hydrocarbon polymers or polymer of nitriles, or a mixture of these two polymers (Wilson et al., 2003).

The simulation experiment, carried out under conditions similar to those of Titan's atmosphere, allows synthesizing solid particles (tholins), considered as analogues of aerosols of Titan. Different analytical methods were used to study the physicochemical composition of tholins. The simulation method was used to accomplish this study, in this thesis only focus on the laboratory simulation method.

This manuscript is divided into four chapters which include three principal parts.

The first chapters describe the prerequisites to understanding this work. It presents some background on Titan, physical characteristics as well as different observation approaches. It also provides a summary of the different compounds, mainly gas identified in the atmosphere of Titan, including the most recent data acquired by the instruments of the Cassini-Huygens mission. It also shows an overview of current knowledge and assumptions about the physical and chemical properties of aerosols of Titan. Conclude several methods to synthesize the analogue of aerosols on Titan (tholins) and especially introduce PAMPRE method in detail which we used to synthesize our samples in this thesis. This chapter also summarizes the results about the PAMPRE tholins synthesis that we have obtained and the analytical techniques have used in the previous studies.

To investigate the physical and chemical properties of the tholins produced by PAMPRE several studies have been done. With this goal many techniques have been used and have been describes in the chapter 1. Information and results about Pyr-GC-MS of tholins is not enough referenced. There is only few research has used this technique to study the tholins. So the second chapter tries to understand the chemical composition and structure of aerosols in Titan relying on it for interpretation of data from the ACP instrument. We used Pyr-GC-MS instrument to study the compounds released when the tholins suffered different pyrolysis temperature.

The third chapter attempts to provide a systematic method to characterize the thermal properties of tholins. In order to study the thermal stabilities of tholins and the physical and chemical properties changed with the temperature varied. Firstly, we used TG-DSC method to

study the tholins thermal behavior curves then we used some complementary techniques to investigate the composition and structure of the heating residues.

Deposition of organic aerosols on Titan's surface, where fluvial, aeolian, and cryovolcanic as well as cratering processes may lead to their subsequent chemical evolution. Experimental assessment of this evolution on Titan's surface is a major interest in the field of the post-Cassini-Huygens data treatment and preparation of future flagship missions. While in the fourth chapter, the study concerning the chemical evolution when the aerosols sediment on the surface of Titan. We used GC-MS instrument to analyze the three different approaches treating the different sample tholins ( $\text{CH}_4$  content in the initial gaseous mixture is different).

The general conclusion will first make a synthesis of our results and offers new ways to go further in the understanding of the physicochemical nature of aerosols of Titan.



# **Chapter1. Introduction**

Titan, the largest satellite of Saturn, has a dense atmosphere composed mostly nitrogen and methane. A complex chemistry initiated by the solar photons and electrons from Saturn's magnetosphere can happen in Titan's atmosphere and leading to the formation of solid particles. The study of this chemistry, involving precursors such as HCN, will improve our understanding of prebiotic chemistry. Moreover, Titan is a body similar to the primitive Earth due to the presence of liquid on its surface in terms of physical properties. Titan is therefore an interest research object in exobiology and planetary science. Titan has been observed both from Earth and space probes. The study of Titan could provide a better understanding to Earth's climate, the processes of prebiotic chemistry, and therefore the conditions of appearance of life on the early Earth. In the 1980s, the Voyagers have provided much information on the structure of the atmosphere. The latest Cassini-Huygens mission provided a large amount of data for the scientists and analyzed by many international teams.

## **1.1 Titan versus Earth**

There are many similarities which can be found when comparing Titan and Earth. Titan is the only moon in the solar system that has a substantial atmosphere. One important point is that Titan's atmosphere is primarily composed of nitrogen like Earth, but in Titan there is also one of the most abundant constituents is methane ( $\text{CH}_4$ ) is unlike Earth. Methane, the main component in natural gas, plays a key role in the makeup of atmospheric conditions on Titan. The organic chemistry that occurs in Titan's atmosphere is an analogue of the processes that may have been present in the early terrestrial atmosphere. Some characteristics of Titan and Earth have been concluded in **Table 1-1**.

Table 1-1. Titan versus Earth (<http://georgenet.net/hubble/titanearth.html>).

	Titan	Earth
Diameter (Km)	5.150(with it's clouds)	12.756
Radius (Km)	2.575	6.378
Mass (Kg)	$1.36 \times 10^{23}$	$5.9742 \times 10^{24}$
Mean Density(gm/cm <sup>3</sup> )	1.881	5.518
Rotation Period (Days; hours; minutes; seconds)	15:23:15:31.5	00:23:56:45
Sideral (Rotation) period (days)	15.945	365
Mean distance orbiting sun (Km)	1.427.163.966	149.597.900
Astronomical Units(AU) from sun	~9.54	1.0
Albedo	0.21	0.39
Escape Velocity(Km/sec)	2.47	11.2
Space Temperature	85-95 Kelvin -168 Centigrade -292 Farenheight	288-290 Kelvin 17 Centigrade 62.6 Farenheight
Major Constituents	N <sub>2</sub> 94-98% CH <sub>4</sub> 1.8-6.0% Ar 0-12% Isotope of argon deduced indirectly	N <sub>2</sub> 76% O <sub>2</sub> 20.9% Ar 0.934% CO <sub>2</sub> 0.031% H <sub>2</sub> O 1.0%
Minor Constituents	H <sub>2</sub> CO CO <sub>2</sub> C <sub>2</sub> N <sub>2</sub> C <sub>2</sub> H <sub>2</sub> C <sub>2</sub> H <sub>4</sub> C <sub>4</sub> H <sub>2</sub> C <sub>3</sub> H <sub>4</sub> C <sub>3</sub> H <sub>8</sub> HCN HC <sub>3</sub> N	H <sub>2</sub> CO Ne O <sub>3</sub> N <sub>2</sub> O O <sub>3</sub> N <sub>2</sub> O He Xe Kr NO <sub>2</sub>

Other interesting characteristics:

- One Titan year is equal to 30 Earth Years
- Both Titan and Earth have a greenhouse effect
- It is believed that Titan also has continents and oceans as determined through radar Second largest moon in our Solar System (Jupiter's Ganymede is the largest)



Titan and the Earth atmosphere also have similar temperature vertical profiles **Figure 1-1** with a troposphere, a tropopause and a stratosphere. Titan exhibits seasonal changes in its stratospheric temperatures and winds that are similar to Earth's have been discovered by other researchers.

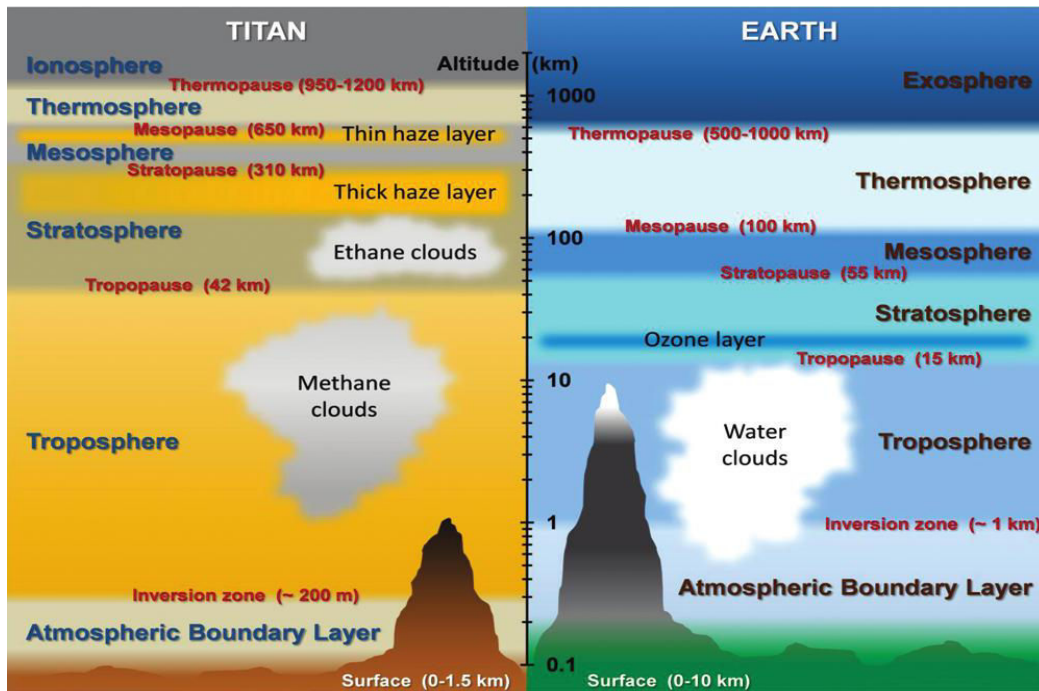


Figure 1-1. Vertical profile of the Titan and Earth atmosphere (cable et al., 2010).

In addition, there is also another characterization is similar with the Earth that is the presence of an active and complex organic chemistry in Titan's environment. The presence of an internal water-ocean was considered since the Cassini-Radar observations. This makes Titan a potential habitable environment and has an important role in astrobiological science field. So by comparison with the Earth, the scientists want to research the present conditions on Titan to see if Titan can give us the explanations about the origin and characteristics of the life on the early Earth. Because of its 94 K surface temperature, Titan offers us a volatile-rich, chemically primitive world trapped in time.

## 1.2 The observation of Titan and in-situ data acquisition

The method which is the most commonly used to observe Titan is the use of ground-based observatories. Observations in all ranges of lengths wave allow obtaining different data points from the different altitudes on the satellite, and thus have a global vision.

Another way to study Titan directly is in situ observation via space missions. Until now, we have launched some missions to study this satellite. Pioneer 11 was launched in 1973 to explore our solar system, and particularly the environment of Saturn's rings in preparation for the Voyager 1. The Voyager 1 and 2 missions were launched in 1977. The Voyager 1 encounter with Saturn and Titan took place in November 1980, while Voyager 2 arrived in the Saturnian system in August 1981, 9 months later. Through these missions we have acquired some knowledge about Titan, but are very little and limit, until the Cassini-Huygens mission launched we have some new and comprehensive understanding to Titan.

### **1.2.1 The instruments for observation in situ on Cassini-Huygens**

#### *The Cassini orbiter*

There are 12 instruments on the Cassini orbiter to collect data studied by 27 international scientific teams and allow to investigating the Saturnian system through several of fields:

#### 1. The optical

The following instruments are used to study the optical properties of Saturn, its rings and satellites throughout the electromagnetic spectrum. They are:

- **CIRS** (Composite Infrared Spectrometer), measurement of infrared data of the atmosphere and rings of Saturn and its moons to study their temperature and composition;
- **ISS** (Imaging Science Subsystem), taking photographs in the areas of visible, near ultraviolet and near infrared;
- **UVIS** (Ultraviolet Imaging Spectrograph), in the ultraviolet field to measure the atmosphere and rings in order to study the structure, and chemical composition;
- **VIMS** (Visible and Infrared Mapping Spectrometer), identification of the chemical composition of the atmosphere and the rings of Saturn and its moons by measuring the visible and infrared energy emitted or reflected.

## 2. The study of fields, particles and waves

These instruments that are dedicated to study of fields, particles and dust, the magnetic field and plasma around Saturn. Two of these instruments are using:

- **CAPS** (Cassini Plasma Spectrometer), study of the plasma in the space of the magnetic field of Saturn.

- **INMS** (Ion and Neutral Mass Spectrometer), examination of charged and neutral particles which are close to Titan, and other Saturn's satellites in order to learn more about the extent of their atmosphere and ionosphere and survey distance in the microwave field.

The instruments using radio waves to map atmospheres, determine the masses of the satellites of Saturn, collecting data on the particle size of the rings, and reveal the surface of Titan. One of these instruments is:

- **RADAR** (Cassini Radar), mapping the surface of Titan using radar imager to "break" the atmospheric haze.

### *The Huygens probe*

On January 14, 2005, the *Huygens* probe landed on the surface of Titan, just off the easternmost tip of a bright region now called Adiri. The probe photographed pale hills with dark "rivers" running down to a dark plain. Current understanding is that the hills (also referred to as highlands) are composed mainly of water ice. Dark organic compounds, created in the upper atmosphere by the ultraviolet radiation of the Sun, may rain from Titan's atmosphere. They are washed down the hills with the methane rain and are deposited on the plains over geological time scales (European Space Agency, 2005).

The Huygens probe included six instruments:

-**ACP-GCMS**: (Aerosol Collector and pyrolyze-Gas Chromatograph and Mass Spectrometer). ACP function was to collect aerosols in the atmosphere and pyrolyzed the sample. The pyrolysis products were then injected into the GCMS. They were either directly analyzed by mass spectrometry or by coupling with gas chromatography (Israel et al., 2002, 2005).

**-DISR:** (Descent Imager/Spectral Radiometer), which was carried out according to images of Titan's surface and spectroscopy measurements (visible and infrared) for the atmosphere (Tomasko et al., 2005).

**-HASI:** (Huygens Atmosphere Structure Instrument), contained sensors measuring the physical and electrical properties of the atmosphere (Fulchignoni et al., 2004).

### **1.2.2 Surface composition from in situ observation**

Before Cassini-Huygens mission carried out, Titan's surface composition was not very well known because observe of Titan's surface directly is very difficult due to Titan's surface has a thick, scattering and absorbing atmosphere. The rich in a varies of geologic characterizations on the surface of Titan was observed from this mission, but its composition remains elusive (McCord et al., 2008; Stofan et al., 2007). The information about the surface composition on Titan is very crucial for establish models of Titan's interior, surface, and atmosphere, especially very useful in the search for an endogenic methane source. The instrument Cassini Visual and Infrared Mapping Spectrometer (VIMS) is a useful orbital tool, the data obtained from this instrument can be used for global studies and mapping the Titan's surface composition. VIMS instrument is an imaging spectrometer that operates in the 0.35-5.17mm spectral region and is composed of two instrumental subsystems that can cover the different spectral ranges (Brown et al., 2004). The presence of "dirty" water ice has been confirmed by (McCord et al., 2008, 2006) on the basis of earlier ground-based studies (Coustenis et al.,1995; Griffith et al., 2003). However, many regions of Titan are not spectrally consistent with water ice as the dominant component, and the identity of the other constituents remains ambiguous. VIMS spectra for 5 mm bright spots have been suggested as attributable to CO<sub>2</sub> and telescopic and VIMS studies have offered that CO<sub>2</sub> might explain the peculiar spectral features in the 2.7-2.8 mm region. VIMS Tui Regio spectra show an absorption feature at 4.92 mm that has been suggested at due to CO<sub>2</sub> (Brown et al., 2009).

After Huygens landed on plain, the GCMS detected a high level of subsurface moisture with a methane humidity of ~50% at the surface. The GCMS surface data also showed traces of ethane and possibly cyanogen, benzene, and carbon dioxide. Aerosol pyrolysis products analyzed by the ACP/GCMS suggest the aerosols may contain nitriles in addition to organics (Brown et al., 2009; Israël et al., 2005). Recently, benzene together with light aromatic species as well as small concentrations of heavy positive and negative ions

have been detected in Titan's upper atmosphere (López-Puertas et al., 2013). They have found that PAHs are present in large concentrations in the upper atmosphere, with a peak concentration of about  $(2-3) \times 10^4$  particles  $\text{cm}^{-3}$  and extending up to about 1250 km, where they present a secondary minor peak.

**Figure 1-2** presents that the spectra mass peaks which obtain by the Huygens GCMS instrument can be attributed to several heavier molecules (Niemann et al., 2005). Their results included the identification of ethane ( $\text{C}_2\text{H}_6$ ) for definitely and tentative detections of cyanogen ( $\text{C}_2\text{N}_2$ ), benzene ( $\text{C}_6\text{H}_6$ ), and carbon dioxide. Cyanogen, benzene, and carbon dioxide show a smaller mass peak regardless of their surface abundances because of the volatile ability is worse than methane.

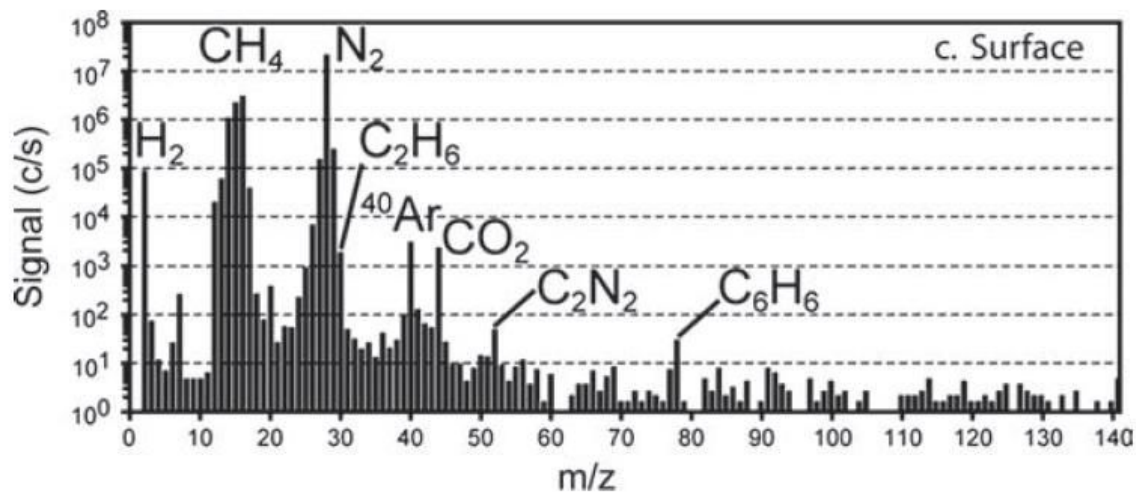


Figure 1-2. Averaged GCMS mass spectrum acquired at the surface showing ion count rates versus mass per charge ( $m/z$ ). Beyond increased methane, compounds found at the surface included firm detection of ethane and tentative detection of cyanogen, benzene, and carbon dioxide (Niemann et al., 2005).

However many compounds have been detected by GCMS, the useful information obtained for us to know the chemical composition of aerosols of Titan, but problems also exist for this instrument. For example the water ice cannot be detected by the instrument in spite of the water ice has a large abundance that because the water ice has a low vapor pressure. Another problem is difficult to detect directly the carbon monoxide because its mass is the same with molecular nitrogen result in the interference in the mass spectra. There was also a dedicated column for CO separation in the gas chromatograph subsystem but none was detected above the detection threshold. But another instrument DISR visible-near-IR reflectance spectrum of the surface suggests a mixture of organics and water ice, in spite of

the evidence for H<sub>2</sub>O is uncertain. The Titan's surface contains complex hydrocarbon and nitrile molecules forming nonvolatile solids, possibly mixed with fine-grained water ice inferred by Huygens data.

Recently the Cassini Solstice mission has discovered what appears to be a miniature version of the Nile River on Titan. The 400 kilometer (250 mile) long feature from 'headwaters' to a large sea **Figure 1-3**. Mission scientists were able to deduce that the feature is indeed a river as the dark, smooth surface within the meanders and channel suggest the presence of a liquid.

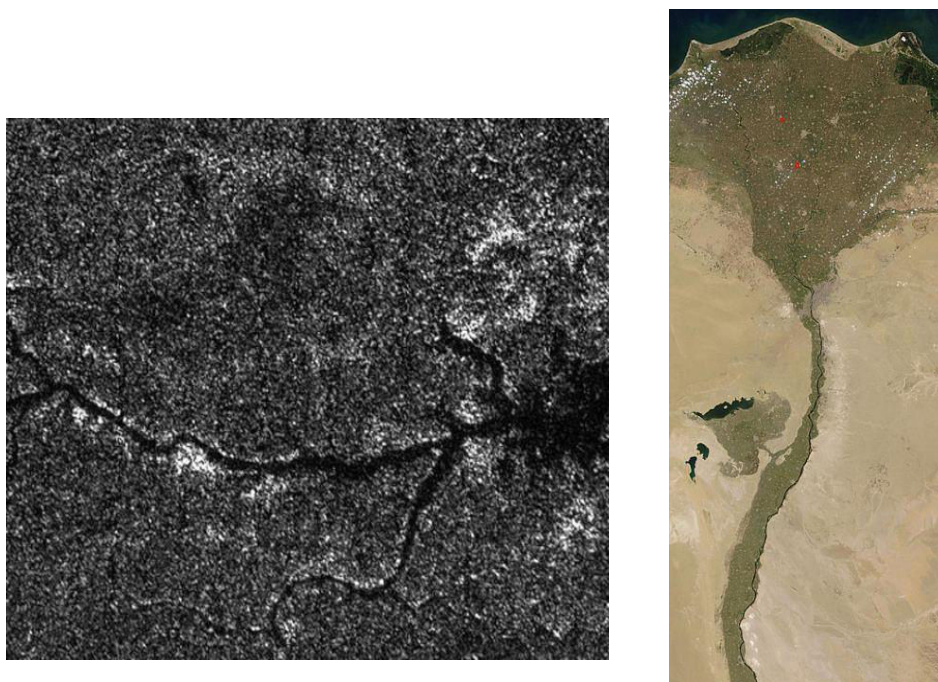


Figure 1-3. Titan's Nile: The radar image on the left taken by the Cassini space probe shows the vast river system as it flows north into the moon's Ligeia Mare sea. The right is a satellite image of the real Nile in Egypt. Image credit: NASA/JPL–Caltech/ASI.

### 1.2.3 Aerosols in Titan's atmosphere from in situ observation

Titan's aerosols play important roles in the atmosphere as they drive many physical and chemical processes occurring in the atmosphere (Tomasko and West 2009). Titan's aerosols have been termed to act as an “anti-greenhouse” agent (McKay et al., 1989) because they have some special optical properties, for example the low albedos of the aerosols at blue and shorter wavelengths absorb sunlight and heat the atmosphere at high altitudes while at longer wavelengths, the aerosols become optically thinner and permit thermal infrared

radiation to escape to space. Their abilities in absorbing and scattering solar and thermal infrared radiation contribute an important role to keep the heat balance of Titan and to provide the forcing for atmospheric dynamics. These optical properties of aerosols will also introduce in the afterward part. In addition, their formation at high altitudes where ultraviolet sunlight penetrates implies that aerosol production provides a sink for products of methane photochemistry that contain large C to H ratios. Because of their important roles in these physical and chemical processes, the Cassini-Huygens mission was carried out in order to better understand size, shape, the composition of Titan's aerosols and the vertical, horizontal distribution.

### 1.2.3.1 Shape and size of aerosols

Preliminary studies have found that these aerosols were made of fractal aggregates of monomers (Cabane et al., 1993). The size of these monomers influences directly on the degree of polarization, whereas the parameters such as opacity or backscatter depend on the total size of the aggregates, and the number of the monomers component.

Comparison of the inferred aerosol properties with computations of scattering from fractal aggregate particles can be used to determine the size and shape of the aerosols. The first in situ information of Titan's aerosols in the main haze layer was obtained by the Descent Imager/Spectral Radiometer (DISR) instrument on the Huygens probe. During the descent of Huygens, DISR measured the degree of polarization linear scattering sunlight at 492 and 934 nm. The phase curves obtained show that the polarization increases to a maximum at a phase angle of  $90^\circ$  and decrease. The curves of successive phase show that the polarization decreases when the opacity of the atmosphere increases. An adjustment of these measures with the values of a code simulating digital broadcasting by fractal aggregates indicates that the monomers have a radius of the order of 0.05 microns. The total size of the aggregates, and the number of the grain component may be evaluated from the opacity of the atmosphere measurements. (Tomasko et al., 2008) through analyze obtained particle phase functions; they conclude that the aerosols have a fractal-aggregate structure of the particles on the basis of their strong forward scattering property. And the wavelength measurement verified the absorbing nature of the aerosol in the visible region. (Lavvas et al., 2009) suggested that the detached haze layer observed by the *Cassini* instruments corresponds to a transition region where the particle growth changes from spherical- to aggregate-type base on the data observed by DISR in the stratosphere, optical properties of the aerosols below the detached

layer corresponded to aggregate particles, but above this altitude region the aerosol optical properties were characteristic of spherical particles.

Most Titan models assume a fractal dimension of two, where aggregates grow under a ballistic cluster-cluster diffusion aggregation process **Figure 1-4** (Cable et al., 2012; Lavvas et al., 2011).

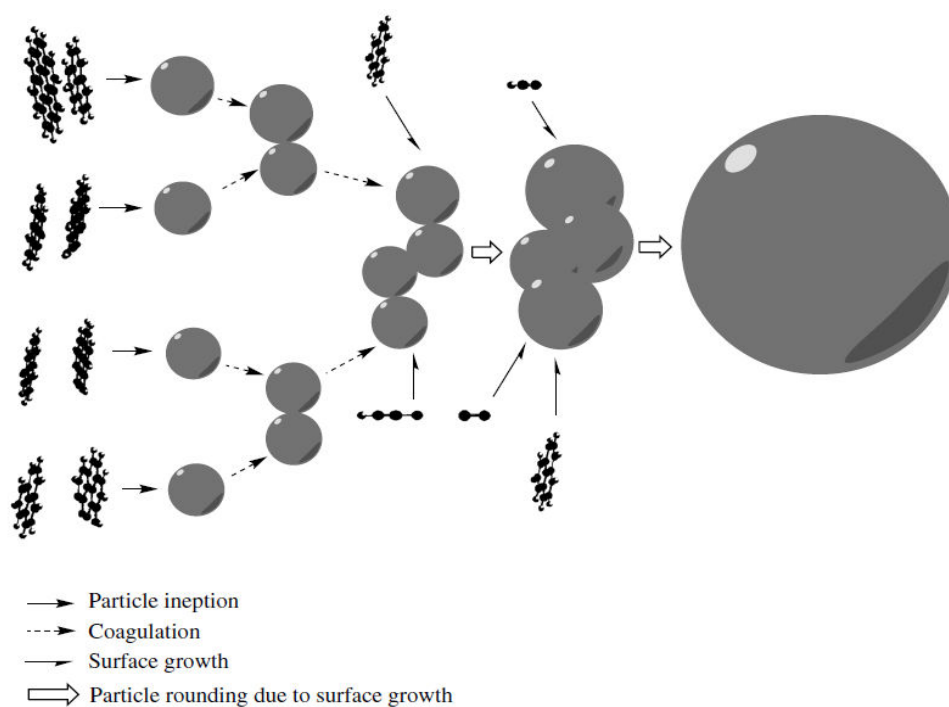


Figure 1-4. Processes included in the model. In this example, the PACs provide primary particles which then coagulate to form an aggregate. Eventually the surface chemistry acting on the aggregate provides a new, larger primary particle (Lavvas et al., 2011).

### 1.2.3.2 Optical properties of aerosols

The optical properties of Titan's aerosols implied the haze is strongly absorbing in the UV and Visible range (Rages et al., 1983).

Through fitting the upward- and downward- looking observations from the measurements during the Huygens descent, we obtained single scattering albedo of the haze aerosols. The measurements from the set of optical measurements on DISR are shown in **Figure 1-5** from (Tomasko et al., 2008).



This figure gives the single scattering albedo as a function of wavelength in the two altitudes region. The significant difference between these two curves for the different region is that the single scattering albedo of the haze aerosols varies with altitude.

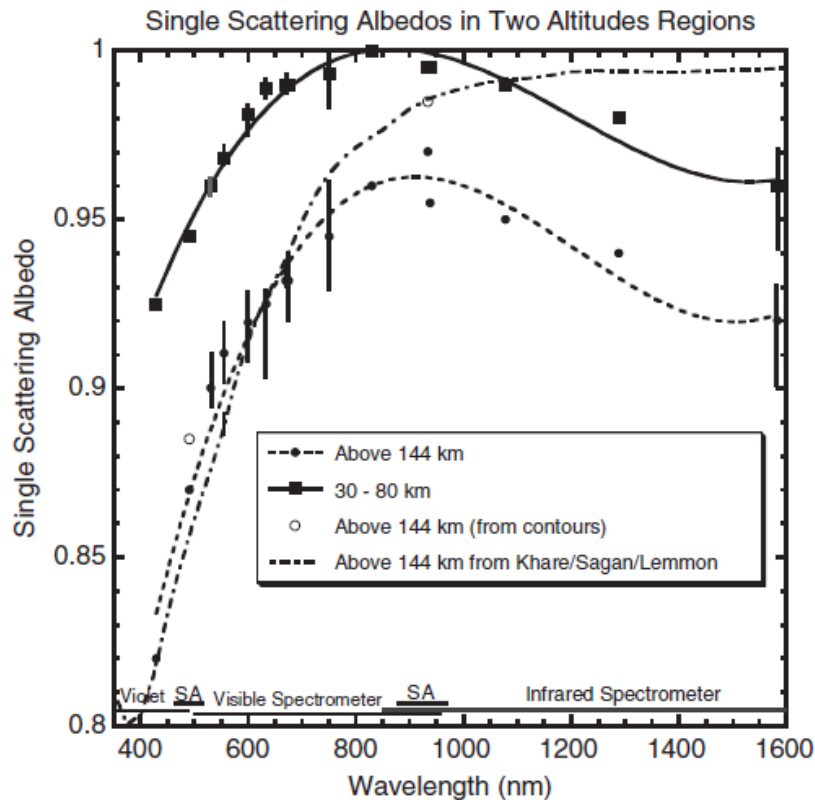


Figure 1-5. This figure shows the variations of single scattering albedo with wavelength at altitudes above 144 km and between 30 and 80 km, as labeled from (Tomasko et al., 2008). The measurements come from different portions of the DISR data set as indicated by the horizontal lines along the bottom of the figure (Note that SA represents the two channels of the DISR solar aureole camera). The error bars approximate one sigma uncertainties in the derived values. The dotted-and-dashed line is the single scattering albedo computed for the haze aggregate particles using 1.5 times the imaginary refractive index reported by (Khare et al., 1984a). The slope toward the blue is in reasonable agreement with the variation of single scattering albedo at high altitudes but does not show the decrease required for the haze aerosols long ward of 900 nm.

(Vinatier et al., 2012) used the volume extinction coefficient; they derived the extinction cross section, which is defined as the ratio of the aerosol volume extinction coefficient to the aerosol number density. The extinction cross-section depends on the imaginary and real parts ( $n_i$  and  $n_r$ , respectively) of the refractive index of the aerosol material. In order to constrain  $n_i$  and  $n_r$  in the  $70\text{-}1500\text{ cm}^{-1}$  spectral range, they employed an algorithm that calculates the extinction cross-section of a given fractal particle. Then they compared the calculated and the observed extinction cross section to derive the optical constants. **Figure 1-6** is the calculated extinction cross section of a fractal particle of 3000 monomers with

individual radii of  $0.05\mu\text{m}$  and a fractal dimension of 2 (dotted line), which are the physical characteristics inferred by (Tomasko et al., 2008) from in situ measurements, and the refractive indices of the tholins of (Khare et al., 1984a).

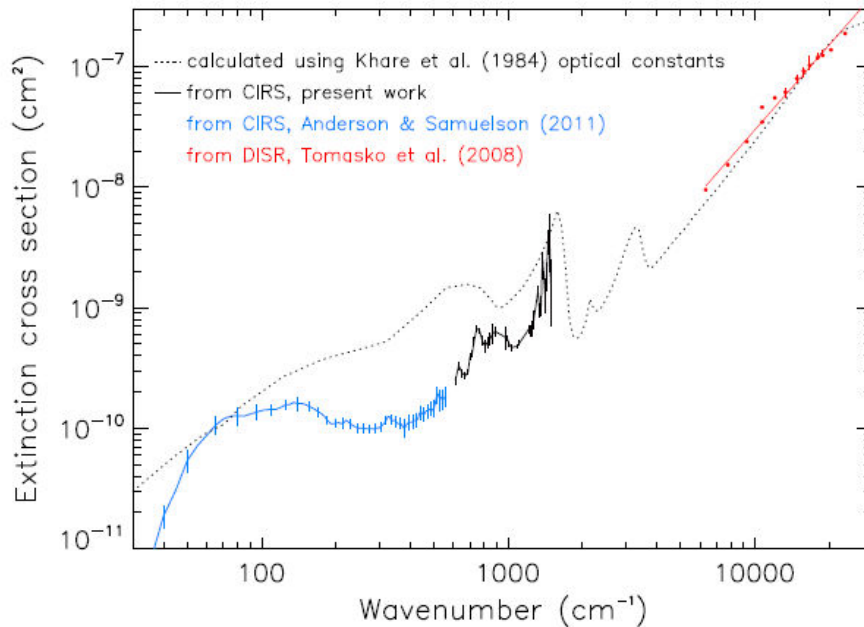


Figure 1-6. Derived extinction cross-section in the  $610\text{-}1500\text{cm}^{-1}$  spectral range (black) using CIRS observations (present work), in the  $30\text{-}560\text{ cm}^{-1}$  spectral range (blue) using CIRS observations (Anderson and Samuelson, 2011) and in the  $6300\text{-}23,000\text{ cm}^{-1}$  region (red) using DISR observations (Tomasko et al., 2008). The extinction cross section of Titan's aerosol is compared with a theoretical extinction cross-section calculated for a fractal aerosol made of 3000 monomers of  $0.05\ \mu\text{m}$  radius and displaying the tholins optical constants of (Khare et al., 1984a).

(Vinatier et al., 2012) found that Titan's aerosols are less absorbent than tholins in the thermal infrared. The most prominent emission bands observed in the mid-infrared are due to C-H bending vibrations in methyl and methylene groups. It appears that Titan's aerosols predominantly display vibrations implying carbon and hydrogen atoms and perhaps marginally nitrogen. In this research Titan's aerosols exhibit the same chemical composition in all investigated latitude and altitude regions.

### 1.2.3.3 Vertical structure of aerosols

The aerosols structure can be separated into a main haze layer located below  $300\text{km}$  and multiple detached layers above, the location and extent of which latitude (Rages et al., 1983). In addition, observations by the Cassini UVIS and ISS instruments reveal the presence

of a detached haze layer at  $\sim 520$  km, while aerosols were detected all the way to the thermosphere (Liang et al., 2007).

Tholins haze formation emphasized the role of photochemical reactions in the stratosphere above about 100 km altitude (Yung et al., 1984; Wilson and Atreya 2003; Liang et al., 2007). Recent results from instruments on the Cassini orbiter inspire the interest to the ion and neutral chemistry in the high atmosphere, around 1,000 km altitude.

Ultraviolet observations of a stellar occultation provide profiles of aerosol extinction in the altitude range 300-1,000km. An aerosol vertical profile derived from the data which obtained by the long-wave (170-190nm) end of the Cassini Ultraviolet Imaging Spectrograph (UVIS) Far Ultraviolet (FUV) spectrograph (Liang et al., 2007) is shown in **Figure 1-7**. This figure shows that the aerosol density vertical distribution derived from the reduction of the  $\lambda$  Sco occultation, compared to the derived  $\text{CH}_4$  profile. The important result is that an aerosol signature in the occultation data is present all the way to 1,000 km. The dip in aerosol density just below 500 km altitude is evidence for a thin haze layer in the altitude region 500-520 km (Tomasko and West, 2009).

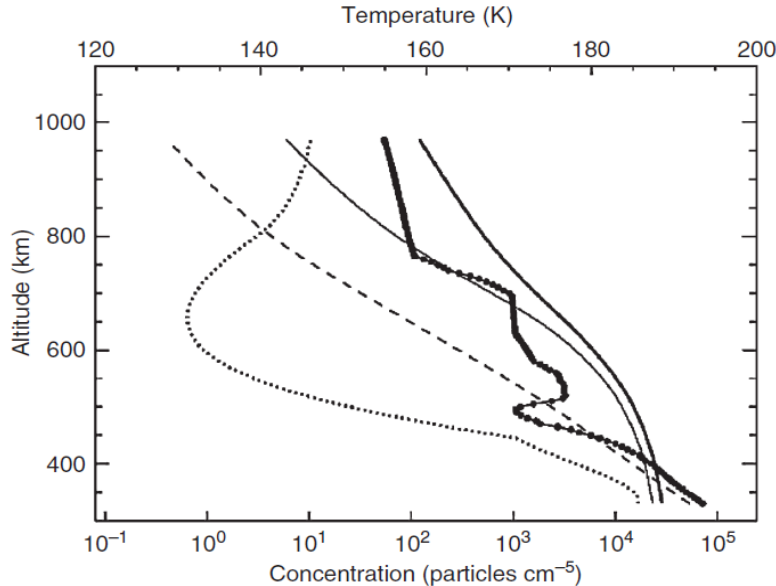


Figure 1-7. From Liang et al., (2007) Aerosol density (filled circles) derived from the UVIS I Sco occultation compared to the  $\text{CH}_4$  density (dashed line) scaled by  $10^{-9}$  (Shemansky et al., 2005; Shemansky 2006). The increase of the mixing ratio of the UVIS aerosols through the mesosphere to at least 1,000 km implies that the production of aerosols must take place at significant rates throughout the mesosphere and thermosphere. The UVIS-derived temperature profile is shown by the dotted line. Model aerosol profiles computed by Liang et al., (2007) are shown by the thin and thick solid lines (Tomasko and West, 2009).

### 1.2.3.4 The chemical composition and structure of aerosols

The ACP experiment on Cassini Huygens was the first to analyse the chemical composition of aerosols of Titan. The results revealed that the main pyrolysis products are  $\text{NH}_3$  and  $\text{HCN}$  and the aerosols are made of an organic refractory core (Israël et al., 2005).

The CIRS instrument on Cassini Huygens mission using IR method found that some absorption bands of aerosols at  $325\text{cm}^{-1}$  and  $515\text{cm}^{-1}$  assignment are not obvious Figure 1-8.  $1380\text{cm}^{-1}$  symmetric bending of C-H in  $\text{CH}_3$ ,  $1450\text{cm}^{-1}$  asymmetric C-H bending of  $\text{CH}_3$  and scissor in plane bending of C-H in  $\text{CH}_3$  (Gautier et al., 2012). That means the C-H functional vibration is mainly due to the methyl group.

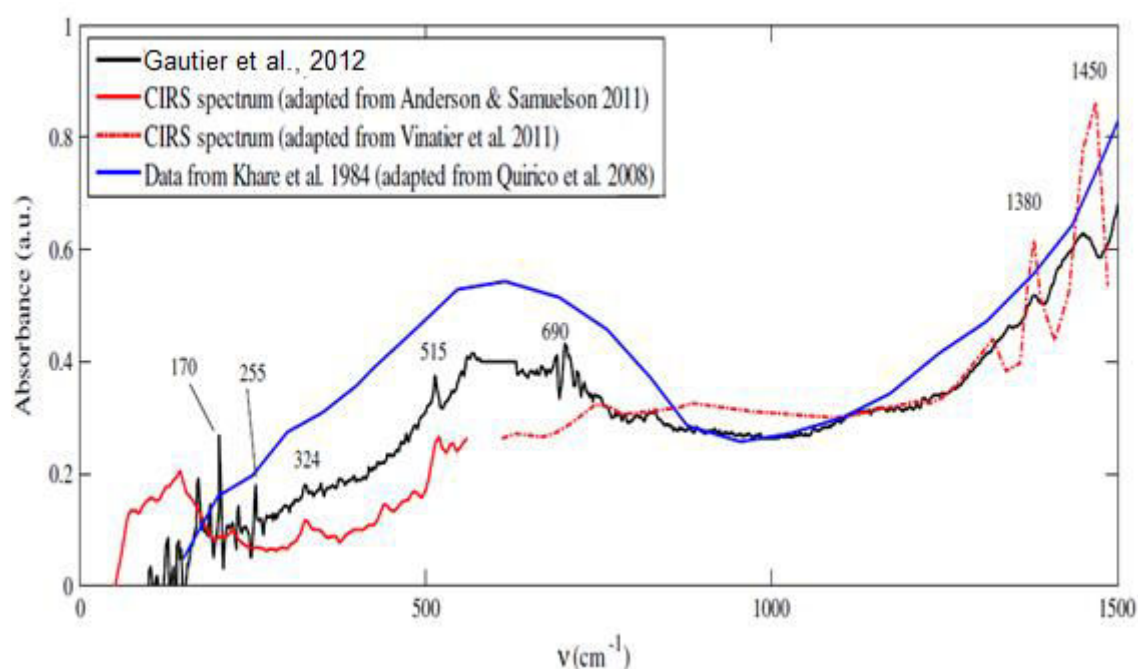


Figure 1-8. Black line represents our tholin 5% spectrum. Titan's aerosols spectra derived from observations with Cassini CIRS (Anderson and Samuelson, 2011; Vinatier et al., 2010) are plotted in red. The blue line represents tholin spectra reconstituted from Khare et al., (1984a) data (from Quirico et al., (2008))

Both the Ion and Neutral Mass Spectrometer (INMS) and the Ion Beam Spectrometer (IBS) on the Cassini Plasma Spectrometer (CAPS) instrument (Young et al., 2004) detected large molecules at altitudes above 950 km in Titan's thermosphere. Mass spectra recorded by INMS show mass peaks that extend to the mass limit of the instrument.

From the CAPS instrument of Cassini Huygens mission, we also got some information about the properties of aerosols of Titan. (Coates et al., 2007) using CAPS electron spectrometer data from sixteen Titan encounters, they revealed the existence of negative ions.

These ions, with densities up to  $\sim 100 \text{ cm}^{-3}$ , are in mass groups of 10-30, 30-50, 50-80, 80-110, 110-200 and 200+ amu/charge. The discovery of negative ions in Titan's ionosphere by the Electron Spectrometer (ELS) (Linder et al., 1998) was reported in this study. Titan's ionosphere contains a rich positive ion population including organic molecules. In this study discovered significant quantities of heavy negative ions in Titan's ionosphere **Figure 1-9**. This result is significant for the chemistry of hydrocarbon atmospheres, the composition of Titan's aerosols, and may have long term effects on the composition of the moon's surface.

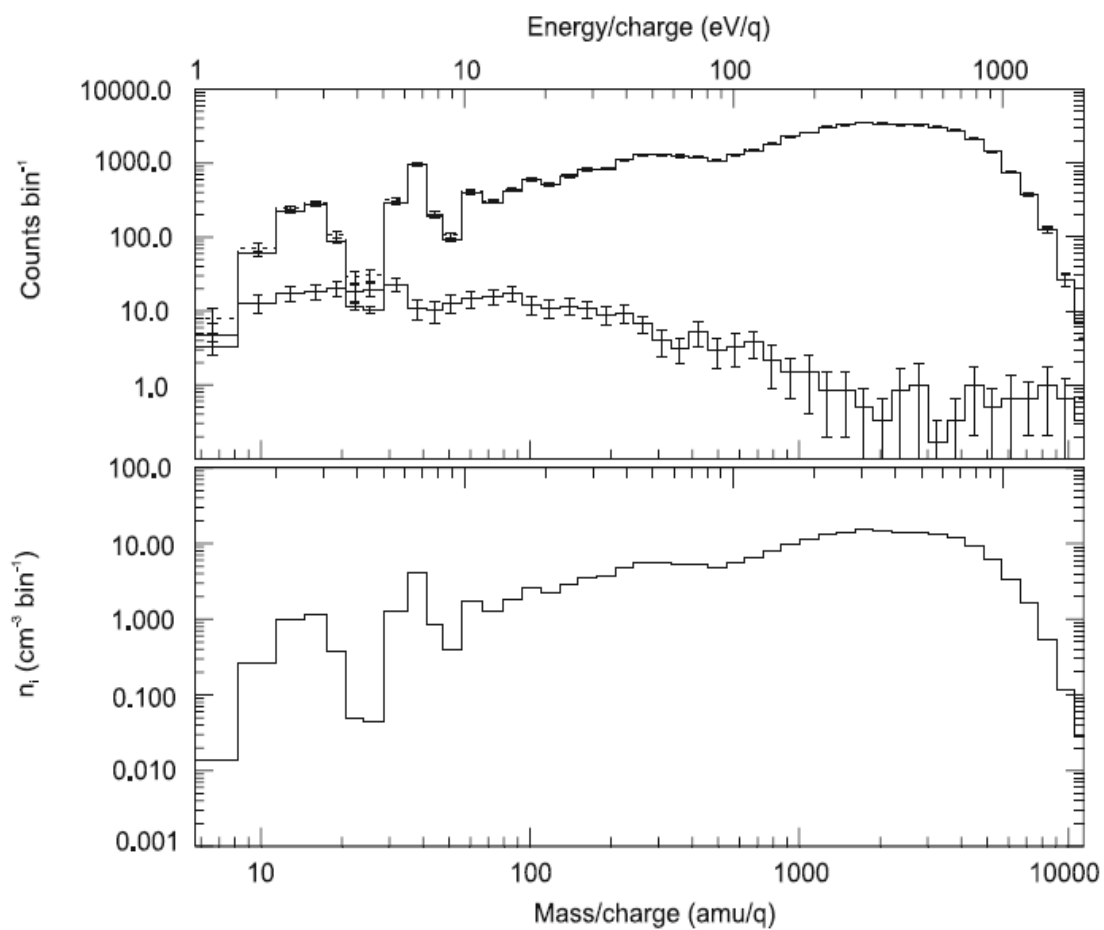


Figure 1-9. Energy (and mass, converted assuming singly charged ions) spectra at an altitude of 953 km during the T16 encounter. (top) Dotted trace shows total counts, dashed trace shows signal due to ionospheric electrons, and solid trace shows counts due to negative ions only. (bottom) Negative ion density measured in each ELS energy bin. In each case error bars are associated with statistical uncertainties on the counts (Coates et al., 2007).

### 1.3 Titan's analogue: Tholins

The term "tholins" was first used to describe the substances obtained in the Urey-Miller-type experiments on the gas mixtures that are found in Titan's atmosphere (Sagan and Khare, 1979). This term can be used in many fields, but it is generally used to describe the reddish, organic component of planetary surfaces. In the laboratory on Earth, the materials produced by the discharge reactor simulated experiment, for example mimic the material believed to be present on Jupiter, Neptune's moon Triton, and other comets, centaurs (minor planets), icy moons, and the early Earth (Sagan et al., 1993; McDonald et al., 1994 ; Ruiz et al., 2007, 2008, 2009) have been called tholins. In this study, we just focus on the Titan's tholins. But we want to keep in mind that tholins it's just a definition, there are no real tholins on Titan. Tholins are useful for us to better think about the chemistry on Titan, but this information may be different with what we actually discover on Titan. Because the conditions used to produce tholins in the experiment are difficult to simulated Titan conditions and environment very exactly and effective reproduction in the laboratory on Earth.

#### 1.3.1 The process of "Tholins" formation

Titan's lower atmosphere has long been known to possess organic aerosols (tholins) presumed to have been formed from simple molecules, such as methane and nitrogen ( $\text{CH}_4$  and  $\text{N}_2$ ). Until now, it has been assumed that tholins were formed at altitudes of several hundred kilometers by procedures as yet unobserved. With the help of measurements from a combination of mass/charge and energy/ charge spectrometers on the Cassini spacecraft, we have obtained evidence for tholins formation at high altitudes (~1000 kilometers) in Titan's atmosphere (Waite et al., 2007).

**Figure 1-10** shows a theoretical model explains formation of tholins by the dissociation and ionization of molecular nitrogen and methane by energetic particles and solar radiation, formation of ethylene, ethane, acetylene, hydrogen cyanide, and other small simple molecules and small positive ions, further formation of benzene and other organic molecules, their polymerization and formation of aerosol of heavier molecules, which then coagulate and deposit on the planetary surface.

Tholins formed at low pressure tend to contain nitrogen atoms in the interior of their molecules, while tholins formed at high pressure are more likely to have nitrogen atoms located in terminal positions.

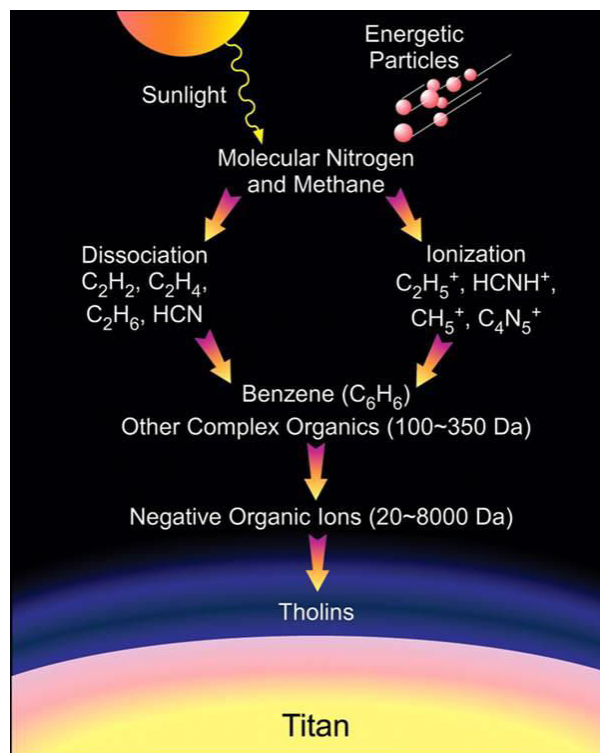


Figure 1-10. Cartoon showing the chemical process leading up to the formation of tholins in Titan's upper atmosphere. The process begins with free energy from solar UV radiation and energetic particles impinging on Titan's atmosphere. The most abundant constituents ( $\text{CH}_4$  and  $\text{N}_2$ ) combine through a number of reaction pathways to form larger organic and nitrile compounds (100 to 350 daltons) that eventually lead to the formation of negatively charged aerosols (20 to 8000 daltons) observed at  $\sim 1000$  km (Waite et al., 2007).

### 1.3.2 Laboratory simulation of Titan's aerosol (Tholins)

As far as now it's very difficult to study Titan's aerosols directly, but some of the difficulties may be overcome with the help of analogues of aerosols of Titan through the simulation experiment in the laboratory. We can use the information provided by the experiments to solve some difficulties and analyze the properties of Titan's aerosols. The major problem of laboratory experiment is to mimic the Titan's aerosols. To reach that goal, many experimental platforms have been developed in international laboratories to produce tholins, analogues of Titan aerosols. The synthesis of aerosol analogues in terrestrial laboratories, was initiated in the 80's (Khare et al., 1981, 1984a, 1984b, 1986; Sagan and Khare, 1979, Sagan et al., 1984) and has been followed until now. There are several teams have carried out the synthesis of Titan's aerosol analogues and have applied a series of analytical techniques to determine their properties. All of these "Titan reactors" use some type of discharge or radiation source to simulate one or several of the energy sources capable of generating radicals and other activated species in Titan's atmosphere.

Energy sources used in the previous studies have been concluded comprehensively in (Sarah Marie Hörst, 2011). For example include protons (Scattergood et al., 1975; Scattergood et al., 1977), laser induced plasma (LIP) (Borucki et al., 1988; Scattergood et al., 1989; Ramirez et al., 2001), gamma rays (Gupta et al., 1981; Ramirez et al., 2001) corona discharge (Navarro-gonzalez et al., 1997 ; Ramirez et al., 2001, 2005), electrical discharge (Khare et al., 1984b; Scattergood et al., 1989; Thompson et al., 1991; Sagan et al., 1993; McDonald et al., 1994; Coll et al., 1995; Ehrenfreund et al., 1995; McKay, 1996; Coll et al., 1999; Khare et al., 2002; Bernard et al., 2003; Coll et al., 2003; Sarker et al., 2003; Imanaka et al., 2004; Somogyi et al., 2005; Bernard et al., 2006; McGuigan et al., 2006; Sekine et al., 2008), UV (Hg or deuterium) (Podolak et al., 1979; Bar-Nun et al., 1988; Scattergood et al., 1992; Clarke et al., 1997; Trainer et al., 2006; Tran et al., 2003a,b; Ferris et al., 2005; Tran et al., 2005; Vuitton et al., 2006; Tran et al., 2008; Vuitton et al., 2009a; Jacovi et al., 2010), and UV synchrotron (Imanaka and Smith, 2007, 2009; Thissen et al., 2009; Imanaka and Smith, 2010). Many of the experiments that used UV lamps included (Thissen and Dutuit, 2009) cannot dissociate  $N_2$  (energy of dissociation = 9.76eV) because the UV radiation below 180nm (corresponding to electron energies above 6.9eV) is blocked by the silica windows generally used to confine both the light source and the reactive medium, or because the radiation flux above 9.76eV is not intense enough (Scattergood et al., 1989, Trainer et al., 2006) thus introducing primary products detected in the atmosphere of Titan as HCN and  $HC_3N$  to simulate the reactivity of the nitrogen in the reaction mixture. (Podolak et al., 1979; Clarke et al., 1997; Clarke et al., 2000; Tran et al., 2003a; Tran 2005, 2008; Vuitton et al., 2009b).

When we chose the method to simulate the aerosols of Titan, we must carefully consider the energy source and make an appropriate choice, because the composition of organic material produced in the context of Titan is very dependent on the type, intensity, and duration of ionization and dissociation processes. Although there are many parameters that can influence the differences among the simulation experiments for example temperature, pressure, composition of the gas mixture, sample collection technique, analysis technique, etc. But the differences in energy sources may account for much of the variability observed between simulation experiments.



The recovered data from tholins' characterization have been described in several articles (see **Figure 1-11** caption and references section)(Coll et al., 2012).

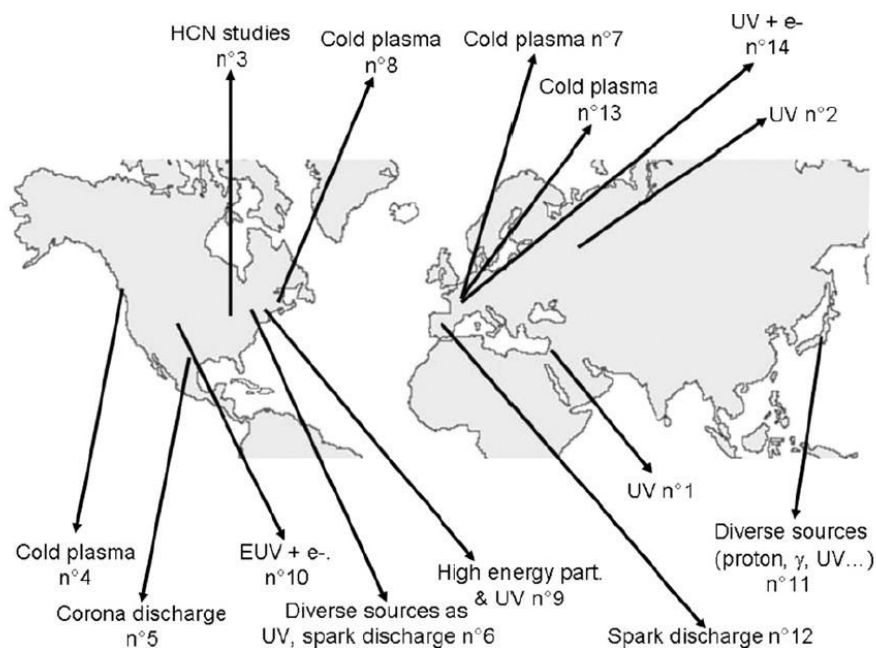


Figure 1-11. The summary of the laboratory teams which interest on Titan's atmospheric chemistry of all over the world. Written next to the energy source used by each team, is the numbered identification of the corresponding reference, where details about the synthesis are provided. n°1= Bar-Nun's team, n°2= Dodonova's work, n°3= Matthews's work, n°4= NASA Ames team, n°5= Navarro-González's team, n°6= Ponnampereana's team, n°7= Raulin's team, n°8= Sagan's team, n°9= Ferris' team, n°10= Smith's team, n°11= Koike et al., 2003, n°12= Centro de Astrobiología, Spain, n°13= PAMPRE team; n°14= SETUP team (Coll et al., 2012).

(Coll et al., 2012) has used a figure to summarize all of the teams in the world to carry out this simulate experiments in order to better understand their properties and the conditions under which they were synthesized. In summary, each tholins simulate experiment method has its own advantages and shortcomings, and it is necessary to determine which method is appropriate to model Titan's atmosphere. To resolve this question, (Coll et al., 2012) has carried out a series experiments. After several Pyr-GC-MS experiments to analyze some different aerosol analogues synthesized by different teams and compare with the results of the ACP experiment on board Huygens probe, they concluded that the experimental setup supported by a "cold plasma" produces aerosol analogues the most similar to Titan's aerosols, in terms of the volatile products they formed ( $\text{NH}_3$  then HCN). Cold plasma consists of a gas or gas mixture that is partly ionized, and keeps the ions at high temperature but the neutral molecules at room temperature. It can be generated when a high-voltage electric field is applied to a low-pressure container. It differs from a "hot plasma" because in this case the

ions and the neutral molecules are all at high temperature. Several laboratory simulation experiments are currently based on “cold plasma” systems.

In my study, we have used the aerosol analogues synthesized at LATMOS (Laboratoire Atmospheres, Milieux, and Observations Spatiales) a laboratory of the Versailles St-Quentin university. To better understand the production of these tholins we will explain in details the PAMPRE (Production d'Aerosols en Microgravite par Plasma Reactifs) method to synthesize the aerosol analogues.

### 1.3.3 The PAMPRE method

The most recent method used in the simulation experiment is the PAMPRE experiment, developed at LATMOS Laboratory also in France (Alcouffe et al., 2010; Szopa et al., 2006). This device is based on a capacitive coupled radio-frequency (RF) cold plasma system (see **Figure 1-12**) at low pressure in a  $N_2$ - $CH_4$  gaseous mixture. In this plasma, solid particles produced from the gas phase are in levitation, thus preventing any wall effect on their production **Figure 1-13**, and allowing the study of the formation and growth of the particles directly in the plasma. The studies developed by this group deals with the determination of the tholins chemical composition and structure (Pernot et al., 2010; Quirico et al., 2008; Vuitton et al., 2010), the solubility of the tholins in various solvent and the determination of aerosol optical properties (Carrasco et al., 2009; Hadamcik et al., 2009), as with gas to solid conversion efficiency (Sciamma-O'Brien et 2010).

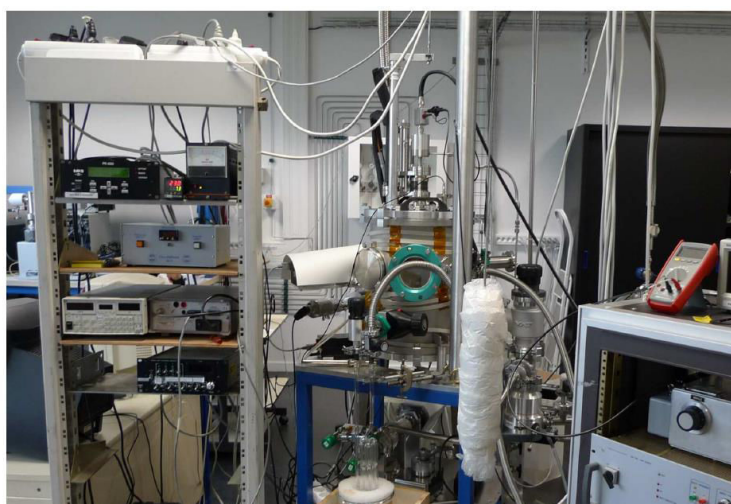


Figure 1-12. PAMPRE instrument at LATMOS laboratory.

The match between tholins of PAMPRE and aerosols of Titan is gradually confirmed by the identification of common signatures to both materials. (Rannou et al., 2010) recently identified a signature for aliphatic functions ( $-\text{CH}_2-$ / $-\text{CH}_3$  stretching modes groups) in aerosols of Titan by use of data transmitted by tangential Cassini VIMS instrument, IR absorption band at 3.4  $\mu\text{m}$  appeared. It underlines the fact that this band is predominant in the same spectral range for tholins of PAMPRE and published in the article (Quirico et al., 2008). Atmospheric transmission of far telluric infrared radiation also analyzed by the Cassini CIRS instrument, which has led to recent identification of spectral signatures of Titan aerosols in the medium and far infrared (Anderson and Samuelson, 2011; Vinatier et al., 2010).



Figure 1-13. Picture for the  $\text{CH}_4\text{-N}_2$  plasma in the PAMPRE reactor, the green trace corresponds to the diffusion of powders suspended at 532 nm green laser.

### 1.3.3.1 The setup for PAMPRE method

The experimental setup on PAMPRE has been described in a previous publication (Szopa et al., 2006). The complete device is shown in **Figure 1-14**.

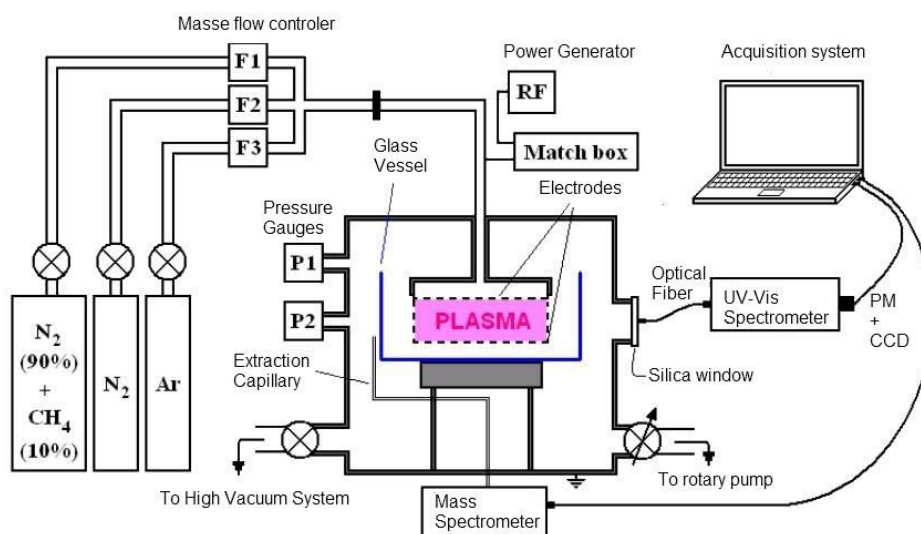


Figure 1-14. Experimental set-up for PAMPRE.

This set-up comprise of some important apparatus, these apparatus will be introduced in detail in the following part.

### *Reactor chamber*

The reactor chamber consists of a cylindrical stainless steel, 40 cm high and 30 cm in diameter. **Figure 1-15** shows a section in the plane for the optical measurements.

Two opposed openings (10 cm in diameter) are closed by a glass window, an opening can be used to inspect the plasma, the other through a window to face silica optical spectroscope. The experiment was designed to take measurements of light scattering simultaneously at multiple phase angles. Twelve holes have been provided for this purpose. For now, one of them is occupied by an inlet valve of air. Three aluminum tubular legs that supporting a plate connected to ground and serving to support a crystallizing glass for collecting the products tholins. This plate acts as an anode when the plasma is not confined. At the bottom of the enclosure, a hole allows the passage of a sampling capillary tube of the plasma towards the mass spectrometer. In the lower part of the enclosure, the openings allow to carry out the primary and secondary pressure measurements.

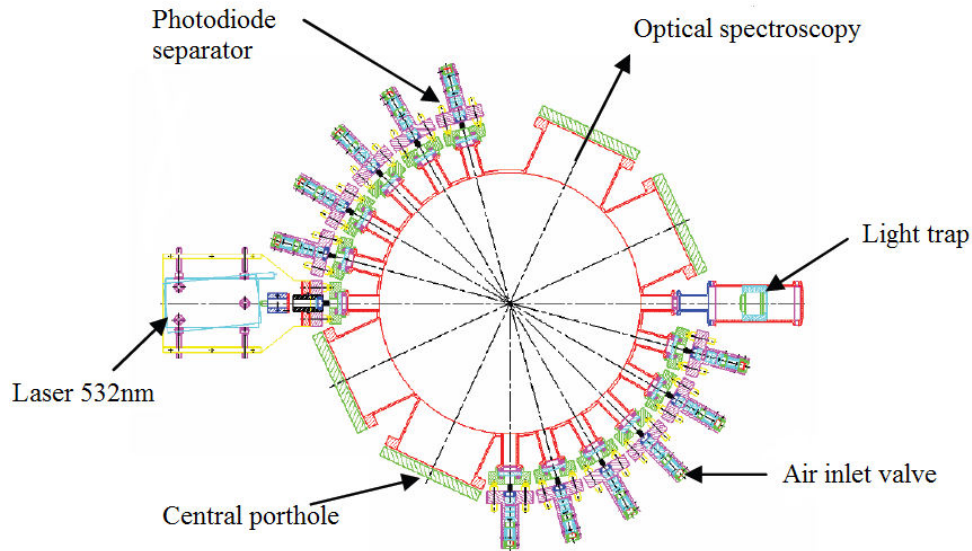


Figure 1-15. The cross section of the upper part of the reactor chamber.

Before each experiment, the reactor chamber, plasma box and crystallizer are cleaned with ethanol. The reactor is then pumped down to secondary vacuum by a turbo molecular pump while baked out at 110°C for several hours in order to remove impurities adsorbed onto the chamber walls. Once the chamber has cooled down, an argon discharge is switched on for 30 min to outgas the plasma confining metallic grid box.

#### *Pumping and gas injection*

Two independent pumping units are used. The first is a primary pump vane. It provides the order of a vacuum  $10^{-2}$  mbar in the chamber. Its role is to establish a vacuum before the secondary pumping with a turbo molecular pump. The primary pump is also used to vent when the experiment work flow of gas. A diaphragm valve between the chamber and the primary pump is used to adjust the pumping speed.

The second group is a turbo molecular pump (Alcatel ACT 200T), allowing to obtain a high vacuum ensuring the cleanliness of the enclosure before the experiments.

A Baratron (MKS PR 4000) pressure gauge is used to measure pressure between  $10^{-2}$  and 100 mbar. To measure the ultimate vacuum in the chamber, a type gauge Penning (Penning Edwards 505), operating between  $10^{-2}$  and  $10^{-6}$  mbar is used. Three-way fuel the gas chamber: the gases employed are argon, and nitrous nitrogen mixture (90%) and methane (10%). By dilution of this mixture in the nitrous pure, all proportions of CH<sub>4</sub> between 0 and 10% in N<sub>2</sub> can be obtained in the chamber. Each channel comprises a bottle (Air Liquid,

purity 99.999%). A flow controller (MKS 247°C) allows the regulation of the quantities of gas injected. These controllers are calibrated for nitrogen, a correction factor is taken into account when using other gases. Debits for gas are between 2 and 100 sccm ( $\text{cm}^3 \cdot \text{min}^{-1}$ , at  $0^\circ\text{C}$  and atmospheric pressure).

The gas mixture is injected through a stainless steel tube into the chamber by the polarized electrode of 12.6 cm in diameter. This electrode shaped "shower head" composed of three superimposed grids, provides an even flow of gas in the plasma (**Figure 1-16**). Around the electrode is placed a cylindrical cage plasma confinement (inside diameter 13.7cm, height of 4 to 5cm). Two diametrically opposed openings of width 1cm, covered with a fine mesh grid to allow both an observation of the plasma optical emission spectroscopy and visual inspection. This configuration is consistent with the "GEC RF reference cell".

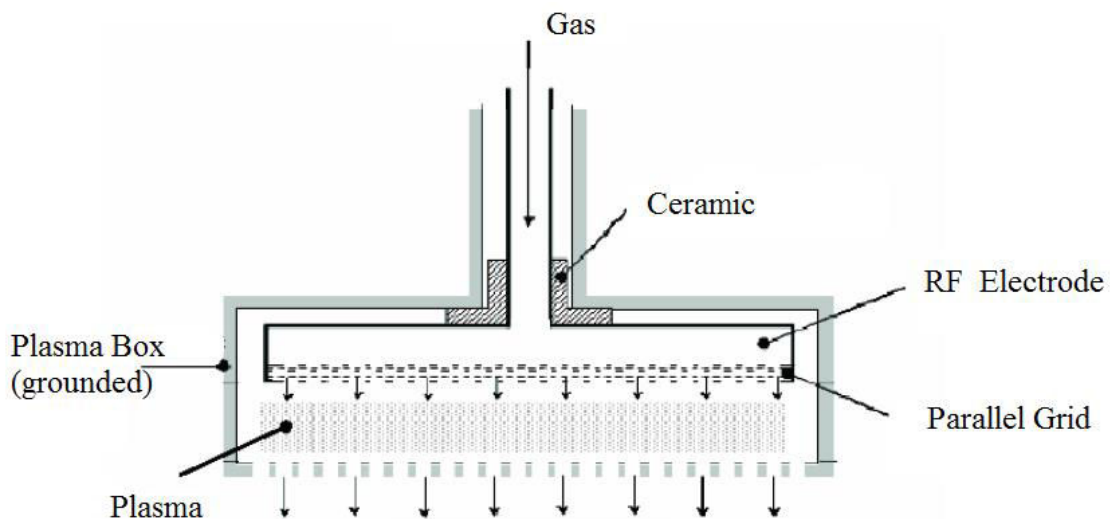


Figure 1-16. Cathode and containment cage.

### *RF discharge*

A radio frequency generator SAIREM GRP 01KE generates 13.56 MHz discharge. The incident power is adjustable from 0 to 100 W. The plasma is generated in continuous mode. It is also possible to obtain pulsed: a function generator (TTi TG550) is then coupled to the system. It delivers a voltage niche, with a rate of symmetry adjustable from 10 to 90%. The frequency of pulses is adjustable from 2 MHz to 5 MHz.

In both operation modes, the coupling is carried out through a tuning box which allows adapting the load to the output impedance of the RF generator, which is 50W. Such an arrangement allows the coupling maximum power to the plasma. The tuning box (**Figure 1-17**) contains two capacitors in parallel, and  $C_F$   $C_C$ , as well as inductance  $L$  and a capacitor  $C_B$  connected in series. The pair of capacitors  $C_c$  (variable 7 to 1000 pF) and  $C_F$  (500 pF) are used as filters against the parasitic capacitances. The capacitor  $C_B$ , variable from 25 to 500 pF, provides a high voltage in the branch of the circuit feeding the RF discharge. This box also includes a bridge agreement divider for measuring the self-bias voltage of the cathode.

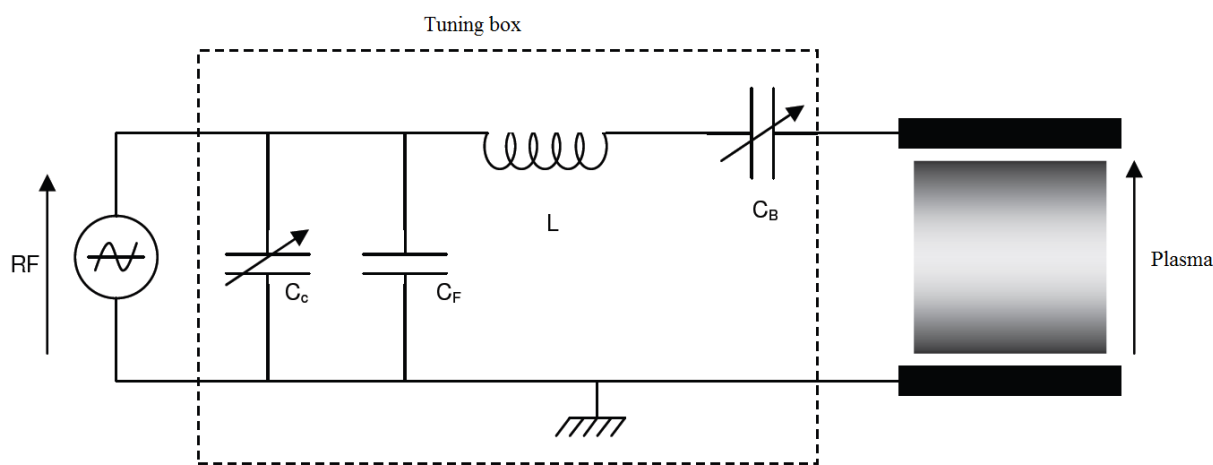


Figure 1-17. Diagram of tuning box.

Electrically charged tholins are produced and grow in levitation in the plasma, held in suspension by the electrostatic force between the electrodes. Once other forces (tholins weight, neutral and ion drag forces) surpass this electrostatic force, the tholins are ejected and collected in a glass vessel (crystallizer) surrounding the confining grid box, for further collection and ex-situ analysis. The tholins formation can be followed by the variations of the self-bias voltage of the polarized electrode. A quasi steady state is obtained after about 100s, supposed to be a characteristic time for dust formation (Cavarroc, 2007).

### 1.3.3.2 The limits in tholins production method (PAMPRE)

No single method has been able to accurately reproduce all observed conditions of the Titan atmosphere where aerosol formation occurs. Moreover, the problems such as contamination during tholins generation, collection and conserve prior to analysis can affect the results. In the following we will address the limitations of PAMPRE techniques and how such limitations can detrimentally affect the properties of the tholins.

## I. Temperature

Titan's atmosphere and surface are at cryogenic temperatures, this temperature is very difficult to maintain over the necessary time periods during a simulation experiment in the laboratory. For this reason the reactor for PAMPRE simulation are operated at room temperature, the temperature condition is not simulated very exactly with Titan. That means certain compounds that would normally condense at 180 K and below are volatile and behave differently with expected on Titan (Mckay, 1996; Raulin et al., 1989). For example, dicyanoacetylene ( $C_4N_2$ ) has been detected in Titan's atmosphere but it was not found in any experimental simulations carried out at room temperature. Only after cooling the reactor to 100-150K we can detect this thermally unstable compound (Coll et al., 1999; De Vanssay et al., 1995). Temperature can also affect the physical adsorption of gases onto particle surfaces, so the process for methane and ethane condensation onto aerosols cannot be understood very well without appropriate temperature simulation. Temperature variations also influence the kinetics of reaction; it can change the concentration of many intermediate products. It has been noted that temperature effects on ion-molecule reactivity in the Titan ionosphere, in particular with regard to branching ratio effects, are largely unknown both in terms of experimental and theoretical studies (Carrasco et al., 2008).

## II. Pressure

The RF discharge can operate at a total pressure ranging from 0.2 to 10mbar (Alcouffe et al., 2010). For plasma generation methods in particular, pressure can affect the densities of the active species (electrons, ions, and radicals) in the plasma and, therefore, the collision frequencies and kinetic energies of these species (Imanaka et al., 2004). Moreover, it has been demonstrated that nitrogen incorporation into tholins and the degree of aromaticity are very dependent on the pressure (Imanaka et al., 2004; Cruikshank et al., 2005). In the light of (Lavvas et al., 2009) study, tholins simulated techniques should be operating at much lower pressures.

## III. Oxygen and water contamination

Titan's atmosphere contains traces of oxygen, a little amount of CO (0.005%) and trace amounts of CO<sub>2</sub> and water vapor have been detected in the atmosphere (De Kok et al., 2007), no oxygen-containing molecules are present. So, the key to successfully produce the tholins in the laboratory is to generate these organics without oxygen. Therefore, the presence



of greater than trace levels of water vapor (or even trace levels of O<sub>2</sub>) in a reaction chamber can lead to unusual incorporation of oxygen in tholins, which changes the properties of the material significantly. It is difficult to realize the tholins synthesized under the oxygen-poor conditions because the oxygen and water are ubiquitous on the ambient atmosphere of Earth. We can adopt some measures to limit the amount of oxygen and water contamination. For example, before the tholins are produced, the chamber is baked out to remove H<sub>2</sub>O adsorbed on the walls of the chamber/electrodes, while being pumped down to 10<sup>-5</sup> mbar. A pure N<sub>2</sub> plasma discharge is then used to help further removing the remaining contaminants. And small leaks maybe result in the introduction of H<sub>2</sub>O, O<sub>2</sub> and CO<sub>2</sub> from Earth's atmosphere, or impurities in the gas bottles. The oxygen and water can also be incorporate into the samples when they were collected after produced and conserve for the further analysis.

### **1.3.4 Previous analysis of PAMPRE tholins**

The tholins produced in the PAMPRE apparatus have been previously analyzed using a number of in-situ and ex-situ analytical techniques. In order to better interpret the results acquired by our works, to understand the results of analyses performed by complimentary techniques is important and necessary.

#### 1.3.4.1 The physical properties analysis

##### *The grain size and morphology*

(Szopa et al., 2006) used optical emission spectroscopy (OES) method during the production of the tholins and detected N<sub>2</sub>, CN and H $\alpha$  emission in the plasma. The size and morphology of the tholins particles were studied by Scanning electron microscopy (SEM) method. The result of SEM revealed that the particles are quasi-spherical with diameters ranging from 0.2 to 2.5 $\mu$ m (average 0.8 $\mu$ m). The surface of the particles appears to be rough. The particles also appear to be sticky as they tend to form aggregates.

Hadamcik et al., (2009) investigated the variation in grain size with gas composition, gas flow rate, absorbed power and production time through analysis of SEM images. They found that grain size increases with increasing CH<sub>4</sub> concentration, with decreasing gas flow, increasing absorbed power and increasing production time (Hadamcik et al., 2009).

### *Solubility*

(Carrasco et al., 2009) investigated the solubility, morphology and composition of PAMPRE tholins. The study process is that they solved a known mass of 98% N<sub>2</sub>/2% CH<sub>4</sub> tholins into three solvents (H<sub>2</sub>O, CH<sub>3</sub>OH (methanol) and CH<sub>3</sub>CN (acetonitrile)), filtered the solvent, evaporated the solvent and then weighed the remaining material. The solubility of tholins in these three solvents are 0.2 mg/ml in water, 0.3 mg/ml in methanol, and 0.43 mg/ml in acetonitrile. The solubility of two samples (90/10 and 98/2) in methanol and toluene (C<sub>7</sub>H<sub>8</sub>) was also measured. For the 98/2 sample in methanol they found that 19±6% of the sample is soluble and that the soluble fraction has a solubility of 2.5±0.2mg/ml. For the 90/10 sample in methanol they found that 35±5% of the sample is soluble and that the soluble fraction has a solubility of 6.5±0.6mg/ml. The tholins had a very low solubility ratio in toluene (3% and 5% respectively). The morphology of these samples was also investigated through the use of SEM. They compared the insoluble and the initial samples morphology, the difference was not very significant.

### *Electron/Ion densities*

(Alcouffe et al., 2010) used optical emission spectroscopy (OES) to monitor the plasma. They also investigated the electron and ion densities as well as the self-bias voltage. The electron density calculations indicate that the electron density reaches a minimum around 0.8-0.9 mbar, which is the pressure at which the majority of the samples used in this work were produced. In this region there is little variation in electron density with CH<sub>4</sub> concentration and the electron density is approximately  $3 \times 10^{14} \text{ m}^{-3}$ . At lower pressures, the electron density decreases with increasing CH<sub>4</sub> in the gas mixture. Due to large uncertainties in the electron densities, they did not provide electron temperatures.

### *Optical indices*

(Mahjoub et al., 2012) studied the effect of initial methane concentration on tholins' optical constants. Samples produced in different methane concentrations (1%, 2%, 5% and 10%) were recorded by the ellipsometric measurements.

They found the optical constants depend strongly on the methane concentrations of the gas phase in which tholins are produced: imaginary optical index (k) decreases with initial CH<sub>4</sub> concentration from  $2.3 \times 10^{-2}$  down to  $2.7 \times 10^{-3}$  at 1000 nm wavelength, while the real

optical index ( $n$ ) increases from 1.48 up to 1.58 at 1000 nm wavelength. The larger absorption in the visible range of tholins produced at lower methane percentage is explained by an increase of the secondary and primary amines signature in the mid-IR absorption. An important decrease of the imaginary optical index, when the  $\text{CH}_4$  concentration increases, has been demonstrated. Mid-Infrared spectra of thin tholins films produced in different  $\text{CH}_4$  concentrations allows to connect this  $k$  variation to nitrogen-rich polymers preferably produced in lower methane percentages.

#### 1.3.4.2 The chemical properties analysis

##### *Chemical composition of tholins*

Elemental analysis method was used to analyze the chemical composition of tholins produced with 90%  $\text{N}_2$  and 10%  $\text{CH}_4$  which showed the C/N ratio is 2.32 and C/H ratio is 0.75 (Szopa et al., 2006). Those tholins were also analyzed through the use of pyrolysis GC-MS (Pyr-GCMS), the sample was heated to 650°C and then the resulting gases were analyzed by GC-MS instrument. Most unsaturated hydrocarbons and nitriles were identified and also identified numerous monoaromatic molecules (including nitrogen heterocycles) but did not observe any polyaromatics (Szopa et al., 2006).

(Sciamma-O'Brien et al., 2010) produced PAMPRE tholins for a variety of gas mixtures ranging from 1%  $\text{CH}_4$  to 10%  $\text{CH}_4$ . They examined production rates, performed elemental analysis on each sample and calculated gas to solid conversion rates for the tholins. They found that an initial concentration of 5%  $\text{CH}_4$  results in a steady state concentration of between 1 and 2%  $\text{CH}_4$ . It indicates that the samples produced with an initial concentration of 5%  $\text{CH}_4$  probably form in conditions more representative of Titan because Titan's atmosphere contains 2%  $\text{CH}_4$  in the region of the atmosphere we are interested in. From the elemental analysis measurements (performed by combustion for C, N and H and by carbon pyrolysis for O), they find that for increasing  $\text{CH}_4$  the molar percentage of H increases, N decreases, while C and O remain approximately constant. The C/N ratios for the 0.9 mbar sample range from 1.1 to 2 (for 2%  $\text{CH}_4$  and 10%  $\text{CH}_4$  respectively) (Sciamma-O'Brien et al., 2010).

Because of the sample tholins is very complexity, ultrahigh resolution mass spectrometry is necessary to determine the chemical composition of the tholins. (Pernot et al., 2010) used this method and two different tholins samples have been generated by changing the relative abundance of  $\text{N}_2/\text{CH}_4$  ratio: either 98%/2% (SA98) or 90%/10% (SA90). The high

resolution of the orbitrap reveals a large number of fine peaks for each mass unit and enables us to assign a  $C_xH_yN_zO_w$  formula to mass peaks, with the contribution of isotopes being negligible. This work confirms the importance of the nitrile chemistry for Titan's aerosol production, in agreement with the large nitrogen incorporation observed by the ACP instrument of the Huygens probe. New routes are proposed for Titan's aerosols formation, compatible with the present knowledge on Titan's atmospheric reactivity. They involve HCN and  $CH_2$  as patterns, in addition to the  $C_2H_2/HC_3N$  pair presently favored in most of Titan's atmospheric chemistry models.

#### *Composition of gas phase product*

(Gautier et al., 2011) used a cold trap (cooled by liquid nitrogen -77 K) to collect the gas phase products of the PAMPRE experiment. The products were then analyzed using GC-MS. They found that the total amount of condensable species changes with the initial concentration of  $CH_4$ . Accordingly, the carbon gas to solid conversion yield decreases with increasing  $CH_4$ . More than 30 different species were detected in their analysis. The predominant species observed in the GC-MS measurements are nitriles; hydrocarbons, some aromatics (mostly heteroaromatics) and 3 oxygen containing molecules (methanol, ethanol, and acetone) were also observed. They investigated the products of experiments using 1, 4, and 10%  $CH_4$ . In all cases, the major peak corresponded to HCN. More hydrocarbons were observed for the 10%  $CH_4$  experiment than the 1% and 4% experiments. They conclude that nitriles are important gas phase precursors to aerosol formation (Gautier et al., 2011).

#### *Stationary gas phase composition*

In the study (Carrasco et al., 2012) various initial  $N_2/CH_4$  gas mixtures (methane varying from 1% to 10%) are studied with a monitoring of the methane consumption and of the stable gas neutrals by in situ mass spectrometry. Atomic hydrogen is also measured by optical emission spectroscopy. A positive correlation is found between atomic hydrogen abundance and the inhibition function for aerosol production. This confirms the suspected role of hydrogen as an inhibitor of heterogeneous organic growth processes, as found in (Sciamma-O'Brien et al., 2010).

Moreover ammonia and methanimine are detected in the plasma in agreement with the detection by INMS in Titan's ionosphere (Yelle et al., 2010), such as ethanimine. The production in the gas phase of such highly polymerizable species provides promising clues to understand the production of tholins.

### *The structure of tholins*

Three different tholins samples (90/10, 98/2, and 99/1 the percentage for initial gaseous mixture) were analyzed by using UV Raman, infrared spectroscopy (IR), X-ray diffraction (XRD) and high resolution transmission electron microscopy (HRTEM) instruments (Quirico et al., 2008). Through the use of FTIR and Raman, they have identified -CH<sub>2</sub>, -CH<sub>3</sub>, -C-CH<sub>3</sub> (2800-2900 cm<sup>-1</sup>IR, 1380 cm<sup>-1</sup>Raman), -NH<sub>2</sub> (3200-3400 cm<sup>-1</sup>IR), -CN (2190-2300 cm<sup>-1</sup>IR, 2325 cm<sup>-1</sup>Raman), and C<sub>3</sub>N<sub>3</sub> (980, 690 cm<sup>-1</sup>Raman). The intensity of the feature attributed to C<sub>3</sub>N<sub>3</sub> increases from 90/10 to 98/2 (and 99/1). HRTEM reveals a very disordered nanostructure, but it is not necessarily as disordered as completely amorphous CNH. XRD confirms this interpretation with the presence of some coherent domains on an nm scale. From the HRTEM data there is evidence of small polyaromatics, most likely less than four rings. The HRTEM and XRD for the 98/2 and 90/10 exhibit no significant differences.

The soluble and insoluble fractions were also compared using IR spectroscopy (Carrasco et al., 2009). The soluble and insoluble fractions only exhibited slight differences. The peaks corresponding to symmetric and antisymmetric stretching modes of C-H in CH<sub>2</sub> and CH<sub>3</sub> are higher in soluble fraction (which is also true of the symmetric and antisymmetric bending modes of CH<sub>2</sub> and CH<sub>3</sub>). This indicates that there are more aliphatic chains in the soluble fraction. Comparisons of a band assigned to -CN (branched on an aliphatic group, 2240 cm<sup>-1</sup>) show that it is more intense in the soluble fraction and indicate that there are fewer conjugated cyanides in the soluble fraction than in the insoluble fraction.

(Gautier et al., 2012) studied various samples N<sub>2</sub>:CH<sub>4</sub> gas mixtures including: 1%, 2%, 5% and 10% of methane. The synchrotron radiation for mid-IR and the internal Globar source for the far-IR were used to analyze these samples. The evolution of the linear absorption coefficient  $\epsilon$  (cm<sup>-1</sup>) is given as a function of the wavenumber. They provided a complete dataset regarding the influence that the concentration of methane vapor in the gas mixture has on the tholins spectra. They found that intensity of the 2900 cm<sup>-1</sup> (3.4 $\mu$ m) pattern (attributed

to methyl stretching modes) increases when the methane concentration increases. More generally, tholins produced with low methane concentrations seem to be more amine based polymers, whereas tholins produced with higher methane concentrations contains more aliphatic carbon based structures. Moreover, it was shown that the position of the bands around  $2900\text{ cm}^{-1}$  depends on the chemical environment of the methyl functional group. We concludes that the presence of these absorption bands in Titan's atmosphere, as measured with the VIMS instrument onboard Cassini is in agreement with an aerosol contribution.

NMR is a powerful tool for structure determination of complex organic molecules and solid state species, providing detailed element-specific information about local structure and chemical environments. In (Derenne et al., 2012) study, they used solid state NMR techniques to investigate the carbon and nitrogen bonding environments in a  $^{13}\text{C}$ - and  $^{15}\text{N}$ - enriched sample recovered from PAMPRE experiment. The gaseous mixture they used to synthesize the sample contained  $2.00 \pm 0.06\%$  of pure  $^{13}\text{C}$ - labelled methane (Eurisotop, Saclay, France) in  $\text{N}_2$  isotopically enriched with 30% of  $^{15}\text{N}_2$  nitrogen (Eurisotope, Fr.). Then sample was examined by solid state NMR using a Bruker AVANCE III 700 spectrometer at  $B_0 = 16.4\text{ T}$  with  $\nu_0(^{13}\text{C}) = 176.07\text{ MHz}$  and  $\nu_0(^{15}\text{N}) = 70.95\text{ MHz}$ , with a 3.2mm triple resonance Bruker MAS probe, spinning at 22 kHz. Samples were spun at the magic angle using  $\text{ZrO}_2$  rotors.

The results of this study indicate that the model tholins structure is mainly based on unsaturated C-N bonded units, contained within  $\text{sp}^2$  bonded species such as imines or aromatic triazine or heptazine units, or nitrile ( $-\text{C}\equiv\text{N}$ ) groups. Amino groups ( $-\text{NH}_2$ ) are also present, most likely linked to  $\text{sp}^2$ -bonded C as are some methyl ( $-\text{CH}_3$ ) groups. Along with previous mass spectrometry and FTIR, UV-visible and FT-Raman investigations, this places additional and new constraints on the likely structures and compositions of the Titan's tholins.

At last, all the previous analysis has mentioned above were summarized in the **Table 1-2**. If we observe this table very carefully, we can find that the analysis used the Pyr-GC-MS technique is only (Szopa et al., 2006) has a little mention, but this technique is very useful to study the fragments of tholins. So in the next chapter, we will introduce this technique comprehensively.

## 1.4 Conclusion

In conclusion, aerosols of Titan play a predominant role in the climate control and organic chemistry happened in the satellite of Saturn. They are consisted of complex organic compounds and can be produced on a global scale, so the scientists are interested in these aerosols in the astrobiology domain. In spite of recent progresses acquired in the determining of their physical and chemical properties, mainly due to observations from the Earth and the results obtained from Cassini-Huygens mission, it still have many key questions about these properties and also some difficulties for interpreting the data obtained by the Cassini-Huygens mission. That is why we have developed some simulated method in the laboratory to produce the analogues of aerosol of Titan (tholins) to study the potential properties of aerosols, and also study their possible mode of formation and growth.

Tholins are complex chemical material, their physical and chemical properties can be varying with the different synthesized conditions used. The experience PAMPRE allows conducting a systematic physical and chemical properties study for tholins. This study aims to assess the impact of environmental conditions on the nature of these particles and to estimate the properties of aerosols of Titan. In order to study the physical and chemical properties of tholins compressively, we must develop and adopt the new and appropriate analytical techniques to accomplish this goal. In this thesis, we have proposed some techniques. In view of the results of ACP experiment and the limitation of the results, so in the next chapter the Pyr-GCMS technique was used to better constrain the chemical composition of aerosols of Titan, the results can be used to as the complementary data of ACP experiment on Cassini-Huygens mission.

Table 1-2. Summary of previous analysis of PAMPRE tholins, on the basis of the summary in (Sarah Marie Hörst, 2011).

Reference	Initial % CH <sub>4</sub>	Measurement Technique	Conclusions
(Szopa et al., 2006)	10	OES Pyr-GC-MS SEM Elem. Analysis	N <sub>2</sub> , CN, H $\alpha$ observed in plasma unsaturated species, rings/heterocycles, no polyaromatics sphere diameter 0.2-2.5 $\mu$ m, avg. 0.8 C/N=2.32, C/H=0.75
(Hadamcik et al., 2009)	var	SEM	grain size increases with increasing [CH <sub>4</sub> ] , decreasing gas flow increasing absorbed power and increasing production time
(Carrasco et al., 2009)	2, 10	Solubility IR APPI-TOF CID MS <sup>2</sup>	2% in CH <sub>3</sub> OH solubility ratio 19 $\pm$ 6%, solubility 2.5 $\pm$ 0.2 mg/mL 10% in CH <sub>3</sub> OH solubility ratio 35 $\pm$ 5%, solubility 6.5 $\pm$ 0.6 mg/mL bulk, soluble and insoluble fractions very similar more intensity at heavier masses in 10%, groups space 13 or 14 u losses of 15, 17, 27 (-more only)
(Quirico et al., 2008)	2, 10	FTIR Raman HRTEM XRD	-H <sub>2</sub> , -CN, -CH <sub>2</sub> , -CH <sub>3</sub> , -C-CH <sub>3</sub> C <sub>3</sub> N <sub>3</sub> , -CN, -CH <sub>2</sub> , -CH <sub>3</sub> , -C-CH <sub>3</sub> small polyaromatics (less than 4 rings) coherent domains on a m scale
(Alcouffe et al., 2010)	var	OES	neutral gas temperature increases ~10% above ambient



(Sciamma-O'Brien et al., 2010)	var	Prod. rate Elem. Analysis in situ MS	0.9 mbar peaks at 4% CH <sub>4</sub> (36.2 mg/h), 1.7 mar at 6% CH <sub>4</sub> (49.3 mg/h) C/N increases for increasing CH <sub>4</sub> from 1.1 to 2 (2% to 10% CH <sub>4</sub> ) initial [CH <sub>4</sub> ] of 4-6% result in steady state [CH <sub>4</sub> ] of 1-2%
(Véronique Vuitton et al., 2010)	2, 5, 10	FTIR HRMS MS <sup>2</sup>	more chemically complex than HCN polymers more chemically complex than HCN polymers some molecules from 98/2 have similar structure to HCN polymer
(Pernot e al., 2010)	2, 10	HRMS	polymeric scheme C $\alpha$ -(CH <sub>2</sub> ) $n$ + $\beta$ (HCN) $n$
(Gautier et al., 2012)	1, 2, 5, 10	Mid-IR Far-IR	percentage of methane impacts the spectrum of tholins in the mid-IR The 2900 cm <sup>-1</sup> pattern is agreement with the Cassini-VIMS spectra
(Mahjoub et al., 2012)	1, 2, 5, 10	SE	optical constants depend on the methane concentrations optical index (n) increases from 1.48 up to 1.58 at 1000 nm wavelength
(Derenne et al., 2012)	2.00 ± 0.06% <sup>13</sup> C 30% of <sup>15</sup> N <sub>2</sub> nitrogen	NMR	tholins structure is mainly based on unsaturated C-N bonded units, contained within sp <sup>2</sup> bonded species nitrile (-C≡N) groups. Amino groups (-NH <sub>2</sub> ) are also present, most likely linked to sp <sup>2</sup> -bonded C as are some methyl (-CH <sub>3</sub> ) groups.

**Chapter 2. Determination of the  
chemical composition of Titan's aerosols  
analogue (Tholins)**

## 2.1 Introduction

Titan's atmosphere has been believed that contains several varieties of hydrocarbons and N-containing organic molecules (mostly nitrile). These species in the atmosphere can form vary complex organic chains and rings through the polymerize process then condense into aerosols. These aerosols contribute to the source of the yellowish haze which covers Titan's surface and they can serve as the nucleus for other organic molecules to condense which forming shells on the particles when they settle down into the atmosphere.

The organics in Titan's atmosphere has been observed by the astronomical observation tools, there are also many laboratory research the organic chemistry in Titan's atmosphere by simulations and theoretical models. It is assumed that aerosols are formed by UV photolysis and charged particles at high altitudes. Eddy diffusion, sedimentation and general circulation distribute these aerosols throughout the atmosphere of Titan (Ehrenfreund et al., 1995). However, the shape and size for the aerosols distribute is not the same, submicron particles dominate the upper atmosphere; in the low regions due to the lower temperature, it contains mostly the larger molecules which can absorb in the visible.

The study of the constituents of these aerosols by Pyr-GC/MS (Pyrolysis Gas Chromatography/Mass spectrometry) is part of the Cassini Huygens mission (Israel et al., 1991). The main objective of the ACP experiments is to analyze the chemical composition of the aerosol particles. For this purpose, the instrument will sample the aerosols during descent and prepare the collected matter (by evaporation, pyrolysis and gas products transfer) for analysis by the Huygens Gas Chromatograph Mass Spectrometer (GC-MS) (Israel et al., 2002). Although this is the first time to study the chemical composition of aerosols of Titan directly, but there also exist some limitations to understand the aerosols comprehensively due to the sensitivity of instrumentation of ACP experiment. Therefore, some complementary tools should be used to analyze the chemical composition of aerosols. In this chapter, the pyrolysis-GC-MS technique was used to better constrain the structure of tholins.

### 2.1.1 ACP experiment

#### 2.1.1.1 ACP scientific objectives

As far as now, the Huygens probe is the first and the only tools that in-situ characterize the Titan's organic aerosols. This technique can provide the first chance to study the real

aerosols on Titan and will provide data on the chemical composition and relative abundances of the organic core and condensed volatiles constituting the aerosols. Based on the many predictions which have been obtained by the scientists used modeling experimental simulations, and Pyr-GC-MS analyses for several different tholins. So there are two classes of scientific objectives for ACP mission (Israel et al., 2002):

The primary objectives are determine the chemical structure of the photochemical aerosol then deduce the relative abundance of constituent (C, H, N, O) composing the aerosol. And obtain the relative abundances of condensed organics (e.g. C<sub>2</sub>H<sub>2</sub>, C<sub>2</sub>H<sub>6</sub>, HC<sub>3</sub>N, and HCN) principally CH<sub>4</sub> in order to compare with the abundance of constituent molecules in the aerosol nucleation sites. These objectives can be accomplished from measurements made during probe entry by ACP coupled with GC-MS.

Secondary objectives of fundamental interest are to determine the absolute abundance of all the condensed species averaged that exist on the stratosphere and upper troposphere respectively and compare the mean sizes of the aerosol nucleation sites over these two regions. At last, detection of non-condensable species, such as CO, eventually trapped in aerosols.

These objectives can also be accomplished under the help of additional information acquired by other Probe instruments (mainly the Descent Imager/Spectral Radiometer).

#### 2.1.1.2 ACP sequences during descent

The operations sequences are designed to meet the following requirements:

1. When the instrument in the position above 80 km, the aerosols need to obtain by the direct impaction on the filter then with the instrument continue to decent until below 80 km the samples are obtained by filtration. This procedure can determine the compositions of the particle cores (non-volatile and volatile components) and are conducted mainly in the low stratosphere and down to the tropopause (above 30 km).

2. The second sample must be collected above the deep methane clouds (20 km) within the troposphere. The instrument because of the mass constraints can only be equipped with a single collector that be used again after the oven, filter and product transfer lines and so on others equipment have been cleaned.

3. As the aerosols condense on the surface, the aerosols may be impacted by the reaction with the surface. This instrument must make at least one direct chromatographic analysis of the atmosphere composition before surface impact.

During the descent of Huygens probe into the atmosphere of Titan, the instrument ACP takes two samples of aerosols, then submitted to different treatments heater. The entire procedure of this sample can be divided into six sequences.

Sequence 1: The ACP instrument began to initialization and preparation for the first sampling operation, the filter in its sampling position at nominal altitude 130 km.

Sequence 2: Firstly collect the sample in the low stratosphere. When the filter retracted into the oven means this sequence finish.

Sequence 3: Heating the filter from ambient to 250°C and 600°C then the gas product transfers to GCMS.

Sequence 4: Oven and transfer lines are cleaned, and prepare for the second sampling operation.

Sequence 5 and sequence 6 is for taking the sample in the upper troposphere then the procedures repeated the sequence 3 and 4.

The first result obtained by ACP experiment revealed that ammonia and hydrogen cyanide as the main pyrolysis products after thermolysis of Titan's collected aerosols. The aerosols are made of an organic refractory nucleus, with a chemical composition that includes carbon(C), nitrogen(N) and hydrogen(H) (Israël et al., 2005).

Although some important results have been obtained by the ACP instrument, and the knowledge of the chemical composition of the real aerosols of Titan has an advance step. But the technique problems have also appeared during the descent of ACP instrument on the Titan's surface, a part of the ACP operation was not nominal. The operation of the coupling between the ACP and GCMS instruments has not been optimal. The effect of pressurization-depressurization to transfer the samples from the ACP to the GCMS did not operated correctly from temperature "ambient" to pyrolyze at 250°C of each sample. Internal pressures oven for these transfers actually not reached 2500 mbar necessary, the thermal conditions of ACP reached values 20 to 30°C lower than expected, and not in agree with the thermal

modelling of the instrument. Even this was the first direct chemical analysis of Titan's aerosols, the interpretation of the results were limited by the absence of detection of additional compounds (mainly due to a lower sensitivity of the instrumentation than originally planned), and by our ignorance of the aerosols building material.

### **2.1.2 Previous analysis of tholins using Pyr-GC-MS method**

Pyrolysis gas chromatography mass spectrometry (Pyr/GC/MS) is an instrumental method that enables a reproducible characterization of the intractable and involatile macromolecular complexes found in virtually all materials in the natural environment. It differs from GC/MS by the kind of sample analyzed and the method by which it is introduced to the GC/MS system. Instead of the direct injection of a highly refined organic solution, a few mg (or in the case of materials with a high organic carbon content, <mg) of the original natural material (e.g. soil, sediment, vegetation, insect cuticle, hair etc.) is analyzed directly. Pyrolysis is simply the breaking apart of large complex molecules into smaller, more analytically useful fragments by the application of heat. The sample is put into direct contact with a platinum wire, or placed in a quartz sample tube, and then the sample is heated at high temperature (500-1200°C). By applying heat to a sample that is greater than the energy of specific bonds, the molecule will fragment in a reproducible way. The fragments are separated by the analytical column then to produce the chromatogram.

Pyrolysis chromatography is also a powerful analytical tool that able to thermally crack (fragment) essentially non-volatile molecules into volatile fragments, making them suitable for chromatographic analysis.

(Sagan et al.,1979) was the first to investigate the tholins chemical properties. They studied tholins which produced by a spark discharge in a CH<sub>4</sub>, NH<sub>3</sub>, H<sub>2</sub>O (2.5%) mixture. They found that their sample thermal dissociation temperature was about 900°C through the pyrolysis-GC-MS method. This dissociation led to release aliphatic and aromatic hydrocarbons, abundant nitriles and other N-compounds. They concluded that this solid was not a polymer (repetition of the same monomeric unit) and the properties of tholins depended on the energy source employed and on the initial abundance of gas.

Tholins obtained from the sparking of He-CH<sub>4</sub> and N<sub>2</sub>-CH<sub>4</sub> mixture have also been studied, with the consider of ACP experiment (Coll et al.,1998; Israel et al., 1991; Raulin et al., 1998). The work leads by (Israel et al., 2002) study the pyrolysis gas chromatography

(Pyr-GC) of tholins produced at 77 K shows that saturated and unsaturated carbon chains are included in their structure; N-containing groups appear in the case of N<sub>2</sub>-CH<sub>4</sub> sparking. The mass spectrometer (MS) study of the evaporated oligomers and pyrolyzates showed that a wide range of alkylated aromatic compounds evolved from the sample, which indicates that such solids contain a 3-D polymer with a high degree of branching.

(Khare et al., 1981) studied the tholins for the planetary aerosols in the outer solar system (CH<sub>4</sub>/NH<sub>3</sub>/H<sub>2</sub>O spark tholins). The compounds released at various temperatures during the sequential vacuum pyrolysis. The result indicates that some of the nitrogen-containing compounds released at 150 and 300°C, such as acetonitrile, acrylonitrile, and benzonitrile, are less tightly bound in the polymer than the majority of hydrocarbons which were not released until 450°C. There is also a few of oxygen compounds, reflecting the low abundance of initial H<sub>2</sub>O. CO<sub>2</sub> is a major product at all pyrolysis temperatures, perhaps indicative of carboxylic acids.

Sequential (the same sample tholins used for different analysis temperature) and non-sequential (the new sample tholins used for different temperature) pyrolytic gas chromatography-mass spectrometry was realized by (Khare et al., 1984b). Titan tholins were generated from a gas mixture of 0.9 N<sub>2</sub> and 0.1 CH<sub>4</sub>. They found that the number and complexity of the pyrolysates increase with the temperature. But the richness of the products decreases slowly at higher temperature to 700°C. More than one hundred compounds were released. They found alkanes, alkenes, many nitriles, aromatic hydrocarbons, alkyl benzenes and other compounds in the pyrolysis compounds.

In other work (Ehrenfreund et al., 1995) the tholins sample was a film produced by a DC coronal discharge through a continuously flowing 90% N<sub>2</sub>/ 10% CH<sub>4</sub> atmosphere. The main peaks related to N-compounds HCN, CH<sub>3</sub>CN, acrylonitrile, proprioniuile and longer chain branched and unsaturated nitriles were observed by a GCMS analysis. Many hydrocarbons were observed as methyl branched and monosaturated isomers. Benzene, pyrrole, pyridine, pyrazine, pyrimidine and alkylated homologues were observed. HCN is a dissociation product during the whole Pyr-GC analysis process, which may imply that the nitriles can form thermal stable structures in the tholins.

The tholins obtained by (Coll et al., 1999) used the initial mixture gas of N<sub>2</sub>/CH<sub>4</sub> passes through a U-tube reactor. After the Pyr-GC-MS analysis under the chosen conditions

(Coll et al., 1997) their tholins yielded 27 hydrocarbons and 19 nitrile. These two families of compounds dominate the composition of tholins. In their results, It does not content aromatic or cyclic compounds other than benzene compared with previous work (Khare et al., 1984b; Ehrenfreund et al., 1995)

The tholins produced by PAMPRE method was first analyzed using Pyr-GC-MS by (Szopa et al., 2006) in order to learn more about the structure of the produced tholins. The sample was heated to 650°C, most of the identified molecules were unsaturated hydrocarbons and nitriles. They also identified numerous monoaromatic molecules (including nitrogen heterocycles) but did not observe any polyaromatics. A full list of the molecules identified through Pyr-GC-MS is shown in **Table 2-1**.

Table 2-1. Molecules identified in PAMPRE tholins from Pyr-GC-MS (Szopa et al., 2006).

Name	Molecular Formula
Methane	CH <sub>4</sub>
Hydrogen cyanide	HCN
C <sub>2</sub> Hydrocarbons	C <sub>2</sub> H <sub>x</sub>
Ethanedinitrile	C <sub>2</sub> N <sub>2</sub>
Propene	C <sub>3</sub> H <sub>6</sub>
Butene	C <sub>4</sub> H <sub>8</sub>
Butadiene	C <sub>4</sub> H <sub>6</sub>
Acetonitrile	CH <sub>3</sub> CN
Propenenitrile	C <sub>3</sub> H <sub>3</sub> N
Pentadiene	C <sub>5</sub> H <sub>8</sub>
Benzene	C <sub>6</sub> H <sub>6</sub>
Butanenitrile	C <sub>4</sub> H <sub>7</sub> N
Butenenitrile	C <sub>4</sub> H <sub>5</sub> N
Toluene	C <sub>7</sub> H <sub>8</sub>
Ethylbenzene	C <sub>8</sub> H <sub>10</sub>
Dimethylbenzene	C <sub>8</sub> H <sub>10</sub>

Recently, (Coll et al., 2012) used Pyr-GC-MS method to resolve the which method of synthesis tholins is more appropriate than the other for instance for ACP mimicking study. They asked for samples of tholins synthesized by different laboratories all over the world, the thermal degradation of some of these tholins performed under conditions similar to the ones used by the ACP experiments. Through comparing the results with ACP experiment, they



conclude that the experimental setups supported by cold plasma produce the aerosol analogues the most similar to Titan's aerosols.

The main goal of the pyrolysis is to form enough fragments of the volatile sample to be qualitatively and quantitatively analyzed by other techniques. The use of GC-MS allows the separation of the pyrolysis fragments, their identification and the determination of their relative concentration. The distribution of the fragment helps identify the nature and structure of the initial sample.

In order to study the fragments of tholins systematically synthesized by PAMPRE method, in this chapter study, we have used Pyr-GC-MS method to analyze two tholins samples 5pc and 10pc (5% and 10% methane respectively in the initial gaseous mixture). We studied the pyrolysis temperature range from 100°C to 900°C (the highest limited temperature for the pyrojector apparatus) to observe the evolution of the compounds with the temperature change, and to determine if the pyrolysis temperature can affect the compounds released and how does it work. In addition, we compared the results of these two samples to investigate if the methane percentage in the initial gaseous mixture has an influence on the pyrolysis compounds.

## **2.2 Experimental Section**

### **2.2.1 Instruments**

The part of pyrolysis we used SGE Pyrojector II as apparatus. It is an economical, continuous mode micro furnace pyrolyzing injection system which is highly reproducible. It is ideally suited for use with High Resolution Capillary GC, with a range of sample introduction systems designed for both liquid and solid samples.

The Pyrojector II is designed to operate on an existing GC injection port. It can easily be removed or attached, as the need arises for pyrolysis analysis. The pyrojector has been coupled to a GC-Trace(ThermoElectron)/Ms polaris Q(ThermoElectron). Sample introduction results in immediate pyrolysis and transfer of the breakdown products to the head of the column. The SGE Pyrojector involves a heated chamber in which a sample is introduced, vaporized and pyrolysed. The micro furnace is designed to operate at temperature up to 900°C for extended periods, without Curie Point gaps.

A flow of carrier gas is maintained through the pyrolysis chamber and then to the head of the capillary column. The flow through the pyrolysis chamber is controlled by a pressure differential between the head of the pyrolysis chamber and the head of the column. The pressure differential is greater; the flow through the chamber is greater. The rate at which the sample travels through the pyrolysis chamber (transit time) may directly affect the extent of pyrolysis, i.e. the shorter the transit time, the lower the time during which the sample is subjected to the pyrolysis temperature. Pyrolysis may not occur if the transit time is too short. On the other hand, if the transit time is too long, secondary pyrolysis may occur. Peak broadening due to slow sampling onto the column may also result from low flow rates (long transit times).

The furnace pyrolyzer is essentially an on-line inlet furnace which is continuously heated to the desired pyrolysis temperature. An inlet carrier gas (helium) flows through the pyrolysis chamber. The advantages of this system are that the pyrolysis conditions can be controlled very accurately and reproducible sample sizes are obtained more easily.

**Figure 2-1** shows a diagram of the furnace pyrolyzer Pyrojector II (S.G.E, Melbourne, Australia). For pyrolysis, a plug of quartz wool should be packed and positioned in the center of the furnace. This plug of quartz wool is required to prevent the sample from passing through the furnace into the cooler, lower part of the tube without undergoing satisfactory pyrolysis. The quartz wool is also of use to prevent particulate matter falling down into the transfer line, resulting in blockages. The desired pyrolysis temperature may be set from ambient temperature to 900°C in 1°C steps and the carrier gas (helium) pressure is controlled by use of an electronic control module.

Three different sample injection heads are supplied with the Pyrojector II. Each is intended for a particular type and size of sample. Generally, they include the conventional septum injection: septumless injection and pelletizer injection. In our case we used the solid sampling kit to accomplish the sample injection.

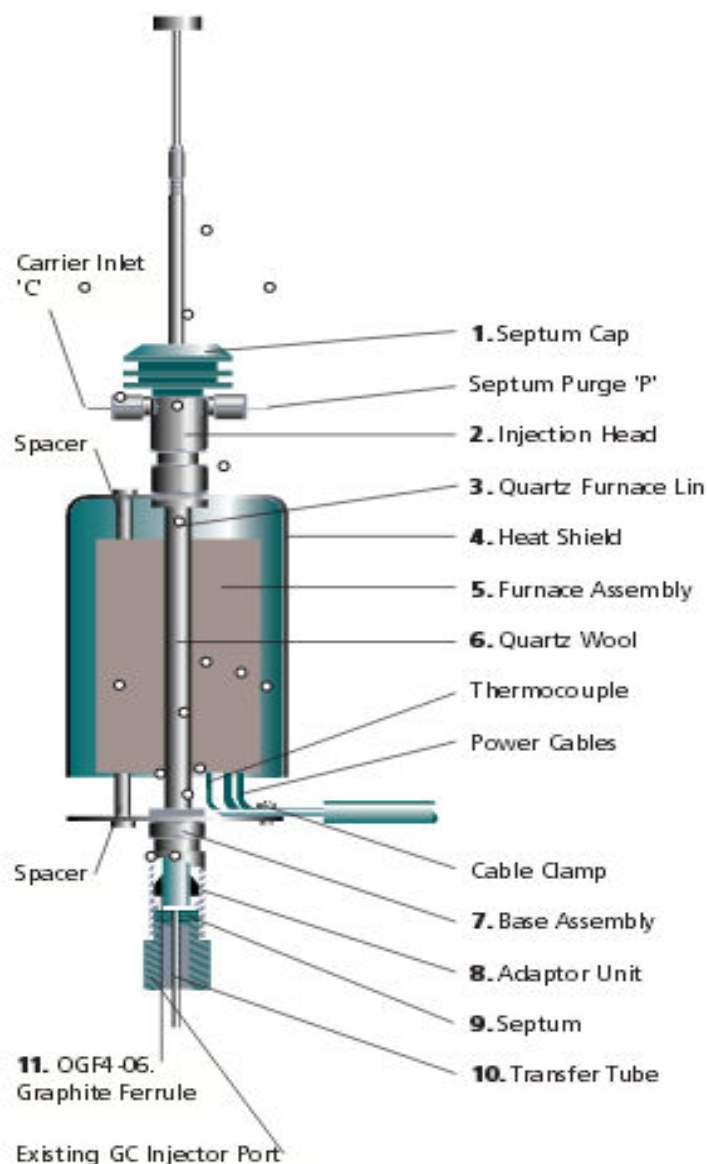


Figure 2-1. Schematic view of the furnace pyrolyzer *Pyrojector II*<sup>TM</sup> (S.G.E., Melbourne, Australia).

## 2.2.2 Experimental method and procedure

### 2.2.2.1 Samples

Tholins were produced in the PAMPRE apparatus (Production d'Aerosols en Microgravite par Plasma Reactifs) (Szopa et al., 2006). This method has been mentioned in detail in the chapter 1.

The tholins analyzed here were produced using  $N_2/CH_4$  gas mixtures of 95%/5.0% and 90%/10% (sample 5pc and sample 10pc). A total pressure of 1 mbar, a flow rate of  $55.0 \pm 0.1$  sccm, and an absorbed radio frequency power of  $30 \pm 2$  W at room temperature.

### 2.2.2.2 The analysis steps

The main steps of the analytical protocol used for Pyr-GC-MS analysis were:

1. Samples are placed inside a disposable quartz tube 50 x 0.53 mm ID in size, which is weighed before and after on an analytical balance, to determine the weight of the sample.

The tube containing the sample is attached to the solids sampling probe by means of a spring hook. The probe is inserted in the injection head and the sample analyzed as per the pyrolysis temperature selected. When the analysis is complete, the probe, sample tube and any residue is removed from the furnace. The tube, after cooling, can be reweighed to determine the residue if desired.

2. Temperature for the pyrojector is changed from 100°C to 900°C. The ramp of temperature is 100°C. For every temperature we have two experimental processes. For the first set, we used the new quartz tube which contains the new sample; for the second set the same sample for each pyrolysis temperature.

3. We inject the sample into the furnace and keep about 30 seconds in order to pyrolyse the sample completely and ensure the fragments completely transfer from the quartz tube into the GC injection port. Then we pull out the injector on the tall position, where the sample residue is cooled.

4. The resulting gas phase products into a GC-MS system. The Helium carrier gas transports the pyrolysate gas through a needle into the heated GC injection port. The injection port is operated in the splitless mode.

5. The different gaseous products are separated by the Gas Chromatography (GC) system.

6. Each gas phase compound is identified by a quadrupole mass spectrometer (MS) used at 70eV operated in a mass range from 10-350 amu.

GC temperature program is 30°C for 10min, and then 4°C/min to 190°C hold for another more 5min. Total GC run is 55min, total MS analysis uses the same time as GC. The GC column is a Restek Rt-QS-BOND 30m×0.32mm×10µm. Helium was used as carrier gas after purification with filters for water vapor, oxygen and hydrocarbons. The flow of the

carrier gas He is 1.2ml/min. Blank using the same temperature program conditions as for the tholins samples was run regularly after every sample in order to check for system contamination. Peak identification is accomplished by use of the NIST mass spectral database.

### 2.3 Results of the Pyr-GC-MS experiment

In order to study the effects of pyrolysis temperature, GC chromatograms were obtained for pyrolysis temperature from 100°C to 900°C. As mentioned above, for one set of experiment, a fresh tholins sample was used for each pyrolysis temperature. For a second set of experiments, the same sample was used for each pyrolysis temperature, and the quartz pyrolysis tub containing the sample was removed from the probe immediately after pyrolysis and placed on the top of furnace in a sealed condition at room temperature.

For the second set of experiments, we encountered some difficulties. Up to 300°C the chromatogram showed the presence of decomposition products. But once the 400°C experiment reaches, there is no peak in the chromatogram. If we continue to raise the temperature to 500°C/600°C/700°C/800°C same results are obtained. So we gave up this set of experiments. In this part we only talk about the results of the first set of experiment. For every pyrolysis temperature we used the new tube with the new sample.

#### 2.3.1 The results for sample 5pc

From the chromatograms of every pyrolysis, we find that at 100°C only the peak for water can be detected, no other peak has been found.

**Figure 2-2** shows a chromatogram (total ion current) of the pyrolysates formed at 200°C from the sample 5pc using the fresh sample. The highest peaks at 12.86min in the chromatogram result from the atmosphere pollution via the gas valve or the atmosphere leak into the furnace when we change the solid sample probe then inject into the GC-MS system. Same air peak is also observed for the others temperatures studied.

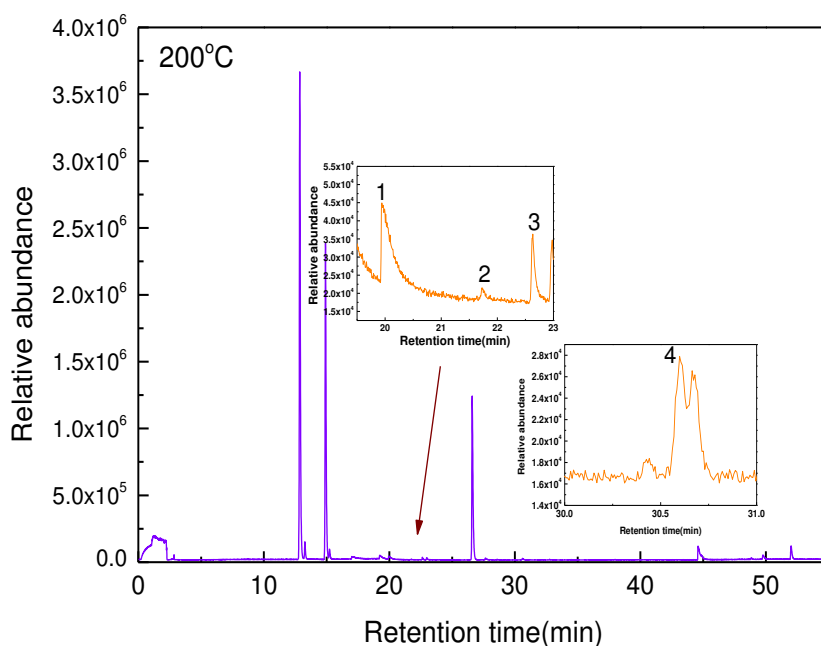


Figure 2-2. The tholins sample 5pc pyrolyzed in He at 200°C.

From this figure we can find that when the temperature rises to 200°C some compounds different from water can be detected, although the quantity of the compounds is low. Some of peaks identified by numbers in **Figure 2-2** are listed in **Table 2-2**.

Table 2-2. Compounds identified in tholins pyrolysate for sample 5% at temperature 200°C.

Peak	Compound	Formula
1	Water	H <sub>2</sub> O
2	Ethylene	C <sub>2</sub> H <sub>4</sub>
3	Hydrogen cyanide	HCN
4	Acetonitrile	C <sub>2</sub> H <sub>3</sub> N

We can observe that the hydrogen cyanide (HCN) appeared which a major compound is obtained by the ACP experiment onboard Huygens probe after thermolysis of Titan's collected aerosols.

At the temperature 300°C, the compounds that can be detected do not change very evidently compared to the results obtained at the temperature 200°C. When the temperature increases up to 400°C, more peaks can be observed including ammonia (NH<sub>3</sub>), one of the main compounds detected during the ACP experiment. It is shown in **Figure 2-3** and the compounds that were not detected in the chromatogram at pyrolysis temperature 200°C are labeled in the chromatogram. The pyrolysis temperature performed at 250°C is more typical of desorption temperature from carbon substrates and may indicate that these compounds are either adsorbed on the tholins surface or are attached to the tholins with very thermally labile chemical bonds (McGuigan et al., 2006).

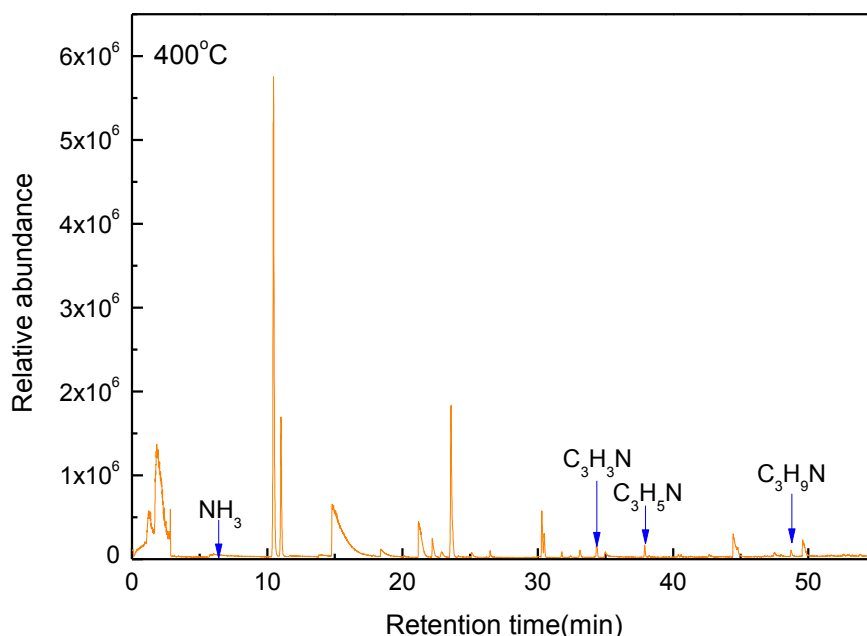


Figure 2-3. The chromatogram for tholins sample 5pc pyrolyzed at 400°C.

As expected, the number of compounds produced during pyrolysis increases with the temperature increasing. But for the sample 5pc when the temperature reaches 600°C **Figure 2-4**, the number of compounds attains a maximum, after 600°C the number of peaks decrease meaning that the temperature 600°C is a turning point and the majority of the compounds have been pyrolyzed. After 600°C only heavy refractory compounds can resist and these compounds are in minority compared to the other.

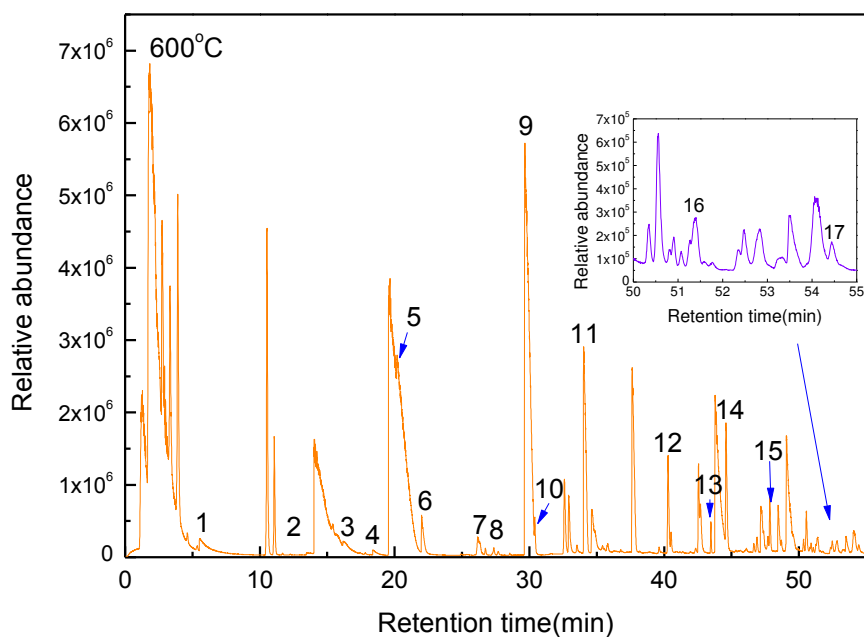


Figure 2-4. The chromatogram for tholins sample 5pc pyrolyzed at 600°C.

The high temperature ensures that the refractory material composing the aerosol particles is thermally decomposed (pyrolysed) into molecular gaseous products. These products contribute to the composition of the gaseous sample to be analyzed by GC-MS. We tried a tentative identification of each observed peak based on MS spectra, most of them were identified and the related results are reported in **Table 2-3**. Due to the complexity of the signal, and sometimes to the low signal-to-noise ratio, it is difficult to clearly identify the species corresponding to each peak, even with the mass spectra obtained and the NIST library.

From this table, we find some compounds have the same formula but different retention time, for example  $C_4H_5N$ , meaning they are isomers. Peaks for corresponding alkenes are also observed, a large number of low-weight molecule nitriles are observed, and very large peaks are observed for acetonitrile. Pyrrole is also detected at this temperature, before to reach 600°C, we did not detect any trace of pyrrole in the pyrolysate. Pyrrole has been previously reported in the pyrolysate of tholins sample (Ehrenfreund et al., 1995; Coll et al., 1998; Pietrogrand et al., 2001) and pyrrole may be more important in tholins structure than previously considered (McGuigan et al., 2006). Here our study suggests that pyrrole may not be initially present in the tholins structure, but produced as a cracking pattern by the pyrolysis process above 600°C.



Table 2-3. Compounds identified in tholins pyrolysate for sample 5pc at temperature 600°C.

Peak	Name	Formula
1	Ammonia	NH <sub>3</sub>
2	Cyclopropene	C <sub>3</sub> H <sub>4</sub>
3	Water	H <sub>2</sub> O
4	Ethylene	C <sub>2</sub> H <sub>4</sub>
5	Hydrogen cyanide	HCN
6	2-Butene	C <sub>4</sub> H <sub>8</sub>
7	Methylenecyclopropane	C <sub>4</sub> H <sub>6</sub>
8	Cyclopropane	C <sub>3</sub> H <sub>6</sub>
9	Acetonitrile	C <sub>2</sub> H <sub>3</sub> N
10	2-Propenenitrile	C <sub>3</sub> H <sub>3</sub> N
11	2-Butennitrile	C <sub>4</sub> H <sub>5</sub> N
12	3-Butennitrile	C <sub>4</sub> H <sub>5</sub> N
13	Butanenitrile	C <sub>4</sub> H <sub>7</sub> N
14	Pyrrole	C <sub>4</sub> H <sub>5</sub> N
15	Propylamine	C <sub>3</sub> H <sub>9</sub> N
16	Butane,1 -isocyano-	C <sub>5</sub> H <sub>9</sub> N
17	Dimethylamine	C <sub>2</sub> H <sub>7</sub> N

After 600°C, with the temperature continued to increase, the compounds do not change very significantly. On the contrary, some compounds happen to disappear and some new compounds appear. For example, ammonia disappears after the temperature 700°C meaning that at this temperature NH<sub>3</sub> is able to react with other generated compounds or to be decomposed. We also observe the formation of benzene at the temperature of 800°C. Moreover, due to the carbonization the total number of compounds we can detect decreases although the peaks in the chromatogram are more in appearance.

**Figure 2-5** shows the chromatogram for a tholins fresh sample 5pc pyrolyzed at 900°C. From this figure, only 13 peaks can be identified amid many peaks presented in the chromatogram. Other peaks identified may be the same compounds with the peaks have been labeled or they were not being identified using the MS database NIST. At this temperature the main released compounds are gas. We reach the carbonization temperature.

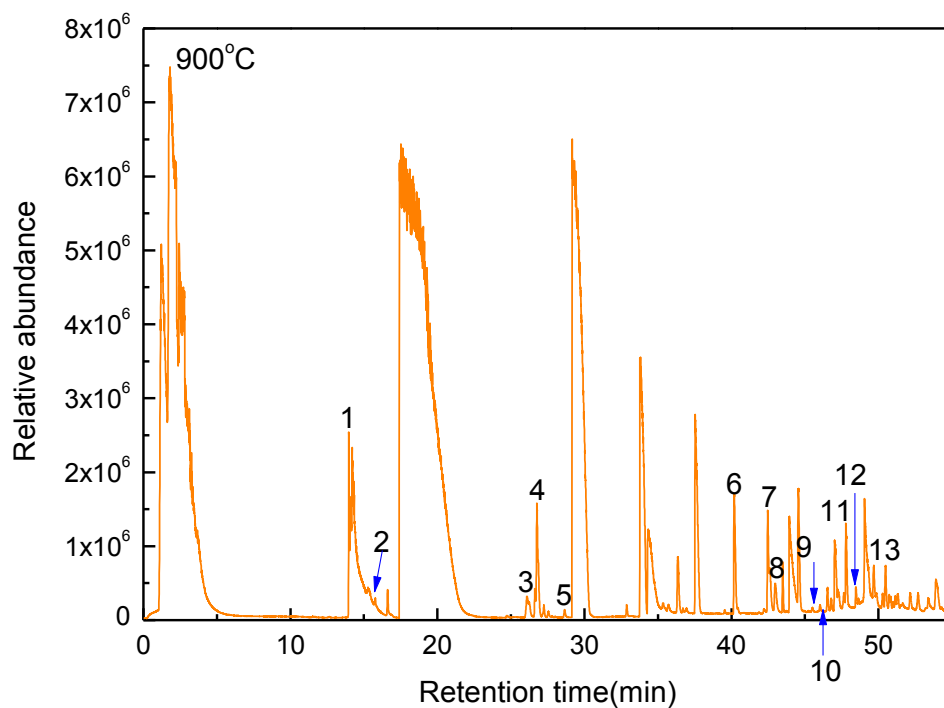


Figure 2-5. The chromatogram for tholins sample 5pc pyrolyzed at 900°C.

### 2.3.2 The results for sample 10pc

Same previous experimental method has been done for the pyrolysis experiment of the 10pc tholins sample. The trend for the change of pyrolyzed compounds as the function of temperature is similar to the results obtained with sample 5pc.

**Figure 2-6** shows the chromatogram for sample 10pc at pyrolysis temperature 400°C. Some of peaks identified by numbers are listed in **Table 2-4**.

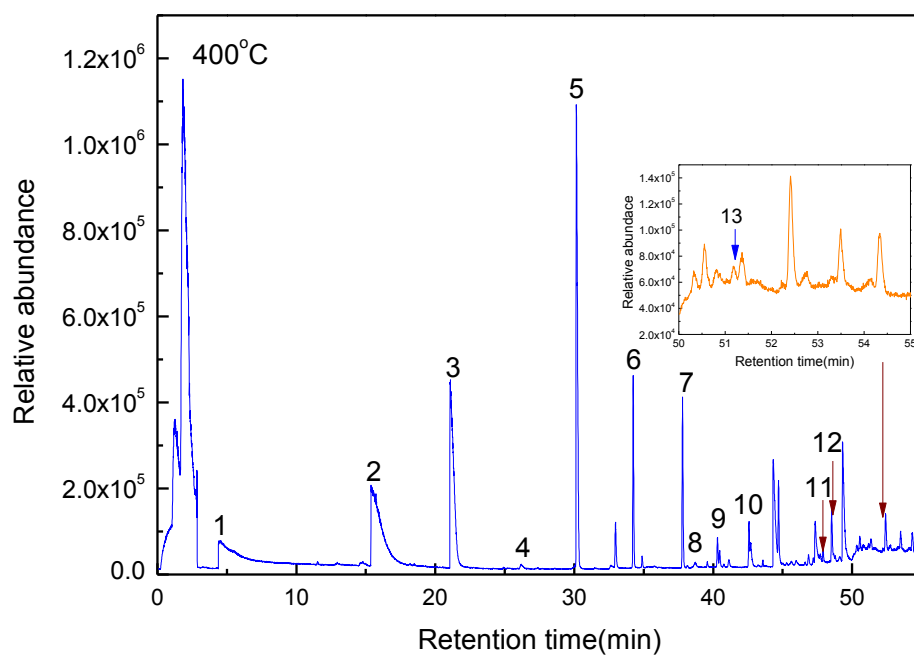


Figure 2-6. The chromatogram for tholins sample 10pc pyrolyzed at 400°C.

Table 2-4. Compounds identified in tholins pyrolysate for sample 10pc at temperature 400°C.

Peak	Name	Formula
1	Ammonia	NH <sub>3</sub>
2	Water	H <sub>2</sub> O
3	Hydrogen cyanide	HCN
4	2-Butene	C <sub>4</sub> H <sub>8</sub>
5	Acetonitrile	C <sub>2</sub> H <sub>3</sub> N
6	2-Propenenitrile	C <sub>3</sub> H <sub>3</sub> N
7	Propenenitrile	C <sub>3</sub> H <sub>5</sub> N
8	Ethylenimine	C <sub>2</sub> H <sub>5</sub> N
9	2-Propenenitrile, 2-methyl	C <sub>4</sub> H <sub>5</sub> N
10	3-Butenenitrile	C <sub>4</sub> H <sub>5</sub> N
11	Pyrrole	C <sub>4</sub> H <sub>5</sub> N
12	Propylamine	C <sub>3</sub> H <sub>9</sub> N
13	Cyclobutylamine	C <sub>4</sub> H <sub>9</sub> N

After comparing the chromatogram of 400°C with the chromatograms obtained for the temperature inferior to 400°C, we found that the ammonia also emerged at 400°C that the same temperature as with sample 5pc. We can also observe pyrrole and its isomer while for sample 5pc we can find these compounds only for pyrolysis temperature above 500°C. However, when the temperature is not very high, the compounds are mainly similar.

The richness of the products is greatest at 600°C and decreases slowly with the temperature increases.

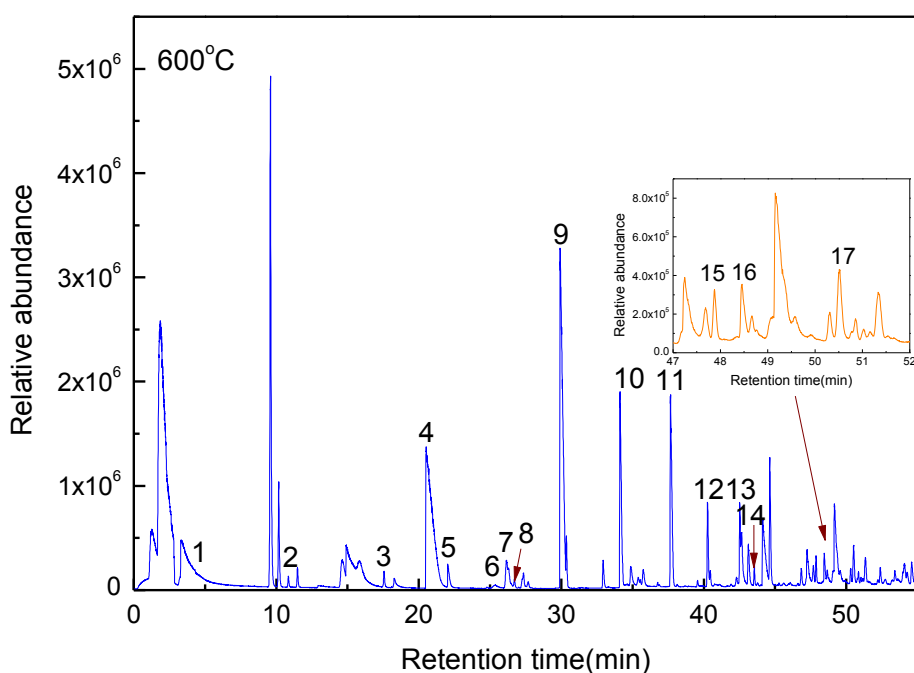


Figure 2-7. The chromatogram for tholins sample 10pc pyrolyzed at 600°C.

**Figure 2-7** shows the total ion current chromatogram for pyrolysis temperature 600°C. The corresponding compounds identified list is given in **Table 2-5**. After comparing the sample 5pc pyrolyzed at 600°C, we found that the major compounds are similar for these two samples. They include hydrocarbon compounds, nitriles, ammonia, hydrogen cyanide, and some pyrrole isomers.

But when the temperature goes up to 700°C **Figure 2-8**, the benzene and toluene emerge among the pyrolyzed products. These two compounds keep appearing until the temperature reaches to the maximum 900°C. For sample 5pc, we can only find benzene at pyrolysis temperature between 800 and 900°C, and the toluene was not observed at all.

Table 2-5. Compounds identified in tholins pyrolysate for sample 10pc at temperature 600°C.

Peak	Name	Formula
1	Ammonia	NH <sub>3</sub>
2	Propene	C <sub>3</sub> H <sub>6</sub>
3	Ethylene	C <sub>2</sub> H <sub>4</sub>
4	Hydrogen cyanide	HCN
5	Isobutane	C <sub>4</sub> H <sub>10</sub>
6	2-Butene	C <sub>4</sub> H <sub>8</sub>
7	1-Butyne	C <sub>4</sub> H <sub>6</sub>
8	Cyclopropane	C <sub>3</sub> H <sub>6</sub>
9	Acetonitrile	C <sub>2</sub> H <sub>3</sub> N
10	2-Propenenitrile	C <sub>3</sub> H <sub>3</sub> N
11	Propionitrile	C <sub>3</sub> H <sub>5</sub> N
12	Cyclopropane	C <sub>4</sub> H <sub>5</sub> N
13	2-Butennitrile	C <sub>4</sub> H <sub>5</sub> N
14	3-Butenenitrile	C <sub>4</sub> H <sub>5</sub> N
15	Pyrrole	C <sub>4</sub> H <sub>5</sub> N
16	Propylamine	C <sub>3</sub> H <sub>9</sub> N
17	Methallyl cyanide	C <sub>5</sub> H <sub>7</sub> N

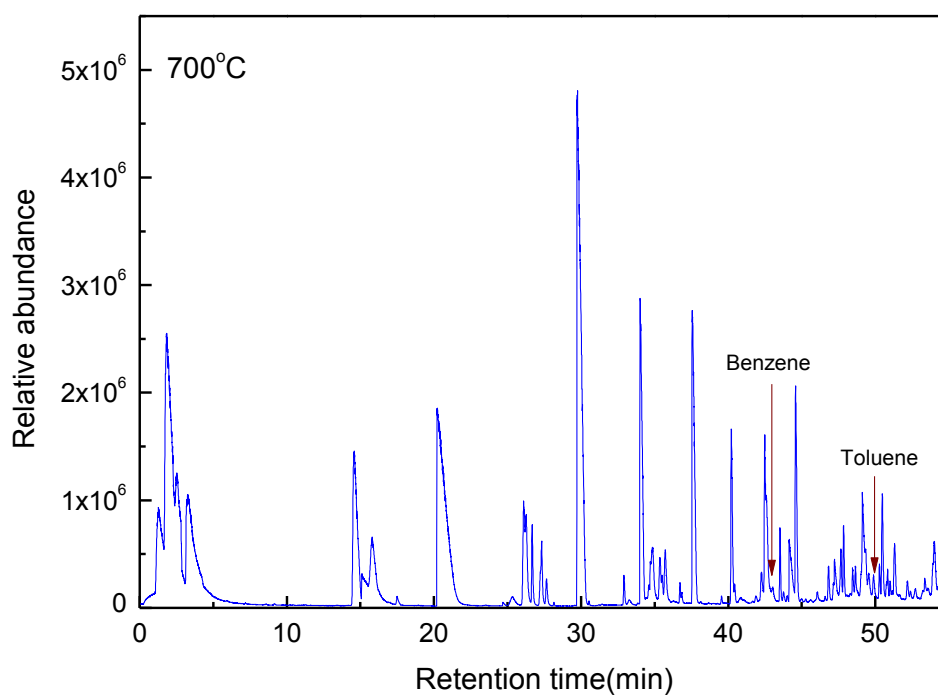


Figure 2-8. The chromatogram for tholins sample 10pc pyrolyzed at 600°C.

The presence of 10% of CH<sub>4</sub> compared to 5% during the tholins production has an influence on the carbon percentage in the tholins structure. By this way the 10% tholins contain more carbon which is the reason why during the pyrolysis the carbonaceous compounds such as benzene and toluene are produced at lower pyrolysis temperature and are produced within more important quantity.

## 2.4 Discussion

As discussed in section 2.1.2, we have described some others studies' results using Pyr-GC-MS method to characterize tholins. Early Pyr-GC-MS studies of tholins have identified numerous organic products, while some of these products may have either been formed during pyrolysis or may also been identified directly on the tholins by spectroscopic method and were probably present in the original sample.

Among the identified species, unsaturated molecules can be noticed as the major pyrolysate products, including hydrocarbons, nitriles, and nitrogenous rings. These results are slightly different from previous pyrolysis studies achieved on tholins produced by other plasma discharges (Ehrenfreund et al., 1995; Khare et al., 1984b). Here we find an absence of aromatic or cyclic compounds other than benzene for sample 5pc; benzene and toluene for sample 10pc at a relative high temperature, in agreement with another study (Coll et al., 1999). The comparison between the different results remains difficult because the various tholins were produced in different laboratories under different conditions, and the specificity of the pyrolysis products is also related to the pyrolyser used. In spite of this difference for all the plasma however seem to produce aromatic species which are part of the tholins, then our results are still basically comparable with these previous studies even though all the identified species are not strictly identical. The tholins produced by all the plasmas seem to release aromatic species which contribute to the part of the tholins. As first proposed by (Sagan et al., 1993) infers that production of aromatic species should be a significant chemical pathway to produce the tholins. But because we did not find trace of polyaromatics in the chromatogram, the kind of aromatics is present in the solid particles, monoaromatic or polyaromatic, this problem is difficult to determine. However the polyaromatics does not appear could be explained by the fact that these polyaromatics maybe decompose during the pyrolysis, and they release the alkylated monoaromatics identified in the chromatogram (benzene and toluene). By inspecting the other species, most unsaturated aliphatic are found, and they constitute the major part of the contribution to the pyrolysates. These species can be result

from the pyrolysis of complex aliphatic molecules mixed with the aromatic ones to form the tholins, or they can be fragments of aliphatic chains that link the aromatic nuclei together (Szopa et al., 2006). But this Pyr-GCMS technique difficult to discriminate between these two origins and another type of characterization method has to be used to resolve this question. Nevertheless, because of the presence of nitriles among the pyrolysates, we can infer that these chains, whatever their origin is, are mostly unsaturated, and can get CN terminal groups. In order to investigate tholins sample comprehensive, it necessary to used further complementary techniques (elemental analysis, ATD-MS, IR, derivatization-GC-MS) to provide a more accurate description of the tholins we produce and compare with other types of tholins.

#### **2.4.1 Compared with two-dimensional gas chromatography-time-of-flight mass spectrometry**

(McGuigan et al., 2006) used flash pyrolysis inlet coupled to two-dimensional gas chromatography GC×GC using time-of-flight MS detection to characterize tholins pyrolysis products. Identified pyrolysis products include low-molecular-weight nitriles, alkyl substituted pyrroles, linear and branched hydrocarbons, alkyl-substituted benzenes and PAH compounds. They also observed that in the tholins chromatogram large peaks for the alkyl-substituted pyrroles with peak amplitude increasing from pyrrole to methyl pyrrole to dimethyl pyrrole. Compared with the chromatogram from the polypyrrole on carbon black, they confirmed that pyrrole is a part of the tholins pyrolysate and the butenenitriles and pyrrole are actually a part of the tholins structure and not the result of a post-pyrolysis reaction. In our results, we also find pyrrole and some of its isomers in the tholins chromatogram.

**Figure 2-9** shows a two-dimensional chromatogram of the pyrolysate formed at 600°C from the tholins sample. Their sample was prepared by the use of a cold plasma discharge (<300K) through a 9:1 mixture of nitrogen and methane at a pressure of 160Pa, a similar to our sample 10pc. In this chromatogram, a number of large alkane peaks are observed (the largest of which is dodecane) low-molecular weight nitriles (very larger peak are observed for acetonitrile) and a few large aromatic hydrocarbon. But in our case, at pyrolysis temperature of 600°C for two samples we only observed some small alkane peaks. The aromatic hydrocarbons were never detected at this temperature for both two samples. That may be because the number of compounds and the complexity of one-dimensional chromatograms

limit the quality of mixture characterization. However in the results of (McGuigan et al., 2006), we didn't find the compounds ammonia and hydrogen cyanide which are the main compounds confirmed by the mission ACP.

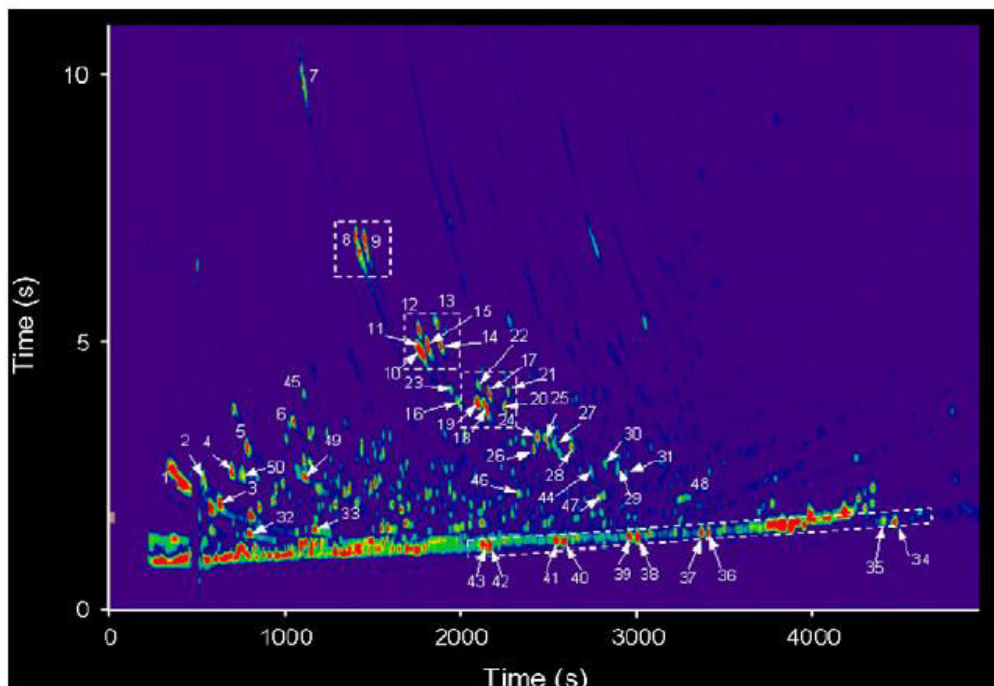


Figure 2-9. Two-dimensional projection of the tholins sample pyrolyzed in  $H_2$  at  $600^\circ C$  (McGuigan et al., 2006).

Acetonitrile is seen as a major peak at all temperatures in our study. It is unlikely that such large quantities of acetonitrile are trapped in the tholins matrix. The tholins are undergoing a degradation reaction that releases acetonitrile, as well as other small organic nitriles, and HCN. The evolution of such large quantities of acetonitrile from  $200^\circ C$  in our case suggests that this reaction is not difficult.

Polyacrylonitrile (PAN) maybe can serve as a useful model system to compare to the tholins structure. (Mellottée and Vovelle, 1982) has studied the thermal degradation of PAN in detail. The mechanism for evolution of HCN and  $NH_3$  is quite complicated, but involves cyclization and aromatization of the polymer, followed by release of HCN (Xue et al., 1997). A simplified overview of the process is shown in **Figure 2-10** (Hodyss, 2006). However compounds like ammonia and HCN are formed as byproducts of the cyclization process at very high temperatures. The end result of the thermal degradation of polyacrylonitrile is an extensively cyclized aromatic chain. Acetonitrile has also been seen in the products of the thermal degradation of polyacrylonitrile (Surianarayanan et al., 1998). Acetonitrile could be



produced by a mechanism similar to the one that produces HCN. Tholins do contain nitriles, and it is likely that some of the processes occurring in the thermal decomposition of polyacrylonitrile occur in tholins as well.

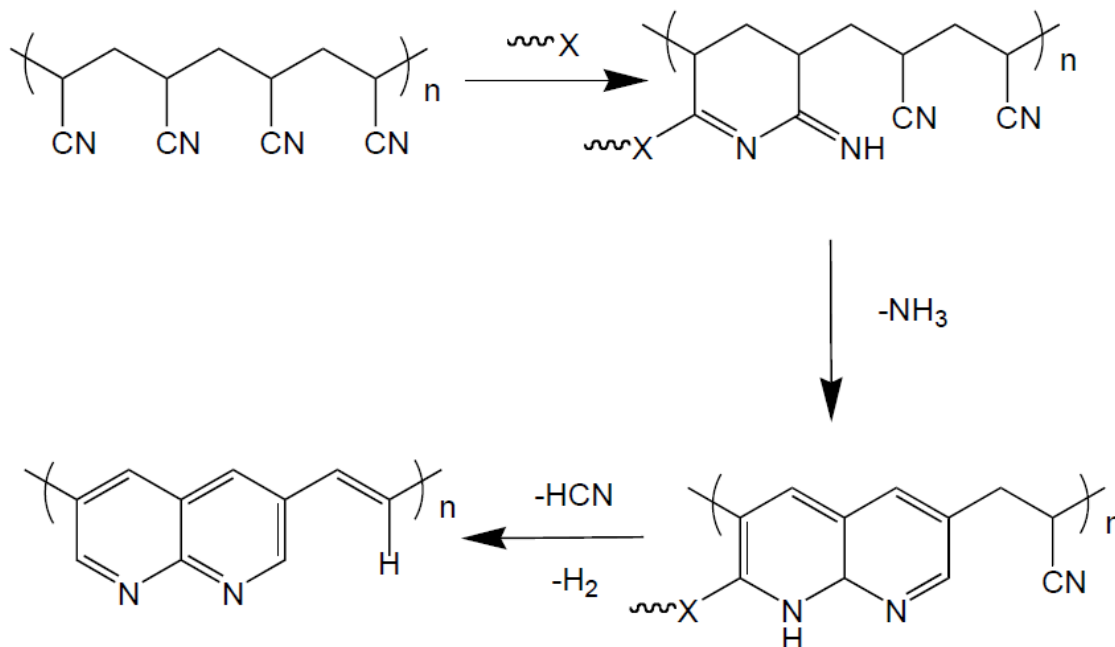


Figure 2-10. Thermal degradation of polyacrylonitrile. X refers to any possible nucleophile, including nitriles (Hodyss, 2006).

In order to study the effects of pyrolysis temperature, (McGuigan et al., 2006) used 250°C, 400°C, 600°C and 900°C as different temperature. The result for (McGuigan et al., 2006) study was that when the sample was pyrolyzed at 900°C, the compounds identified are similar to those detected at 600°C. But we find benzene and toluene after temperature 600°C, the others compounds seem to decrease. So that means aromatic species are part of our tholins sample.

#### 2.4.2 Comparison to the results obtained by the ACP experiment

From the ACP experiment ammonia ( $NH_3$ ) and hydrogen cyanide ( $HCN$ ) have been identified as the main pyrolysis products during the ACP experiment (Coll et al., 2012). Moreover, ACP data shows that Titan atmospheric aerosols are composed of an organic refractory part, as well as a particle nucleus made of carbon, hydrogen and nitrogen atoms. This clearly shows that the aerosol particles include a solid organic refractory core **Figure 2-11**.  $NH_3$  and  $HCN$  are gaseous chemical fingerprints of the complex organics that constitute this core, and their presence demonstrates that carbon and nitrogen are in the aerosols (Israël

et al., 2005). Some of the results from the ACP experiment done during the Huygens probe descent in Titan's atmosphere are shown in **Figure 2-12**.

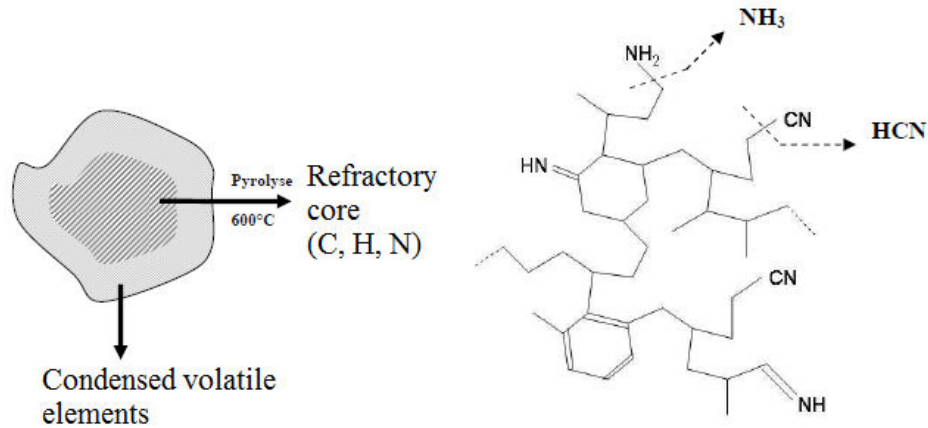


Figure 2-11. The diagram summarizing the detection of HCN, NH<sub>3</sub> and the refractory core for the aerosols of Titan after pyrolysis at 600°C (Mai-Julie NGUYEN, 2007).

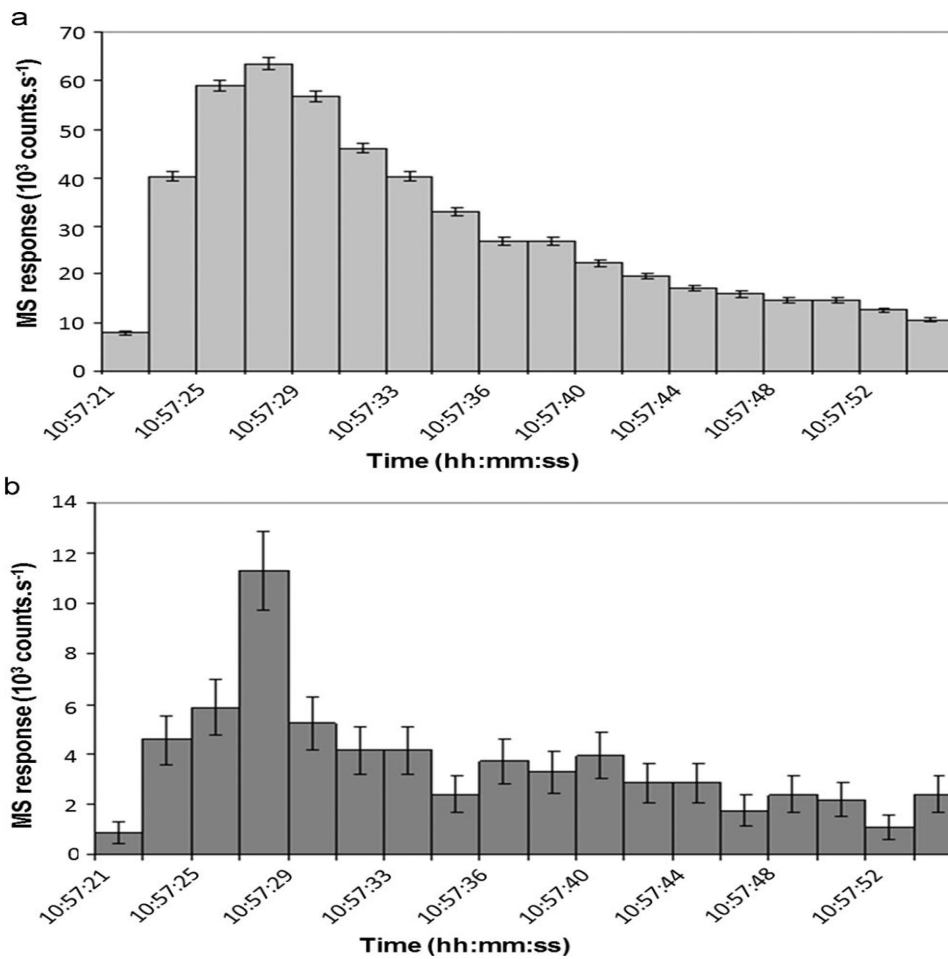


Figure 2-12. Temporal evolution of the intensity of the MS signatures attributed to ammonia for the second aerosol sample pyrolysis by the ACP experiment (Coll et al., 2012).

(Coll et al., 2012) has used Pyr-GC-MS method and compare with the result of ACP experiment to prove that the category of aerosol analogues that appear to be more representative of Titan's aerosols is the "cold plasma". The tholins samples synthesized by the PAMPRE method belong to this category. And the result for Pyr-GC-MS technique can release the  $\text{NH}_3$  and HCN these two main ACP compounds, we can confirm the conclusion that the aerosol analogues produced in PAMPRE set-up is the most similar to Titan's aerosols.

## 2.5 Conclusion

In the previous studies, the methods used to analyze the properties of tholins have not produced much useful information about the structure. These materials may be kerogen-like in structure containing a variety of functionalities extensively cross-linked. Pyrolysis appears to break covalent bonds liberating smaller, volatile and semi-volatile compounds that can be separated and characterized by GC-MS.

In this chapter, we used Pyr-GC-MS technique to study tholins 5pc and tholins 10pc. The number of pyrolysates increases with the temperature increases most of them are nitrogen compounds, while pyrolysis temperature  $600^\circ\text{C}$  is a turning point. Only a few differences have been found out between tholins 5pc and tholins 10pc. Pyrrole and its isomers appear at lower temperature for sample 10pc. The benzene and toluene emerge behavior is also different for these two samples. As they are heated, tholins are chemically altered. The evolution of HCN and acetonitrile can be explained through a mechanism similar to the one by which polyacrylonitrile thermally degrades, involving cyclization and aromatization.

The presence of both  $\text{NH}_3$  and HCN can demonstrate that nitrogen can be incorporate into Titan's aerosol in different ways, and the general presence of nitrogen in the aerosol suggest that the aerosol acts as an important sink for atmospheric nitrogen (Israël et al., 2005). After comparing with the result of ACP experiment, confirm that the aerosol analogues produced in PAMPRE set-up capable to simulate Titan's aerosols, as found in Coll et al., 2012.

## **Chapter 3. The thermal degradation behavior of Tholins**

Some chemical and physical properties of tholins produced with PAMPRE method have already been investigated (Carrasco et al., 2009; Gautier et al., 2011; Hadamcik et al., 2009; Mahjoub et al., 2012; Pernot et al., 2010; Quirico et al., 2008). Through these investigations, we have obtained a lot of results about the properties of tholins. But the thermal characterization of tholins produced with PAMPRE has little mention, except in order to study the oxygen question (Sciamma-O'Brien et al., 2010). The thermal properties of tholins we don't know very clearly. We have used the Pyr-GCMS technique to study the tholins sample in the chapter 2. Nevertheless, the harsh pyrolysis does not inform on the pyrolysis process itself, preventing any inference about the initial aerosol structure and its progressive evolution with the temperature increase.

Therefore another analysis technique for this purpose is developed in this chapter. A systematic study for thermal degradation behavior of tholins was carried out in this part.

### **3.1 Research methods**

#### **3.1.1 Thermogravimetry analysis**

Thermal analysis (TA) comprises a family of measuring techniques that share a common feature; they measure a material's response to being heated or cooled (or, in some cases, held isothermally). The goal for this technique is to establish a connection between temperature and specific physical properties of materials.

##### **3.1.1.1 The principle of TGA and DSC**

Thermogravimetric analysis (TGA) is an experimental technique in which physical and chemical properties of materials are measured as a function of temperature or time. The sample can be heated at a constant temperature (isothermal measurement) or using a constant heating rate (dynamic measurement), but may also be subjected to non-linear temperature programs such as those used in sample controlled TGA experiments.

The results of a TGA measurement are usually displayed as a TGA curve in which mass or percent mass is plotted against temperature and/or time. An alternative and complementary presentation is to use the first derivative of the TGA curve with respect to temperature or time. This shows the rate at which the mass changes and is known as the differential thermogravimetric or DTG curve.

TGA is commonly used to determine selected characteristics of materials that exhibit either mass loss or gain due to decomposition, oxidation, or loss of volatiles (such as moisture). This generates steps in the TGA curve or peaks in the DTG curve.

DSC (Differential scanning calorimetry) is a technique in which the difference in the amount of heat required to increase the temperature of a sample and reference is measured as a function of temperature. A DSC analyzer measures the energy changes that happen when the sample is heated, cooled or held isothermally. The energy changes can be used to characterize a material for melting processes, measurement of glass transitions and a range of more complex events.

#### 3.1.1.2 Experimental instrument (Sensys evo TGA-DSC)

This instrument has a 3D DSC sensor totally surrounds the sample and reference crucibles so that the entire energy of any transformation is monitored thereby giving an unequalled accuracy of measurement.

The symmetry of the microbalance, with its sample and reference suspended vertically from the beam guarantee reproducible positioning of the sample over time and excellent stability of the TG signal baseline.

The sample and the reference are heated inside the same calorimetric block (symmetrical furnace), which means that the buoyancy effect is automatically compensated. CALISTO software is used for data treatment.

The performances of the SENSYS evo TG-DSC result from the absolute symmetry of this unique system in which the TG and DSC transducers, which are mechanically independent, retain their specific characteristics.

### **3.1.2 Infrared absorption and Raman spectroscopy**

The vibrational modes of a molecule can be measured completely by the complementary techniques Infrared absorption and Raman spectroscopy. Some vibrations may be active in both Raman and IR, although these two forms of spectroscopy due to the different processes and different selection rules. In general, IR spectroscopy is used to better characterize the asymmetric vibrations of polar groups while Raman spectroscopy is best at symmetric vibrations of non-polar groups.

### 3.1.2.1 The Infrared absorption spectroscopy principle

The vibrational spectrum of a molecule is considered to be a unique physical property and is characteristic of the molecule. In this chapter, this technique was used to analyze the heating residues and initial tholins samples in order to compare the functional groups change with the temperature increase.

The typical IR spectrometer frequencies of interest can be divided into the near-IR region  $14,000\text{-}4000\text{ cm}^{-1}$ , the mid-IR region  $4000\text{-}400\text{ cm}^{-1}$  and the far-IR region  $400\text{-}10\text{ cm}^{-1}$ . The relationship between the intensities of transmitted IR radiation and the analyte concentration is governed by the Lambert-Beer law. The IR spectrum is obtained by plotting the intensity (absorbance or transmittance) versus the wavenumber, which is proportional to the energy difference between the ground and the excited vibrational states. The radiation frequency and the molecular dipole moment are the two important components of the IR absorption process. The interaction of the radiation with molecules can be described in terms of a resonance condition where the specific oscillating radiation frequency matches the natural frequency of a particular normal mode of vibration. The dipole moment change of the molecule is a crucial point that can cause the energy to be transferred from the IR photon to the molecule via absorption (Larkin, 2011).

A molecule can vibrate in many ways, and each way is called a *vibrational mode*. For molecules with  $N$  atoms in them, linear molecules have  $3n-5$  degrees of vibrational modes, whereas nonlinear molecules have  $3n-6$  degrees of vibrational modes (also called vibrational degrees of freedom). As an example  $\text{H}_2\text{O}$ , a non-linear molecule, will have  $3 \times 3 - 6 = 3$  degrees of vibrational freedom, or modes. **Figure 3-1** shows the fundamental vibrations for the simple water (non-linear) and carbon dioxide (linear) molecules.

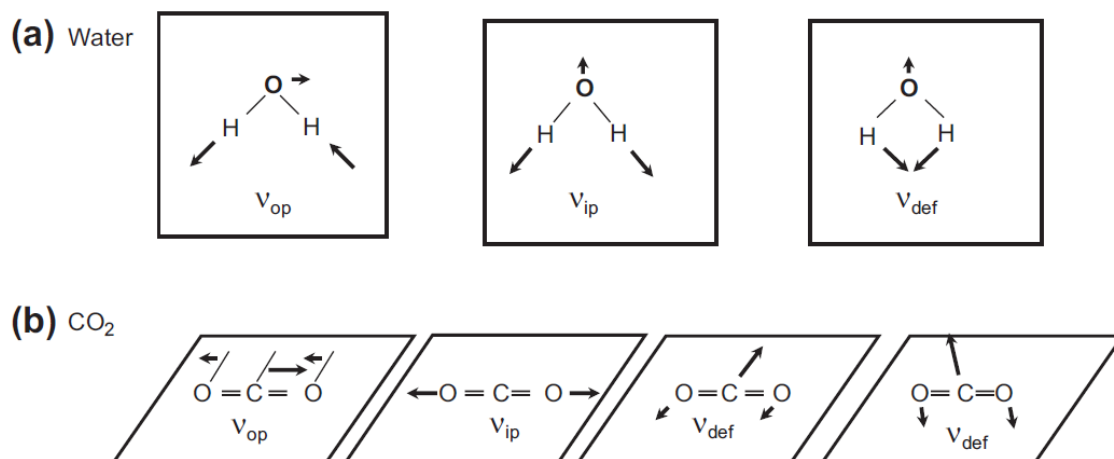


Figure 3-1. Molecular motions which change distance between atoms for water and CO<sub>2</sub>.

The internal degrees of freedom for a molecule define  $n$  as the number of atoms in a molecule and define each atom with 3 degrees of freedom of motion in the X, Y, and Z directions resulting in  $3n$  degrees of motional freedom. Here, three of these degrees are translation, while three describe rotations. The remaining  $3n-6$  degrees (non-linear molecule) are motions, which change the distance between atoms, or the angle between bonds.

### 3.1.2.2 Experimental instrument for infrared spectroscopy

The Perkin-Elmer Spectrum One FTIR Spectrometer was used in the wavenumber range  $4000$  to  $450\text{ cm}^{-1}$ . It was configured to run in single-beam, with a resolution of  $4\text{ cm}^{-1}$ . A mid-range Deuterated triglycine sulfate infrared detector processes signals with a 68340 integrated chip.

### 3.1.2.3 The Raman spectroscopy principle

Raman spectroscopy is a spectroscopic technique used to observe vibrational, rotational, and other low-frequency modes in a system. It relies on inelastic scattering, or Raman scattering, of monochromatic light, here from a laser in the visible range (524 nm) (Quirico et al., 2008). The laser is used to irradiate the sample with monochromatic radiation. The Rayleigh and Raman processes are depicted in **Figure 3-2**.



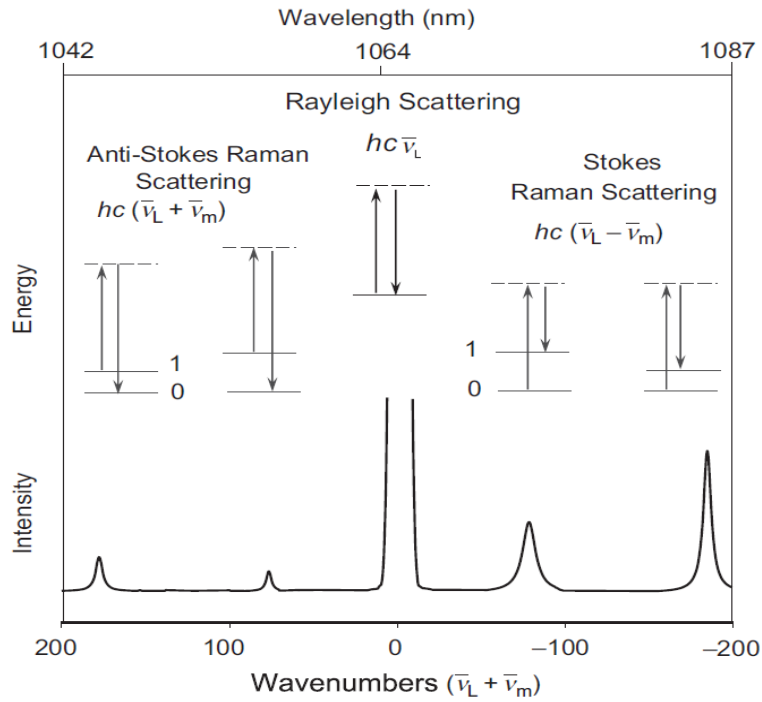


Figure 3-2. Schematic illustration of Rayleigh scattering as well as Stokes and anti-Stokes Raman scattering. The laser excitation frequency ( $\nu_L$ ) is represented by the upward arrows and is much higher in energy than the molecular vibrations. The frequency of the scattered photon (downward arrows) is unchanged in Rayleigh scattering but is of either lower or higher frequency in Raman scattering. The dashed lines indicate the “virtual state” (Larkin, 2011).

As shown in **Figure 3-2** two types of Raman scattering exist: Stokes and anti-Stokes. Molecules initially in the ground vibrational state give rise to Stokes Raman scattering  $hc(\bar{\nu}_m - \bar{\nu}_L)$  while molecules initially in vibrational excited state give rise to anti-Stokes Raman scattering  $hc(\bar{\nu}_m + \bar{\nu}_L)$ . The intensity ratio of the Stokes is relative to the anti-Stokes. Raman bands are governed by the absolute temperature of the sample, and the energy difference between the ground and excited vibrational states. At thermal equilibrium Boltzmann’s law describes the ratio of Stokes relative to anti-Stokes Raman lines. The Stokes Raman lines are much more intense than anti-Stokes since at ambient temperature most molecules are found in the ground state (Larkin, 2011).

The intensity of the Raman scattered radiation  $I_R$  is given by:

$$I_R \propto \nu^4 I_0 N \left( \frac{\partial \alpha}{\partial Q} \right)^2 \quad \text{equation 3-1}$$

where  $I_0$  is the incident laser intensity,  $N$  is the number of scattering molecules in a given state,  $\nu$  is the frequency of the exciting laser,  $\alpha$  is the polarizability of the molecules, and  $Q$  is the vibrational amplitude.

The above expression indicates that the Raman signal has several important parameters for Raman spectroscopy. First, since the signal is concentration dependent, quantitation is possible. Secondly, using shorter wavelength excitation or increasing the laser flux power density can increase the Raman intensity. Lastly, only molecular vibrations which cause a change in polarizability are Raman active. Here the change in the polarizability with respect to a change in the vibrational amplitude,  $Q$ , is greater than zero.

$$\left(\frac{\partial\alpha}{\partial Q}\right) \neq 0 \quad \text{equation 3-2}$$

The Raman intensity is proportional to the square of the above quantity (Larkin, 2011).

### 3.1.3 Elemental analysis

Elemental composition analysis of the tholins produced in PAMPRE and residues of thermal analysis has been achieved by the instrument FLASH 2000 Serie CHNS/Oxygen Automatic Elemental Analyzer, in order to measure the C, H, N, and O mass percentages in the tholins and the change of these elements after heating by different final temperatures.

Elemental analysis is a process where a sample of some material (soil, waste or drinking water, bodily fluids, minerals, chemical compounds) is analyzed for its elemental and sometimes isotopic composition. Elemental analysis is qualitative (determining what elements are present), and quantitative (determining how much of each elements are present).

In our case, the analysis of organic materials, carbon, nitrogen and hydrogen were measured by flash combustion. The sample is weighed in Tin capsules **Figure 3-3** (for analyze the content of oxygen, the silver capsules is used) placed inside the Thermo Scientific MAS200R auto sampler at a preset time, and then dropped into an oxidation or reduction reactor kept at a temperature of 900-1000°C. The exact amount of oxygen required for optimum combustion of the sample is delivered into the combustion reactor at a precise time. The reaction of oxygen with the Tin capsule at elevated temperature generates an exothermic reaction which raises the temperature to 1800°C for a few seconds. At this high temperature both organic and inorganic substances are converted into elemental gases which, after further

reduction, are separated in a chromatographic column and finally detected by a highly sensitive thermal conductivity detector (TCD).

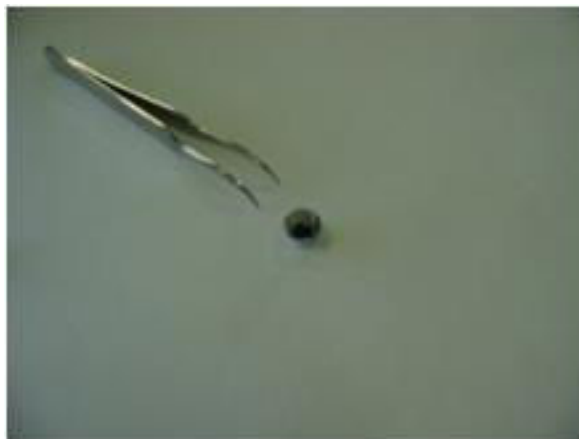


Figure 3-3. The sample to be analyzed is placed in a capsule of Tin for CHNS analysis, a capsule of silver for O analysis. It is compacted in a small pellet form before being introduced into the analyzer to be burn.

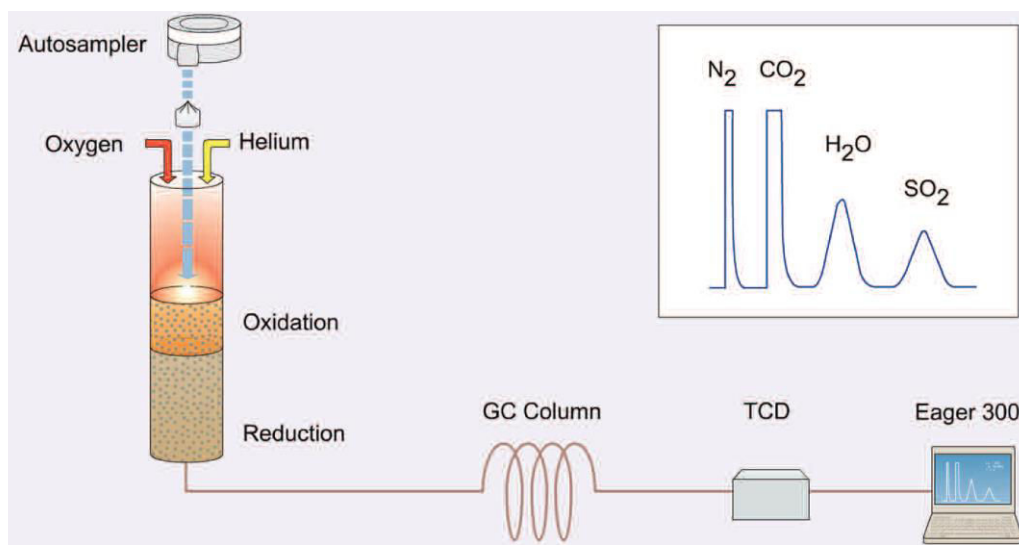


Figure 3-4. The principal schematic of CHNS elemental analysis.

**Figure 3-4** shows the principal of CHNS elemental analysis. On this chromatogram, the first peak corresponds to the  $N_2$  and then  $CO_2$ ,  $H_2O$  and finally  $SO_2$  if sulfur is present. The typical duration of a CHNS elemental analysis is about ten minutes and required sample mass of about 1-2 mg. The chromatogram is analyzed follows. That is to say that we will measure the peak area to determine the mass fraction of element in the initial sample. First, before analyzing the sample of interest, an important step is the calibration of the instrument.

This step of work is critical because the quality of the determination of mass fractions of different elements in real samples will depend on the quality of the calibration curves.

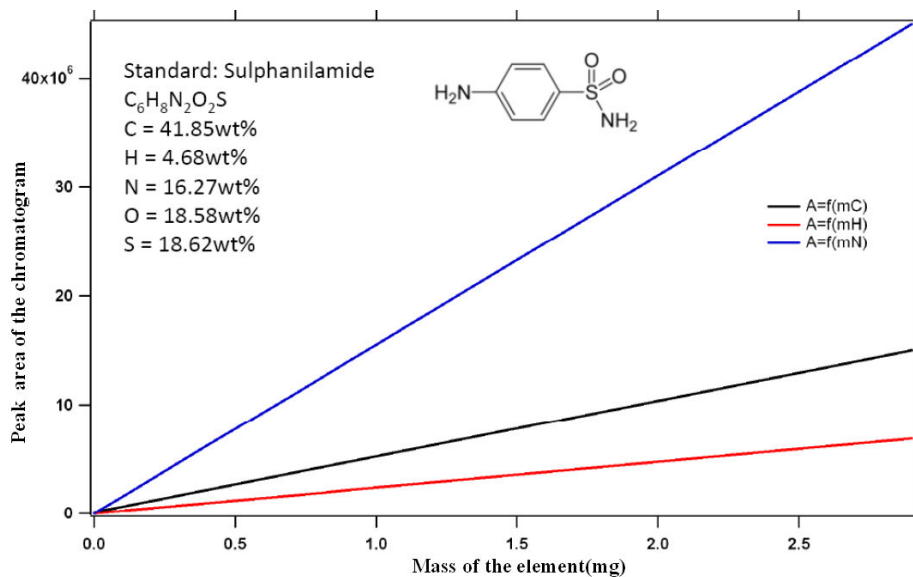


Figure 3-5. Calibration curves obtained during the calibration of the instrument for elemental analysis.

The calibration and establishment of calibration curves are made by assaying the elements in a standard substance which has a known elemental composition. We can consult these informations from the user's guide. In our case, we used the sulfanilamide molecular formula  $C_6H_8N_2O_2S$  as for our standard. In this standard, the mass percentage of carbon is 41.85%, hydrogen 4.68%, nitrogen 16.27%, oxygen 18.58% and 18.62% sulfur. This standard is well known in terms of content of various elements to be determined.

To obtain a useful calibration line, several different masses of standard will be introduced into the analyzer in order to identify areas associated with different elements as **Figure 3-5** shows. In case these areas measured, and knowing the theoretical mass fractions of different elements in the standard, it is possible to trace the calibration line connecting the peak area on the chromatogram and to calculate the mass percentage of the element in the samples.

### 3.1.4 TG-MS (thermogravimetry-mass spectrometry)

Evaporation or decomposition effects are observed when many materials are heated or conditioned. These effects can be detected with DTA, DSC or TGA. Unfortunately, these measurement techniques provide no information on which products or fragments are formed, information which would be very useful in many situations.

We have used a coupling with mass spectrometry (TG-MS coupling). By heating a sample on the TGA, a sample will release volatile materials or generate combustion components as it burns. These gases are then transferred to the MS, where the components can be identified. From TG-MS, curves can be constructed for selected species. A mass spectrometer (MS, Bruker Omnistar) coupled with a thermogravimetry (TG, Setaram Sensys EVO) system has been used to detect the volatile species emitted by the thermal decomposition and fragmentation processes of the tholins samples.

## **3.2 Samples and Experimental conditions**

### **3.2.1 Samples**

Two samples were analyzed in this chapter. The first sample (5pc) was produced with a gaseous mixture containing 5% of methane, while the second sample (10pc) was produced with a mixture containing 10% of methane. The method and conditions for synthesizing these two samples are the same as in chapter 2. We used these two samples to observe the thermal behavior of tholins and compared these two samples to investigate if the differences of this thermal property exist between these two samples.

### **3.2.2 Experimental conditions**

Our TG-DSC analyses were performed using the SENSYS evo TG-DSC instrument, CALISTO software for analyzer. The samples were placed in a platinum 100 $\mu$ l crucible. The average sample weight in the crucible was approximately 20 mg. The samples were heated from the ambient temperature to 300°C, 400°C, 500°C and 800°C as final temperature respectively. At beginning, the temperature was kept 20°C for 20 minutes in order to expel the air and some pollution substance that exist in the instrument. Then the temperature was increased by a heating rate 10°C/min until the temperature reaches to the final temperature we have set. In the end, the temperature was hold for another more one hour. The argon was used as the protected inert atmosphere with a pressure about 2 bars.

The same conditions with the TG-DSC experiment were used for the TG-MS, meaning a temperature increase from the room temperature to 800°C at a heating rate 10°C/min under argon atmosphere. This analysis is important as it focusses on the species released by pyrolysis from the solid sample.

### 3.3 Results for TG-DSC and TG-MS analysis

#### 3.3.1 Repeatability of the TG-DSC measurement

For the sample 5pc and 10pc, the representative thermogravimetric curves for the four different final temperatures are shown in **Figure 3-6**.

From this figure we can find that for every sample, the TG curves have an identical behavior for the different final temperature. We can conclude that our experiments have the repeatability of the measurement which means the tholins produced in PAMPRE are homogeneous. Once the final temperature is reached the sample is kept one hour long at this final temperature, the absence of any additional loss shows that there is no kinetic effect and the temperature ramp is appropriate. This higher temperature limit of 800°C was chosen as it is the maximum achievable temperature with the TG-DSC instrument.

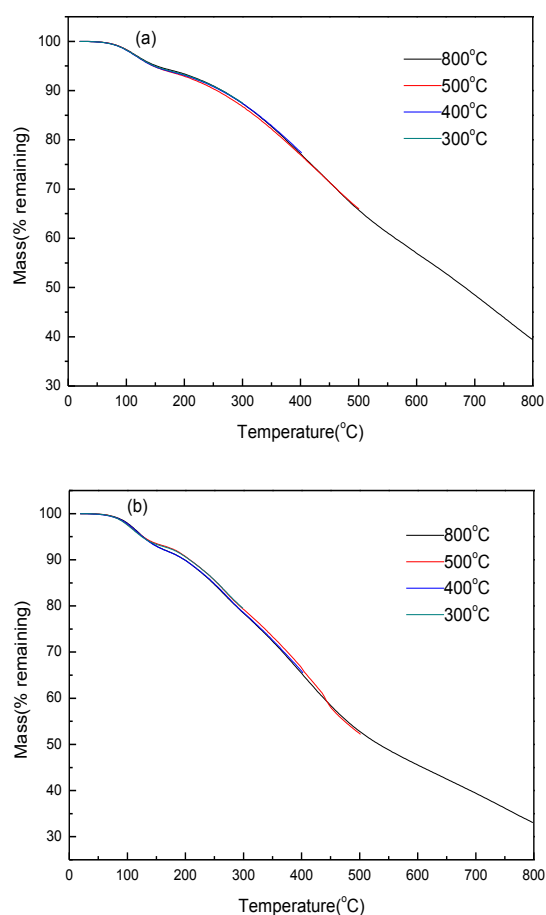


Figure 3-6. Thermogravimetric curves for 800°C, 500°C, 400°C, 300°C (a) sample5pc, (b) sample10pc.

### 3.3.2 Analysis of TG-DSC results

Because the TG curve of the final temperature 800°C includes the reaction stage of final temperature 500°C, 400°C, 300°C, the TG curve for the final temperature 800°C of these two samples was adopted to analyze the thermal characterization of tholins and compare the thermogravimetric behavior of sample 5pc and sample 10pc.

#### 3.3.2.1 Thermal characterization of sample 5pc

The results of the thermal gravimetric analysis for sample 5pc are shown in **Figure 3-7(a)**. It presents that at the beginning of experiment temperature when the temperature (<80°C), the change of mass is not evident, it infers that almost nothing has been volatilized during this stage. Then the temperature get to 200°C during this period (80°C<T<200°C) the mass loss about 10% which is the stage corresponding to the vaporization of moisture vaporization of mainly water, as confirmed by the TG-MS study presented afterwards. (Sciamma-O'Brien et al., 2010) used thermogravimetry analysis method to study the oxygen question in the sample tholins. In my study, When the temperature exceeds 200°C and arrives at approximately 550°C, a change in the slope of the mass loss is visible, suggesting that a difference in the process leading to desorption is occurring. Overall, only 60% of the mass of the sample was lost on heating to 800°C.

**Figure 3-7(b)** is the first derivative thermogravimetry DTG curve corresponds to TG curve for sample 5pc. We can see the weight change rate clearly from this curve. The inflection points indicate thermal transitions. The first peak is happening at the temperature about 110°C and the second peak appears at about 470°C and there is also a more attenuated peak on 750°C.

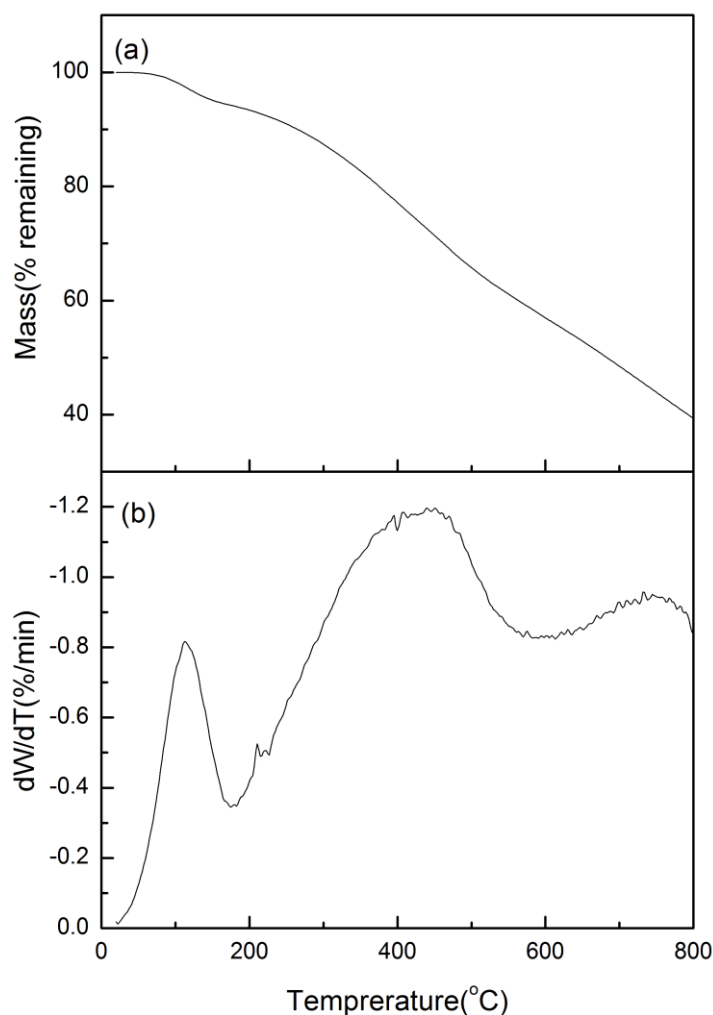


Figure 3-7. TG (a) and DTG (b) curves for sample 5pc, the final temperature is 800°C.

The DSC thermogram of the sample is showed in **Figure 3-8** and compared to the DTG results. Tholins are complex polymers (Pernot et al., 2010) so their thermal decomposition process is also complicated.

The first endothermic peak and the first DTG peak appear at a similar temperature which corresponds to the moisture vaporization. However the second DTG stage, which reveals a major degradation step for tholins, is not accompanied by any clear DSC signal. The absence of heat change is a compromise between exothermic and endothermic processes, such as carbonization and desorption respectively, occurring concurrently for this decomposition period (Sazanov and Griбанov, 2009). For the last stage, the carbonization process becomes dominant, leading to an exothermic DSC curve increasing until the final temperature.



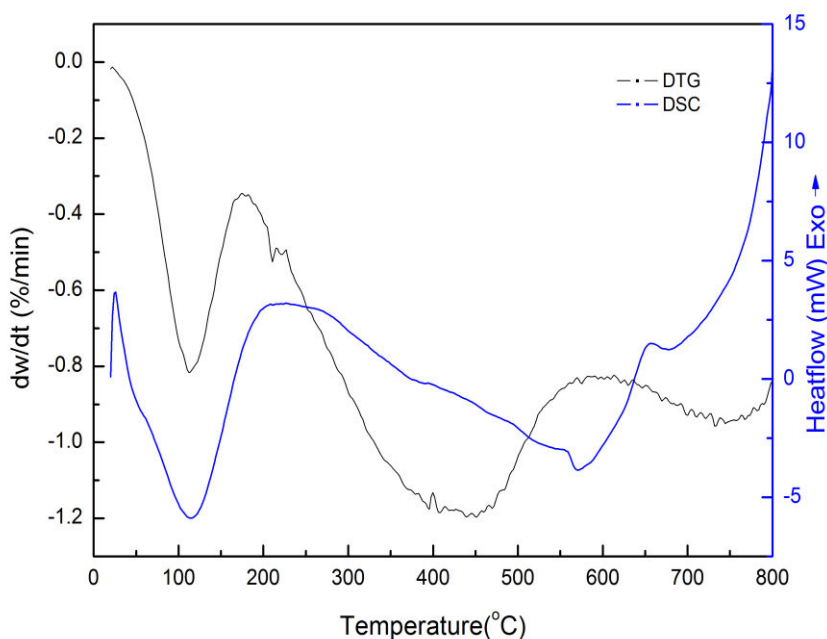


Figure 3-8. DSC and DTG curves for the sample 5pc, heating rate is 10K/min and under the argon atmosphere.

### 3.3.2.2 Thermal characterization of sample 10pc

The following **Figure 3-9** is the TG and the first derivatives of thermograms (DTG) curve of final temperature 800°C for the sample 10pc. **Figure 3-10** the DSC thermogram of the sample and compared to the DTG results.

From **Figure 3-9** (a) the TG curve shows that the sample 10pc has a similar thermal degradation behavior with sample 5pc. It also has three main stages for mass loss. At the beginning of experiment (temperature <80°C), the change of mass is negligible. Then (temperature 80°C<T<200°C) the mass loss is about 10%, corresponding to the vaporization of moisture, which may be water and volatile organic compound. When the temperature exceeds 200°C and till 500°C, during this temperature period, it is the stage maybe the loss of the major thermal compositions about 40%.

The DTG curve **Figure 3-9** (b), the first peak is happening at the temperature of about 100°C and the second peak appears at about 275°C, the third peak presents at about 450°C and there is also the last little peak on 700°C. This information will be mentioned in details later, when comparing sample 5pc and sample 10pc.

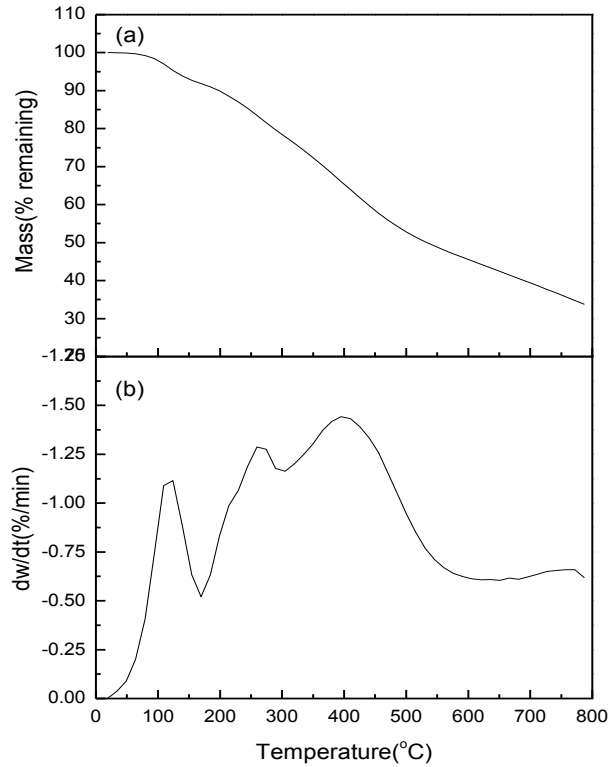


Figure 3-9. TG (a) and DTG (b) curves for sample 10pc, the final temperature is 800°C.

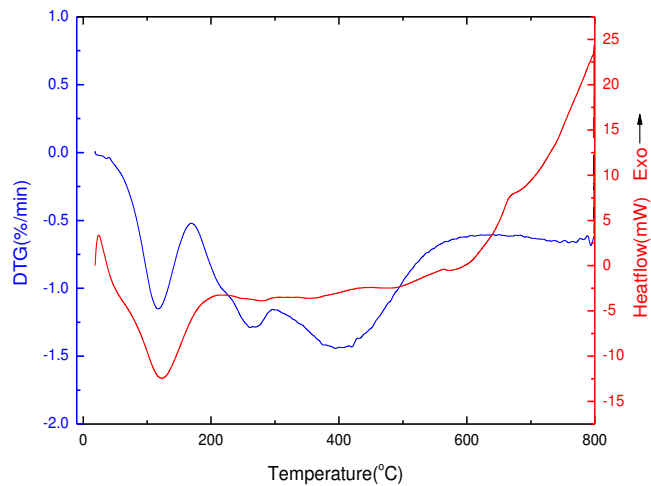


Figure 3-10. DSC and DTG curves for the sample 10pc, heating rate is 10K/min and under the argon atmosphere.

Through comparing the curves DSC and DTG of sample 10pc **Figure 3-10**, we can find that the temperature for the first endothermic peak appears is similar. For the second stage, the value of heat change during the staple degradation stage is not very important. It has

the similar behavior with the sample 5pc. The reasons for this phenomenon are also the same with that we have mentioned to explain the DSC curve of sample 5pc.

### 3.3.2.3 Compare sample 5pc with sample 10pc

In order to compare the thermal characterization of these two samples the following **Figure 3-11** is the TG curves for sample 5pc and sample 10pc at the final temperature 800°C.

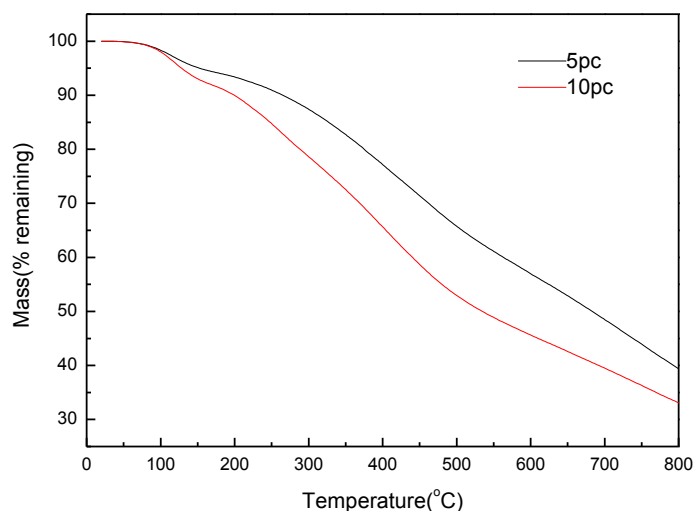


Figure 3-11. Thermogravimetric curves for sample 10pc and sample 5pc at the final temperature 800°C.

In this figure, the red curve is sample 10pc while the black curve is sample 5pc. As can be seen from this figure, we can find that when the temperature about is under 80°C the TG behavior is similar for these two samples, showing a constant weight. But when temperature is above 80°C, the differences between these two TG curves are enlarging with the temperature increase. The mass loss for sample 10pc is obvious more than sample 5pc for the same temperature. When the temperature reaches the final temperature of 800°C, the mass loss for sample 10pc is about 65% while about 60% for sample 5pc. In this case, we can infer that the thermal stability for sample 10pc is worse than sample 5pc. Maybe sample 10pc includes more substances that degrade more easily. However, tholins still have a rather high thermal stability, although it must be remembered that the material that remains at 800°C will be chemically quite distinct from original tholins. A comparable stability against high temperature was found for other tholins mimicking possible planetary aerosols either in the outer solar system (CH<sub>4</sub>/NH<sub>3</sub> atmospheres with a small water) (Khare et al., 1981) or in primitive Earth-like environments obtained from a gaseous mixture CH<sub>4</sub>/N<sub>2</sub>/H<sub>2</sub> with spark

discharge activation of liquid water (Ruiz-Bermejo et al., 2007). If we carefully observe the figure, we also find that when the temperature under 500°C, the TG difference between two samples is increased with increasing temperature. When the temperature is above 500°C, the situation is the opposite.

We can see the small difference between the two samples in the thermal decomposition behavior more clearly on **Figure 3-12** DTG curves. Because the DTG curve indicates that the rate of weight change of the sample, we can clearly find that less than 500°C, the DTG value of sample10pc is more than sample 5pc, than sample 5pc is more than sample10pc. This can explain the situation of TG curves we have mentioned above.

The **Figure 3-12** also shows that during the major decomposition period, sample10pc has one more peak than sample 5pc in the DTG curve. The detail information about these peaks has been displayed in **Table 3-1**. The first DTG peak appears at 100°C, probably resulted from de desertion of water and/or organic volatile material. The second peak for sample 5pc and the second, third peaks for sample 10pc are happening at the second reaction stage of the main degradation stage.

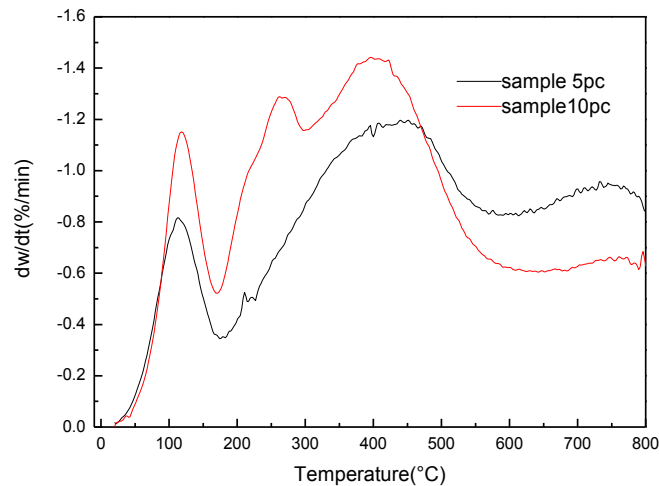


Figure 3-12. DTG curves for sample 10pc and sample 5pc, the final temperature is 800°C.

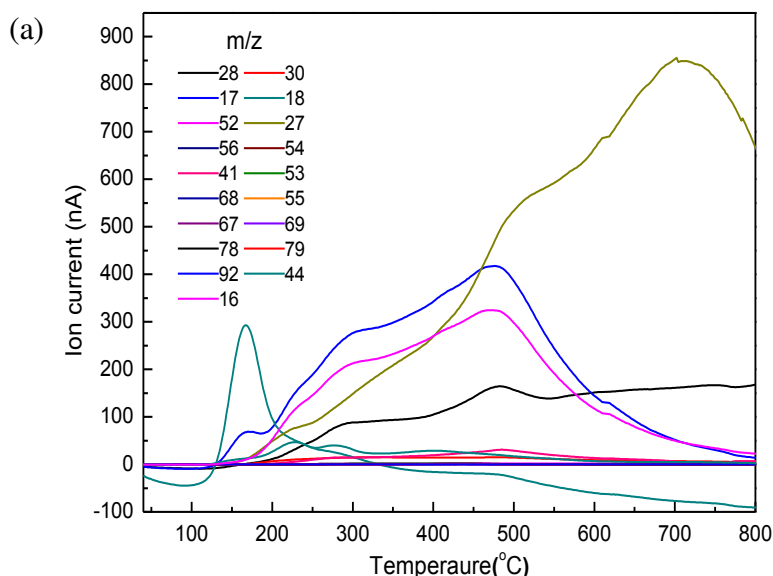
Table 3-1. The temperature of DTG maximal with corresponding rates of mass loss for sample 10pc, sample 5pc.

sample	$T_{\max 1} (^{\circ}\text{C})$	$dw_1/dt (\%/min)$	$T_{\max 2} (^{\circ}\text{C})$	$dw_2/dt (\%/min)$	$T_{\max 3} (^{\circ}\text{C})$	$dw_3/dt (\%/min)$
10pc	117	-1.152	269	-1.286	395	-1.442
5pc	112	-0.816	470	-1.174	761	-0.665

### 3.3.3 TG-MS results

The following figures show the result of TG-MS analysis for sample 5pc and sample10pc. **Figure 3-13** (a) shows that all of the volatile species of thermal decomposition and fragmentation. But because the intensity for some components is very low, we cannot see the curves of them very clearly. So **Figure 3-13** (b) presents the ion current intensity for  $m/z$  as a function of temperature for tholins 5pc. Most of the major signals are observed between 200°C and 600°C, which is the second step highlighted by DTG and DSC analysis. This step is characterized by a flat DSC curve and a DTG curve peak at 450°C. In this temperature range, the MS signal of the gas released shows most often a double structure: a first maximum at about 275°C, and a second one at about 450°C. This is for example the case for ion  $m/z$  54. This double structure can be explained by a release of two types of fragments. First at 275°C labile components are emitted either by desorption or by rupture of fragile terminal fragments. Then at 450°C, more internal molecular structures are cracked and released by the pyrolysis process.

It is for example the case for a major peak at  $m/z$  28 appearing at temperature 275°C and at 475°C. This ion is preferentially attributed to  $C_2H_4^+$  as  $CH_2$  is a well identified polymeric pattern in the initial tholins (Pernot et al., 2010). But it can also involve a small contribution of carbon monoxide  $CO^+$ , as oxygen may exist in tholins resulting from oxidation contamination. Another relevant signal at  $m/z$  41 can be assigned to acetonitrile  $CH_3CN^+$  and follow a similar double structure shape.



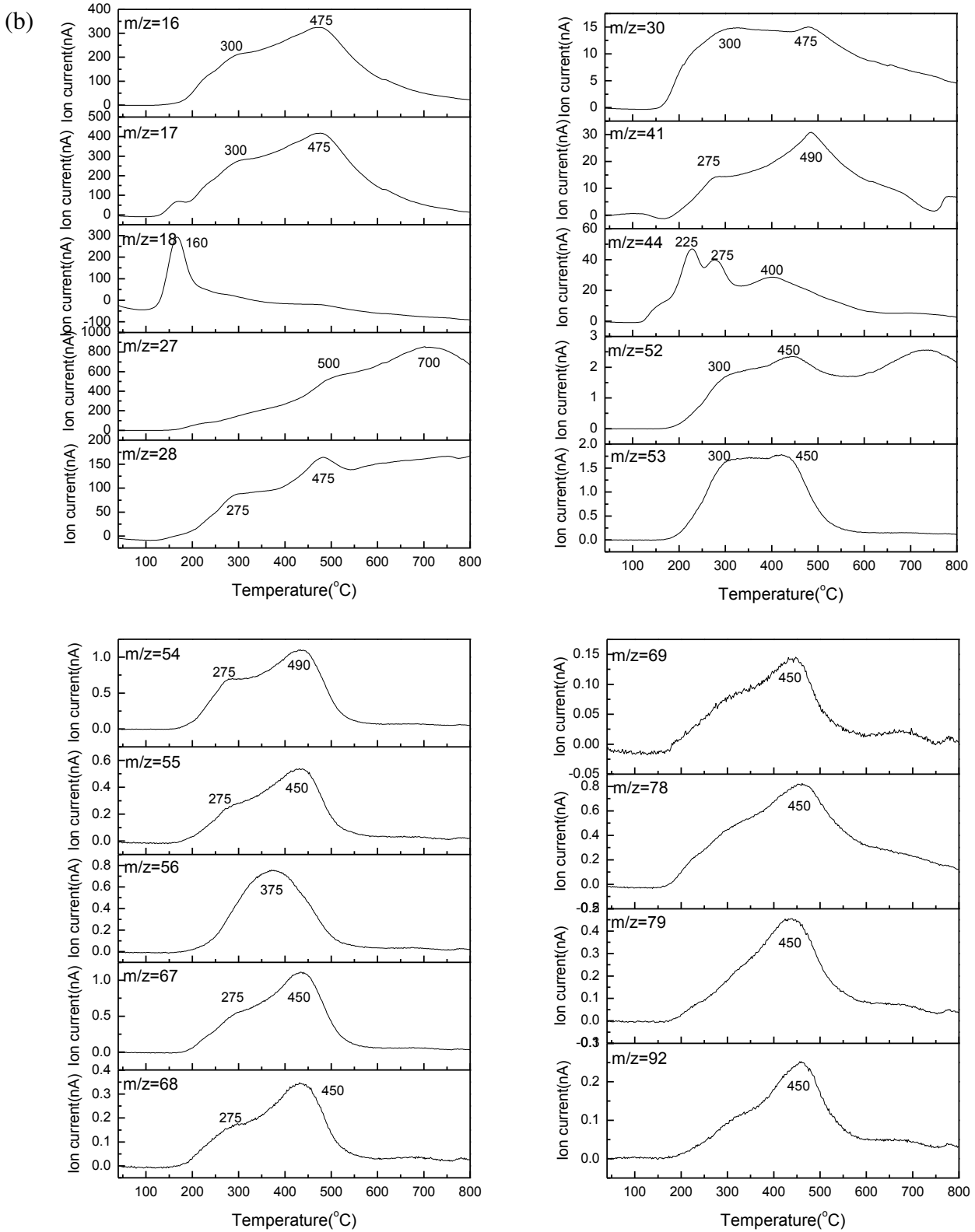


Figure 3-13. Ion intensity curves for tholins sample 5pc (a) all of the volatile species (b) ion current intensity for every m/z as a function of temperature.

Signal at  $m/z$  44 can be assigned to  $C_3H_8^+$ , but  $CO_2^+$  can also contribute to the total intensity due to the partial oxidation of tholins shown by elemental analysis: the contribution of both molecules possibly explain the slightly more complex structure of  $m/z$  44 around 200-300°C, with a successive emission of both species. The TG-MS profiles for the  $m/z$  56 and 55 are consistent with  $C_4H_8^+$  and  $C_4H_7^+$  respectively, maybe with further decomposition patterns producing signals at  $m/z$  15 ( $CH_3^+$ ). Ions with  $m/z$  values larger than 56, 67, and 69 may be derived from hydrocarbons containing five carbon atoms. The signals for the highest  $m/z$  values (78, 79, and 92) suggest the existence of aromatic fragments, inferring aromatic hydrocarbons and heteroaromatics to be a part of the tholins structure. These aromatics species are not emitted beyond 500°C, showing that the pyrolysis process is too harsh in this region to preserve these structures.

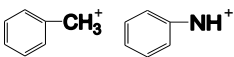
Only a few gaseous species show a third release step beyond 500°C. This very destructive phase for the material only enables the emission of small fragments coming from the most refractory part of the material. In this case, only HCN at  $m/z$  27,  $C_2H_4$  at  $m/z$  30,  $C_2N_2$  at  $m/z$  52 are observed. This HCN and  $C_2N_2$  releases coming from the cracking pattern of the internal structure of tholins are in agreement with the important contribution of nitrogen found in the residue by elemental analysis even at 800°C. HCN and  $C_2H_4$  had been also identified as a dominant pattern in the initial tholins structure by high resolution mass spectrometry (Pernot et al., 2010).

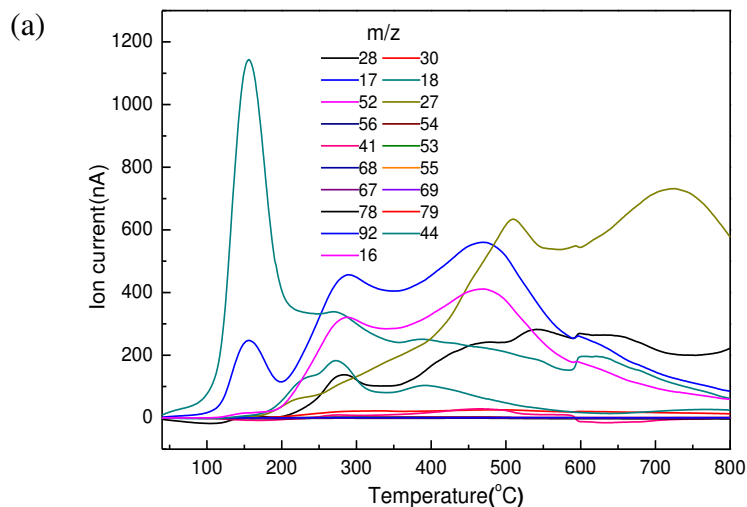
Finally, the second major signal, observed at  $m/z$  17, shows also main release at three temperatures: at 300 and 475°C like all the other organic compounds detected, but also at 150°C. The ion can be mainly attributed to ammonia  $NH_3^+$ , with two peaks of the MS response occurring at 300°C and 475°C. The third additional contribution at low temperature corresponds to  $OH^+$ , a water fragment (correlated with  $H_2O^+$  ion at  $m/z$  18) appearing by moisture degasing below 200°C. The ion current curve at  $m/z$  16 corresponds to  $NH_2^+$ ; fragment ion of ammonia, and shows actually a correlation with the structures at 300 and 450°C. It is important to note that ammonia is not emitted beyond 500°C. This result is consistent with the absence of amine functions in the residue as seen in the infra-red absorption spectrum of the residue at 800°C.

**Figure 3-14** shows the ion intensity curves as a function of temperature for sample 10pc. The same method was used to analyze the result. We can find from **Figure 3-14(a)** that the shape for all the ion intensity curves is a little different with sample 5pc. We can see

clearly on **Figure 3-14(b)** that there are some compounds with one more peak at about 300°C during the thermal degradation process. The ion attribution is proposed in **Table 3-2**, in agreement with the study of the volatile precursors found in the plasma experiment during the tholins production (Carrasco et al., 2012).

Table 3-2. Summary of the possible gaseous organic and inorganic compounds obtained during TG-MS analysis. Heating rate was 10°C/min, final temperature is 800°C, in the argon atmosphere.

m/z	compound	m/z	compound
16	NH <sub>2</sub> <sup>+</sup>	17	NH <sub>3</sub> <sup>+</sup> OH <sup>+</sup>
18	H <sub>2</sub> O <sup>+</sup>	27	HCN <sup>+</sup> C <sub>2</sub> H <sub>3</sub> <sup>+</sup>
28	C <sub>2</sub> H <sub>4</sub> <sup>+</sup> CO <sup>+</sup> N <sub>2</sub> <sup>+</sup>	30	NO <sup>+</sup> C <sub>2</sub> H <sub>6</sub> <sup>+</sup>
41	C <sub>3</sub> H <sub>5</sub> <sup>+</sup> CH <sub>3</sub> CN <sup>+</sup>	44	CO <sub>2</sub> <sup>+</sup> C <sub>3</sub> H <sub>8</sub> <sup>+</sup>
52	NC-CH=CH <sup>+</sup> C <sub>2</sub> N <sub>2</sub> <sup>+</sup>	53	C <sub>4</sub> H <sub>5</sub> <sup>+</sup> C <sub>2</sub> H <sub>3</sub> CN <sup>+</sup>
54	NC-CH <sub>2</sub> -CH <sub>2</sub> <sup>+</sup> C <sub>4</sub> H <sub>6</sub> <sup>+</sup>	55	C <sub>4</sub> H <sub>7</sub> <sup>+</sup> C <sub>2</sub> H <sub>5</sub> CN <sup>+</sup>
56	C <sub>4</sub> H <sub>8</sub> <sup>+</sup> C <sub>3</sub> H <sub>6</sub> N <sup>+</sup>	67	C <sub>5</sub> H <sub>7</sub> <sup>+</sup> C <sub>4</sub> H <sub>5</sub> N <sup>+</sup>
68	C <sub>5</sub> H <sub>8</sub> <sup>+</sup> C <sub>4</sub> H <sub>6</sub> N <sup>+</sup>	69	C <sub>5</sub> H <sub>9</sub> <sup>+</sup> C <sub>4</sub> H <sub>7</sub> N <sup>+</sup>
78	C <sub>6</sub> H <sub>6</sub> <sup>+</sup>	79	C <sub>4</sub> H <sub>3</sub> N <sub>2</sub> <sup>+</sup>
92			





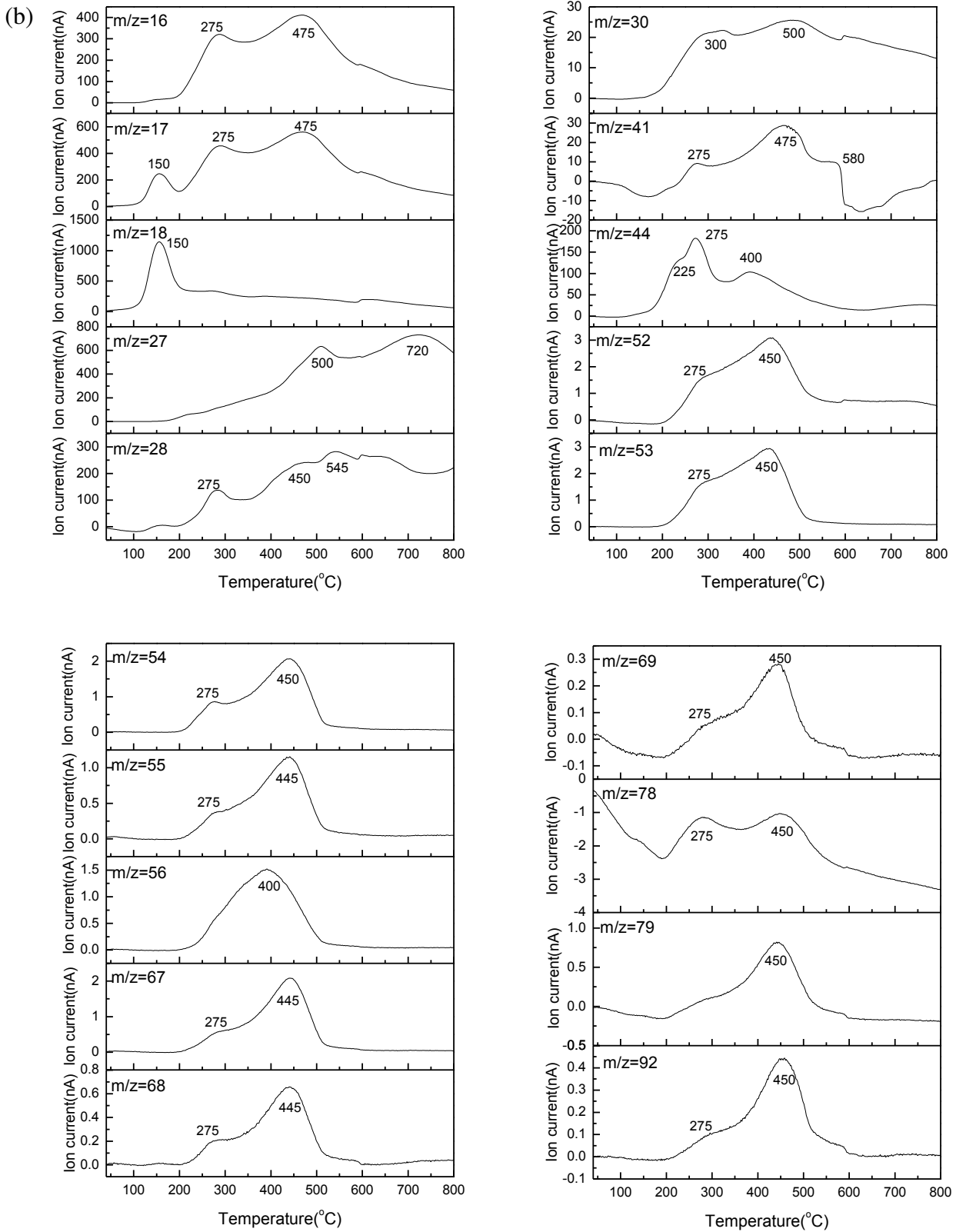


Figure 3-14. Ion intensity curves for tholins sample 10pc (a) all of the volatile species (b) ion current intensity for every  $m/z$  as a function of temperature.

**Figure 3-15** compares the ion current curve for the main thermal decomposition gases for tholins under study, with the strongest signals at  $m/z=16, 17, 18, 27, 28$  for sample 5pc and  $m/z=16, 17, 18, 27, 28, 44$  for sample 10pc. As is shown in this figure, the shape of the main peaks of mass spectrometry resembles those of DTG curves. This phenomenon can explain why there is one more peak in DTG curve of sample 10pc (the peak appeared about  $300^{\circ}\text{C}$ ) than sample 5pc in the major decomposition stage. When the temperature increase to about  $300^{\circ}\text{C}$  there are also some major compounds released for sample 10pc, so the mass loss is more than sample 5pc, the rate of weight change also faster. The MS signal of sample 5pc  $m/z=44(4.69\times 10^{-8}) > m/z=41(3.09\times 10^{-8})$  also are the important products. This indicates the majority of thermal decomposable components in the tholins can release hydrocarbons, such as methane, ethylene, amongst other monomeric components. These results are consistent with some articles studying the thermal decomposition of tholins. Some of these studies used the pyrolysis method, the results of these studies have revealed that tholins after flash pyrolysis, a lot of varieties of organics, such as hydrocarbons (saturated and unsaturated), aromatic hydrocarbons, nitriles and so on could be produced (Khare et al., 1984b; Ehrenfreund et al., 1995; la Fuente et al., 2012; McGuigan et al., 2006; Pietrogrand et al., 2001; Takano et al., 2004).

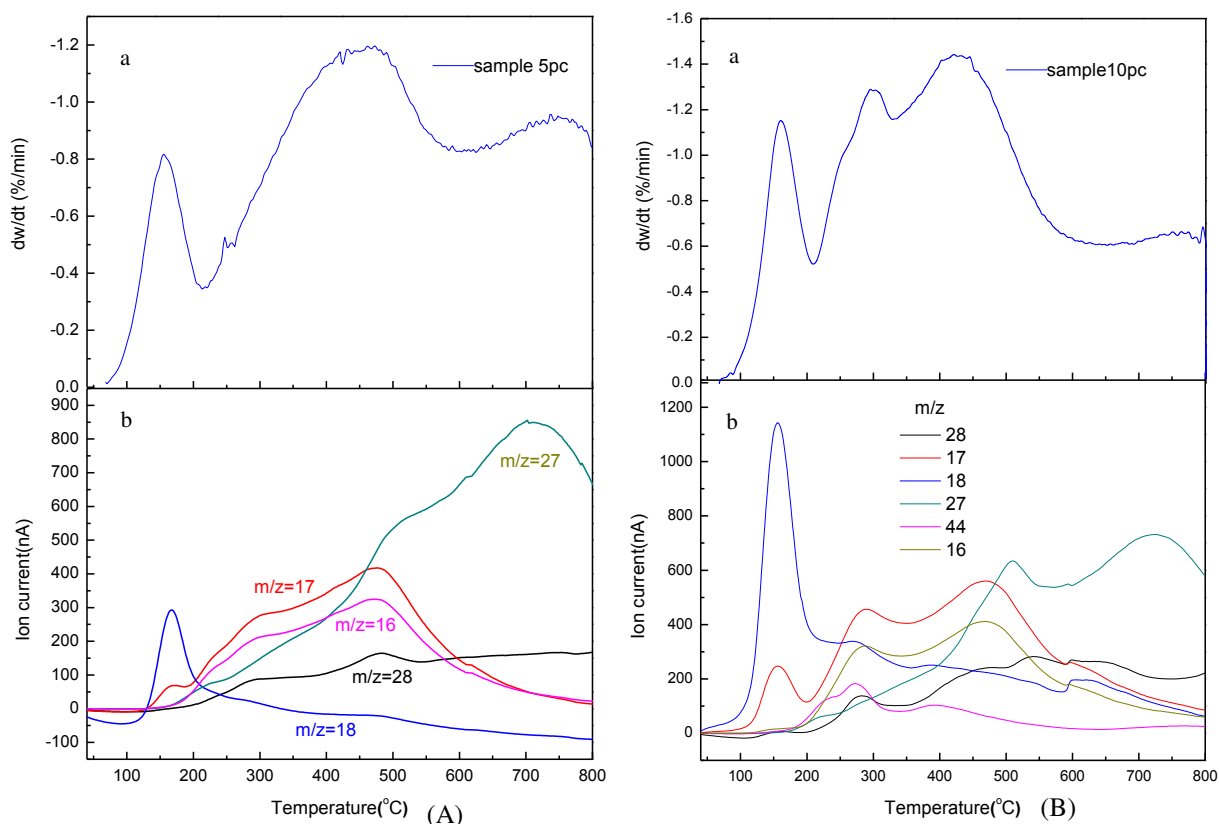


Figure 3-15. DTG curve (a) and MS principal signal comparison (b) as a function of temperature for sample 5pc (A) and sample 10pc (B).

### 3.4 The analysis of sample heating residues

In order to observe the change of sample tholins after every final heated temperature, systematic methods were used to realize this object. For example, infrared spectrometry analysis, raman analysis and elemental analysis. The principal and the experimental process about these techniques have introduced simply in the front part of this chapter. The results of these techniques will be presented and discussed in the following part.

#### 3.4.1 The result of Infrared Spectroscopy

The infrared spectra of the various tholins have been studied by many investigates. (Ruiz-Bermejo et al., 2008) used this method to study the functional groups of CH<sub>4</sub>/N<sub>2</sub>/H<sub>2</sub> spark hydrophilic tholins. Others used infrared spectroscopic measurements to reveal the characteristic bonding structure of tholins formed at different deposition pressures (Imanaka et al., 2006). The bulk, soluble, and insoluble tholins fractions are found to be very similar and reveal identical chemical signatures of nitrogen bearing functions and aliphatic groups (Carrasco et al., 2009). (Quirico et al., 2008) studied the principal functions of the three different tholins samples obtained using different initial gas mixtures and compared with poly-HCN and g-CN materials.

In this study, the tholins and heating residues for different temperature were characterized by their infrared spectrum. Only qualitative analyses have been carried out in this work, revealing many chemical functional groups in the product and their change with the temperature.

**Figure 3-16** presents the infrared spectra result for sample 5pc and the heating residues. For clarity, the spectrogram is divided into four sections: region I (3000-3700 cm<sup>-1</sup>), region II (2700-3000 cm<sup>-1</sup>), region III (2000-2300 cm<sup>-1</sup>), and region IV (900-1800 cm<sup>-1</sup>), in agreement with (Quirico et al., 2008).

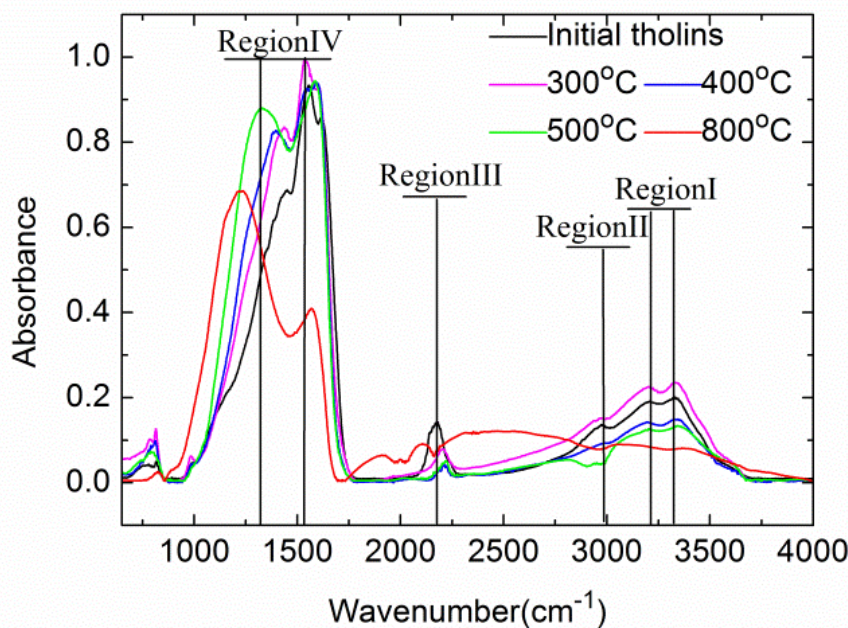


Figure 3-16. The infrared spectra for initial sample 5pc and different temperature heating residues. (The range of wave frequencies investigated from 600 to 4000  $\text{cm}^{-1}$ . Each spectrum was obtained by addition of 4 scans with a resolution of 4.0  $\text{cm}^{-1}$  and the baseline is modified automatic by the software of instrument).

As discussed in (Quirico et al., 2008), region I corresponds to the presence of  $-\text{NH}_2$  and possibly  $-\text{NH}$ -functional groups, primary and secondary amine functions respectively. So for region I correspond to amines. The figure shows a gradual decrease of the band up to 500°C, temperature above which the band is no more observed. Primary and secondary amine functional groups are therefore to be discarded for most of the nitrogen content remaining in the tholins above 500°C and highlighted by elemental analysis.

The region II, consistent with the alkyl bands, contains first the  $-\text{CH}_3$ - symmetric, asymmetric stretching mode and  $-\text{CH}_2$ - asymmetric stretching mode. The bending modes of these chemical groups peak at 1450  $\text{cm}^{-1}$ . In this region II, the alkyls are gradually degraded and disappear between 400 and 500°C. This is in good agreement with a dehydrogenation of the carbonaceous compounds followed by a carbonization. More interestingly, a broad feature appears in the spectrum of tholins residue obtained at 800°C. This large band is visible in the graphitic carbon nitride spectrum, named g-CN, in the work of (Quirico et al., 2008).

Region III shows a band centered at about 2200  $\text{cm}^{-1}$ , which can be assigned to the presence of terminal  $-\text{CN}$  (cyanide), or possibly isocyanide  $-\text{NC}$  units (Lin-Vien et al., 1991; Mutsukura and Akita, 1999). (Liu et al., 1997; Imanaka et al., 2004) have also proposed the

carbodiimide function (-N=C=N-) to explain this feature. In this region, the intensity of the functional group decreases with the temperature increase, and even disappears between 500°C and 800°C. The broad feature detected in region II and consistent with a carbon nitride structure is large enough to cover the region III in the residue spectrum at 800°C.

The spectral region IV exhibits a complex pattern, with two major structures in the initial tholins sample. The first is in the 1500-1600  $\text{cm}^{-1}$  wavelength range and involves C=C and C=N bonds contributions within olefinic chains (Quirico et al., 2008). This structure remains stable in the residue up to 500°C. In the spectrum at 800°C, this band is drastically reduced. The second initial structure is found at about 1450  $\text{cm}^{-1}$  and can be mainly attributed to the bending vibrations of -CH<sub>2</sub> and CH<sub>3</sub> groups. This structure is modified with the temperature since 300°C, and disappears in the 500°C spectrum. The evolution of these both initial bands reveals an important modification of the carbon structure of the residue since 500°C, corresponding to the second thermal transition identified in the DTG analysis. Moreover, in the 500 and 800°C residue spectra, a broad band in the 1200-1300  $\text{cm}^{-1}$  appears, shifting progressively from 1330  $\text{cm}^{-1}$  at 500°C to 1200°C at 800°C. This large structure is consistent with an amorphous material and the increase of graphitic contributions, as seen in the graphitic carbon nitride structure of g-CN in (Quirico et al., 2008).

According to the IR spectrum, the initial nitrogen-rich tholins seem to evolve, first beyond the first thermal transition at 110°C by losing terminal structures such as nitrile and amine functions; then beyond the second thermal transition at 470°C, by reorganizing the initial olefin structure towards a carbon nitride through graphitization process, generating a N-rich graphitic residue.

**Figure 3-17** presents the infrared spectroscopy result for sample 10pc. It has the similar behavior as sample 5pc. There are also four regions consistent with different structure functions. We can observe the change of these functions with the temperature increase.

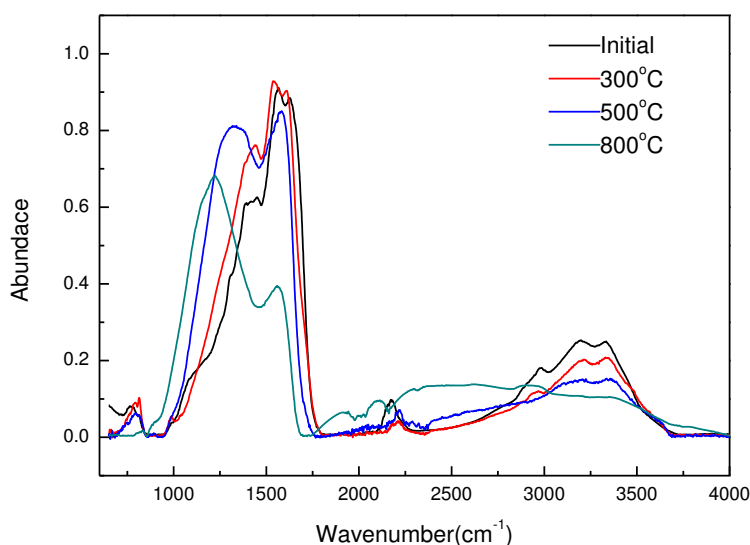


Figure 3-17. The infrared spectra for initial sample 10pc and different temperature heating residues.

### 3.4.2 The result of Raman spectroscopy

For the result of Raman spectroscopy, it will take the residues of sample 5pc as an example. The **Figure 3-19** shows the curves of all the tholins residues after heating used visible Raman spectra (514nm green), centered on the D and G bands of carbon materials between 1200 and 1800 $\text{cm}^{-1}$  Raman shift. In amorphous carbon, the G band at 1500-1600 $\text{cm}^{-1}$  arises from the bond stretching motion of pairs of  $\text{sp}^2$  C atoms, in aromatic rings or olefinic chains. G-band is allocated to the mode symmetry of the corresponding movements  $\text{E}_{2g2}$  of folding of conjugated carbon-carbon bonds. The D band is attributed for  $\text{A}_{1g}$  symmetry breathing mode corresponding to aromatic rings **Figure 3-18** (Ferrari et al., 2000). There is no D mode if the  $\text{sp}^2$  sites form only olefinic chains.

Raman spectroscopy of tholins initial samples was attempted but these studies gave no useful information on vibrational excitations because of strong fluorescence that marked the relatively weak Raman spectra from the samples. This is because the photons emitted in this process, mainly in the visible range. So here we present the Raman spectra of the residues of the heating tholins.

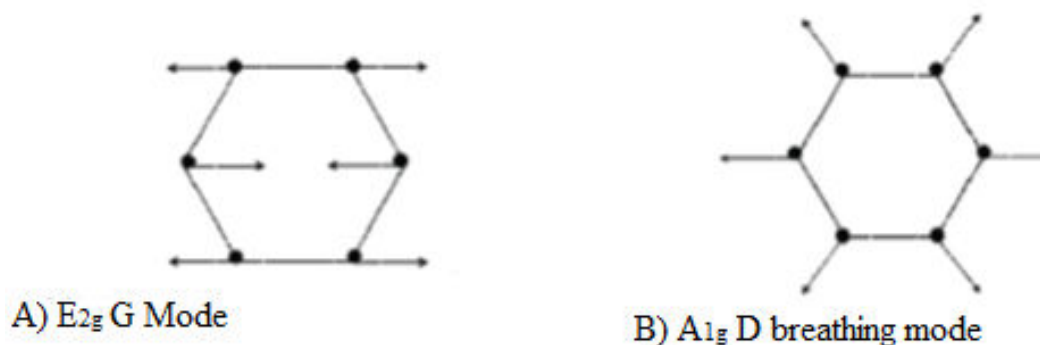


Figure 3-18. Modes of vibration bands related to Raman spectra of carbonaceous materials. G-band is allocated to the mode symmetry  $E_{2g}$  corresponding to movements of folding of conjugated carbon-carbon bonds are shown in cycles; or in olefin chains. The D band is attributed for its mode of  $A_{1g}$  symmetry breathing mode corresponding to the aromatic ring (Ferraris al., 2000).

The black spectrum in corresponds to the residue at 300°C, the blue is residue at 400°C, the red is residue at 500°C and the green is residue at 800°C. From this figure we can find that the intensity of D and G band is increase with the heating temperature increases, the width at half height in turn decreases. However, their positions don't seem to vary significantly. The G band seems its position shift towards high Raman shift as the temperature increases and, simultaneously, its full width at half maximum decreases drastically. All these observations are consistent with a degree of order increases as we increase the heating temperature (Ferrari et al., 2000).

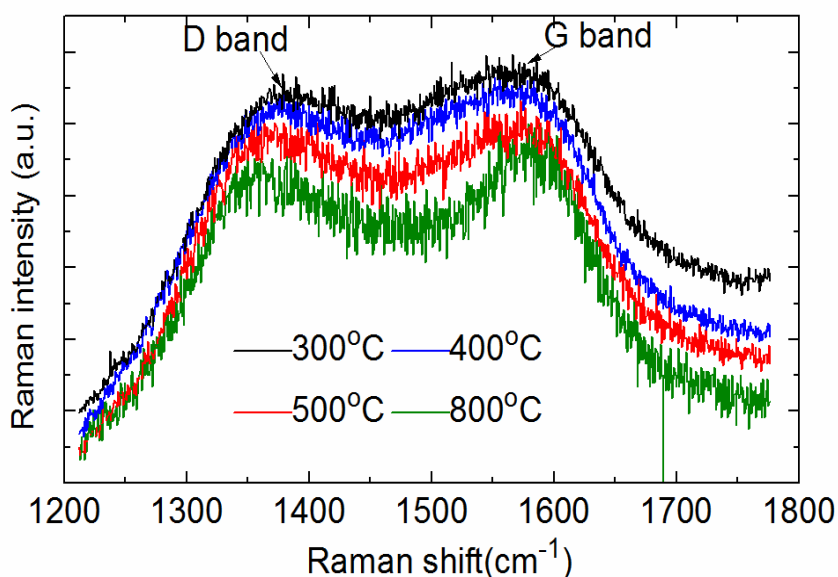


Figure 3-19. Typical Raman spectra of all the tholins residues for different temperature. The G-band and D-band are clearly seen.

On the base of **Figure 3-19** the spectral variations mentioned above were quantified with double profile LBWF (Lorentzienne, Breit-Wigner-Fano) defined in (Quirico et al., 2006), used for the analysis of Raman spectra. Band D was adjusted by profile Lorentzian and G-band by an asymmetrical profile type Breit-Wigner-Fano to take into account valley inter-band (Bonal et al., 2006). Any baseline corrections were made assuming a linear background. This adjustment is shown in **Figure 3-20**. It can allow adjusting the position of  $\omega_G$  and  $\omega_D$  of the band G and D respectively the intensities  $I_G$  and  $I_D$  and their full widths at half height  $FWHM_G$  and  $FWHM_D$ . This adjustment can follow more precisely the evolution of the spectra with temperature. For residues of every temperature, the fit was carried out six times then the average value was adopted to connect a line and observer the change trend of every parameter of band D and band G.

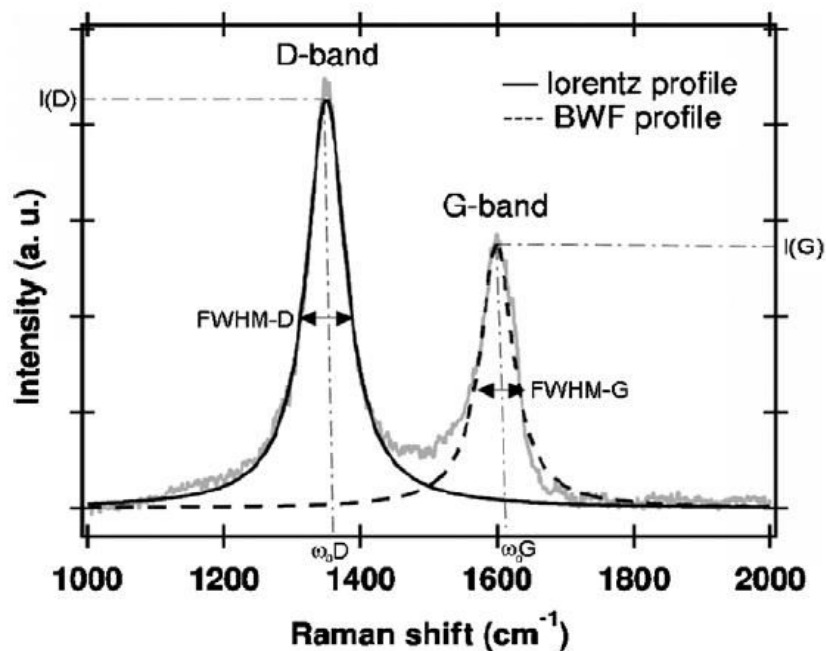


Figure 3-20. Raman spectra are fit by a double band profile, band D is adjusted by a Lorentzian and a G band profile Breit-Wigner-Fano to obtain the spectral parameters  $FWHM_D$ ,  $FWHM_G$ ,  $I_D$ ,  $I_G$ ,  $\omega_{0D}$ ,  $\omega_{0G}$  (Bonal et al., 2006).



The BWF line has an asymmetric line shape, which should arise from the coupling of a discrete mode to a continuum (Cardona et al., 1982). The BWF line shape is given by equation 3-3.

$$I(\omega) = \frac{I_0[1+2(\omega-\omega_0)/Q\Gamma]^2}{1+[2(\omega-\omega_0)/\Gamma]^2} \quad \text{equation 3-3}$$

where  $I_0$  is the peak intensity,  $\omega_0$  is the peak position,  $G$  is assumed as the full width at half maximum (FWHM) and  $Q^{-1}$  is the BWF coupling coefficient. The Lorentzian line shape is recovered in the limit  $Q^{-1} \rightarrow 0$ . The BWF+Lorentzian line pair is an excellent means to fit Raman spectra of all carbons, from graphite to *ta*-C. A Lorentzian line shape is used for the *D* peak as it is from the same family as the BWF line, while the various enhancement mechanisms for the *D* peak are consistent with a Lorentzian (Ferrari et al., 2000). The following figures are the results according to this fit treatment method.

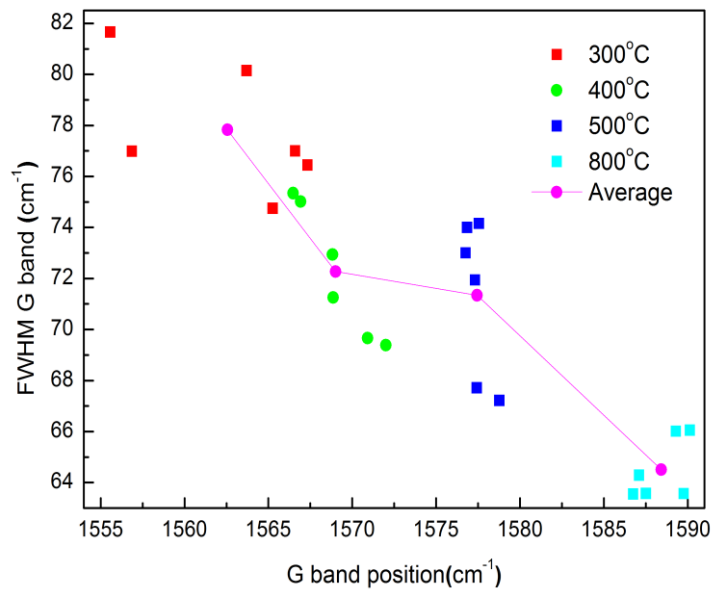


Figure 3-21. The parameter change of the G band Raman spectra for residues of heating tholins sample 5pc.

Parameters are both very well correlated with each other when the temperature rises.

The **Figure 3-21** shows the evolution of the full width at half maximum (FWHM) according to its G position for different heating temperature residues. In this figure, there is clearly a correlation between the two parameters with increasing temperature. Both parameters change in anti-correlated, the width at half height of the band G, decreasing with increasing position.

**Figure 3-22** shows the separate evolution of these two parameters with the level of temperature thermal degradation.

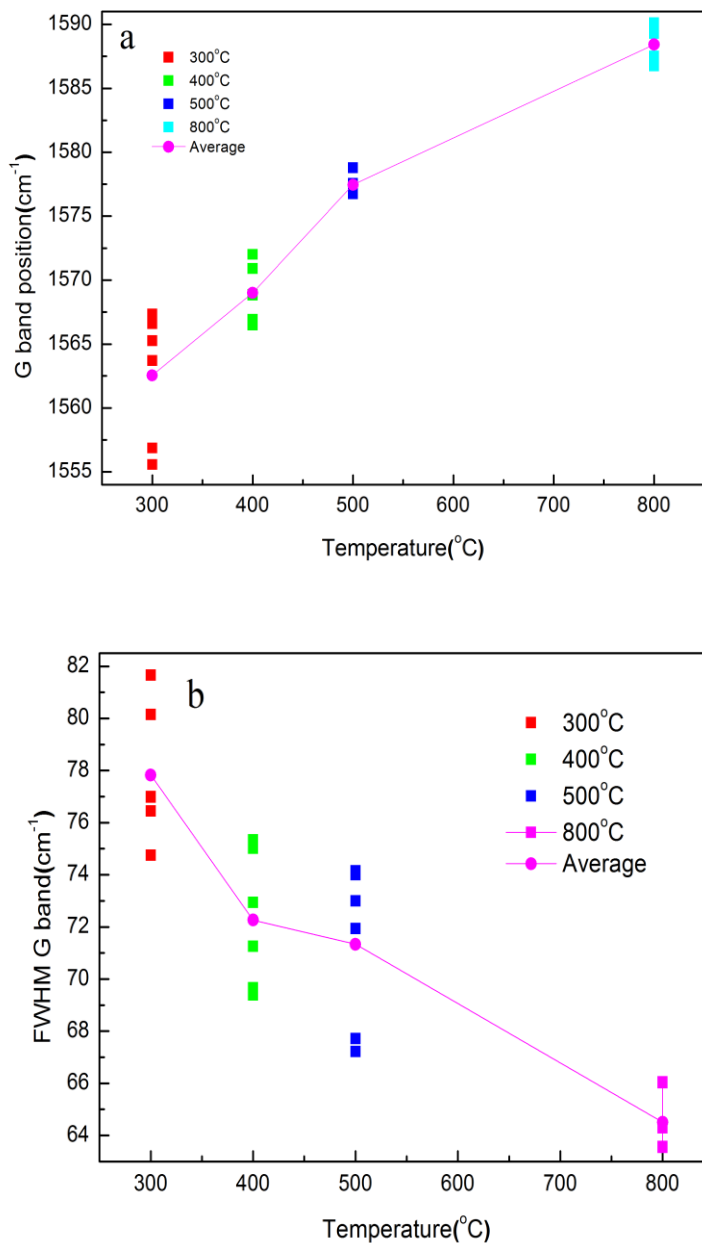


Figure 3-22. The change of G band position (a) and FWHM (b) as a function of temperature.

The G band position increases when the heating temperature increases, in contrast, the G band full width at half maximum (FWHM) is decreases. That means both parameters change in anti-correlated, FWHM decreasing with increasing position **Figure 3-21**. This behavior reflects a growth of polyaromatic units.

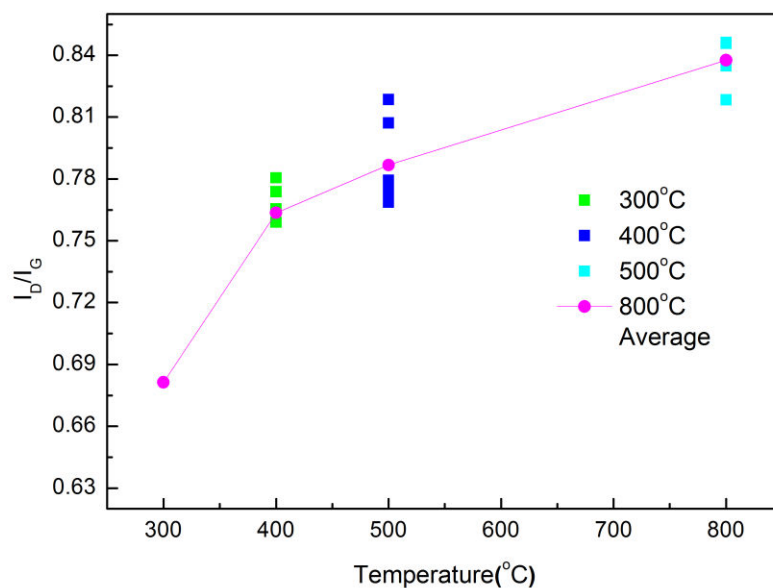


Figure 3-23. The intensity ratio of the D-band and G-band,  $I_{(D)}/I_{(G)}$ , as a function of heating temperature.

In microcrystalline graphite, the intensity ratio of the D and G modes,  $I_{(D)}/I_{(G)}$ , increases as the grain size decreases. However, for amorphous carbon, the disorder is so great that the intensity ratio of the D and G modes,  $I_{(D)}/I_{(G)}$  decreases with decreasing cluster size of fused aromatic rings (Ferrari et al., 2000; Rodil et al., 2001). The intensity ratio of the D-band and G-band  $I_{(D)}/I_{(G)}$  **Figure 3-23**, increases when the heating temperature increases. This increase suggests larger cluster size of aromatic rings at higher temperature. The variation of this ratio infers the structure variation of aromatic in tholins.

### 3.4.3 Elemental analysis

An elemental analysis of the residues and initial tholins were achieved to determine their composition. The C, H, N and O mass percentages were determined. From the obtained elemental mass percentages; we calculated the C, H, N and O molar percentages. Because the mass of residue of every sample is limited, only once measurement can be realized in this study.

Evolution of the elemental analysis with the temperature is shown on **Figure 3-24**. The oxygen content detected in the bulk tholins has been previously discussed (Sciamma-O'Brien et al., 2010). However its stability with temperature suggests that tholins oxygen content is more due to a partial oxidation process than to water adsorption.

For sample 5pc, in the 300 to 500°C temperature range, the 40 to 50% carbon relative enrichment of the residue is mainly anti-correlated with the 35 to 25% hydrogen relative loss, whereas the nitrogen content is stable. This loss of hydrogen can therefore be attributed to the dehydrogenation of the carbonaceous materials present in the tholins. However above 500°C, the nitrogen and hydrogen losses are similar relatively to the carbon whose elemental composition increases from 50% at 500°C up to 60% at 800°C due to a carbonization process of nitrogenous and carbonaceous compounds at high temperatures.

The elemental composition molar percentage change for sample 10pc also has a similar trend.

For these two samples, the nitrogen relative content remains stable up to 500°C, and decreases for temperature above 500°C, from 20% in the initial tholins down to only 10% in the residue at 800°C. This significant remaining fraction of nitrogen not released even at 800°C, highlights a strongly attached contribution of nitrogen in the tholins structure.

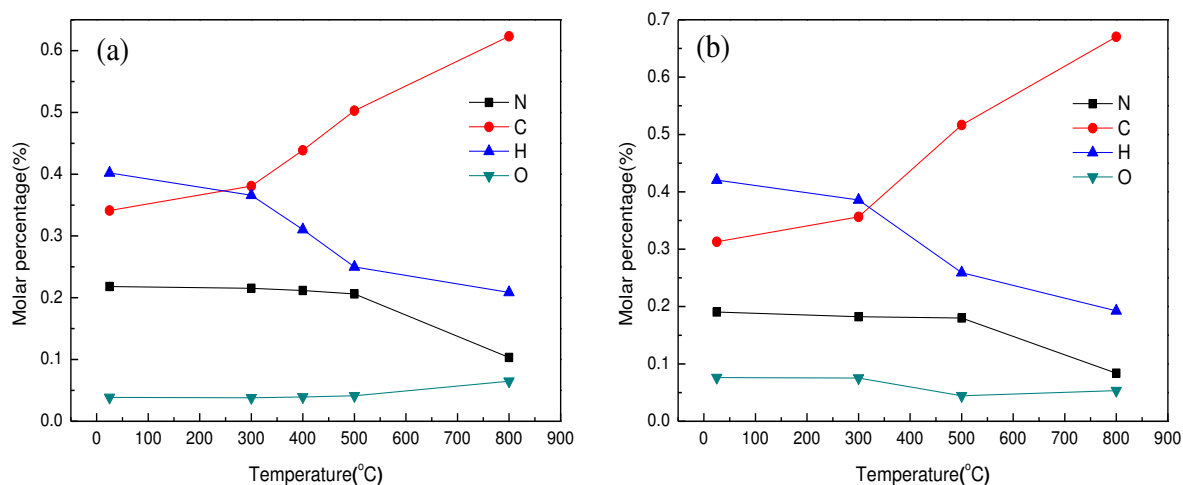


Figure 3-24. Elemental composition of initial tholins and the residues as a function of temperature (a) sample 5pc; (b) sample 10pc.

If we neglect the oxygen content, we can obtain their C/N and C/H ratios **Figure 3-25** the trend is similar for these two ratios. In the beginning, when the heating temperature is low just 300°C the increase for C/N and C/H almost the same, this phenomenon is changed with the temperature increases, the increases for C/H is faster than C/N until 500°C, but the condition is reverse after heating 800°C because the content of nitrogen decreases drastically. That because the most nitrogen functions in the structure of tholins disappeared after 500°C,

we can see this phenomenon from the result of infrared spectra. If we consider the oxygen content, that means there is maybe some water in the sample so the content of hydrogen can also come from water, in this case we can only get C/N ratio.

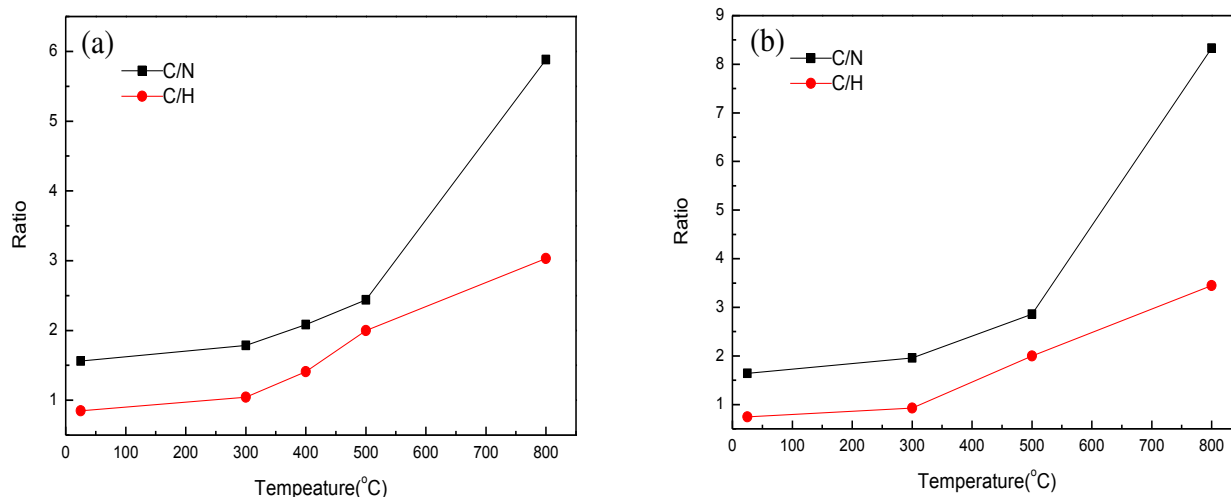


Figure 3-25. Variation of elemental compositions (C/N and C/H) as a function of temperature (a) sample 5pc (b) sample 10pc.

### 3.5 Discussion

The characterization methods used, the results of which have been described above, allow us to monitor physicochemical evolution of tholins during and after thermal degradation. This can be summarized in a few major points.

#### 3.5.1 Thermal stability of tholins

Tholins are complex mixtures of molecules with a  $H_xC_yN_z$  general composition (Pernot et al., 2010; Quirico et al., 2008). Those are often compared to HCN polymers which have an important role in astrophysics as they are thought to be present in cometary ices (Matthews and Minard 2006). From previous studies, tholins were shown to be chemically different, and actually more complex than poly-HCN materials (Véronique Vuitton et al., 2010), but the importance of the HCN pattern in tholins (Pernot et al., 2010; Somogyi et al., 2005) as well as in Titan's aerosols (Israël et al., 2005) was also found out. For these reasons, we compared the thermal stability of a poly-HCN material with our sample.

In part 3.3.2.3, the thermal stability has been compared between sample 5pc and sample 10pc. We found that the thermal stability of sample 10pc is worse than sample 5pc.

But further studies are needed to evaluate if the content of methane in initial gaseous mixture can affect the thermal stability of tholins.

However thermal characterization of HCN polymers by TG and DSC method has been carried out (De La Fuente et al., 2011). In this study, HCN polymers were synthesized from the reaction of equimolar amounts of NaCN and  $\text{NH}_4\text{Cl}$  in water, they conclude that the thermal degradation of all the samples was divided into three stages: drying stage, main pyrolysis stage and carbonization.

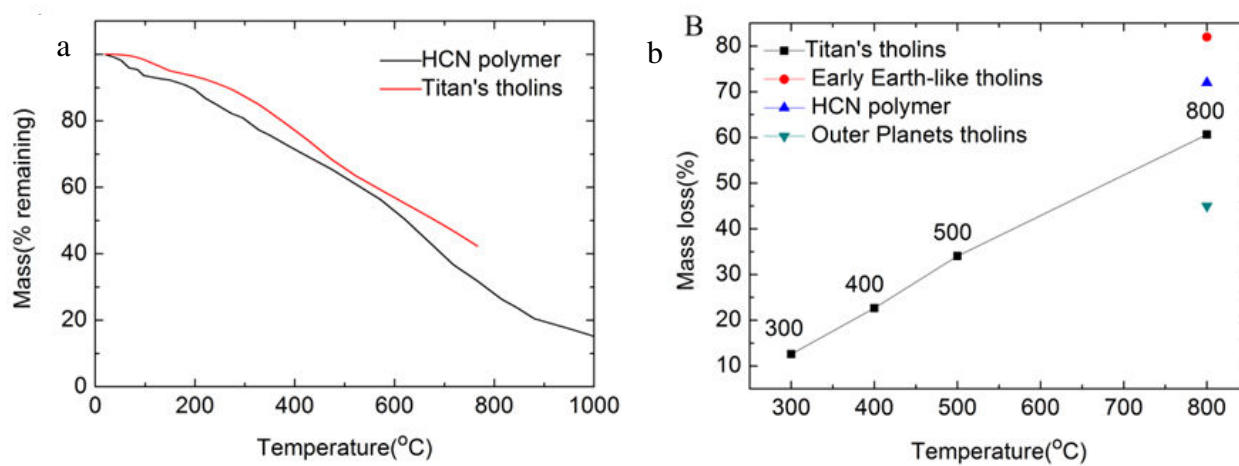


Figure 3-26. Compare thermal properties of Titan's tholins, HCN polymer and other tholins. (A) TG curves of HCN polymer (De La Fuente et al., 2011) and Titan's tholins; (B) mass loss for Titan's tholins, other tholins (Khare et al., 1981; Ruiz-Bermejo et al., 2007), and HCN polymer.

As **Figure 3-26** (A) depicts TG curves for HCN polymer and Titan's tholins. When comparing these curves, we observe that both materials are rather resilient to high temperatures, with tholins being slightly more resistant than HCN polymers up to 800°C. **Figure 3-26** (B) shows the mass loss for Titan's tholins at four final temperatures, from 300 to 800°C. At 800°C, it is compared with relative mass losses of HCN polymer and other types of tholins (planetary aerosols in outer solar system, and in primitive Earth environment). Titan's tholins sample lost about 60%, HCN polymer lost about 70%, and the primitive Earth environment tholins lost more than 80% of its mass. The mass loss for the  $\text{CH}_4/\text{NH}_3/\text{H}_2\text{O}$  spark tholins at 800°C which is the candidate constituents of planetary aerosols in the outer solar system is only about 45%, showing a high thermic stability of this material.

The chemical composition of HCN polymer is simpler than of Titan's tholins, as revealed by IR and NMR spectrometry (Vuitton et al., 2010). The HCN polymer thermal

degradation is also easier than Titan's tholins, as illustrated by the higher mass loss observed for poly-HCN. Beyond the simple chemical structure, this thermal behavior could also be explained by a higher density of the tholins material which could moderate the bonds rupture compared with poly-HCN.

The primitive early Earth tholins were produced with a similar  $\text{CH}_4/\text{N}_2/\text{H}_2$  gas mixture as Titan's tholins, but the reactive plasma mixture also contained some water in the early Earth case. The hydrolysis of the molecules composing the tholins seems therefore to thermally weaken the material.

### **3.5.2 Evolution of elemental and chemical compositions of tholins**

From the point of view of the composition, heteroatoms, that is to say mainly nitrogen and hydrogen are expelled from the material. Both C/H and C/N progressively increases as the temperature increases. The nitrogen containing functions, such as amines and nitriles are degraded with increasing heating temperature.

The functions that contain hydrogen atoms such as alkyl are also gradually degraded as the temperature increases. They disappeared completely from the infrared spectrum when the temperature attained 500°C. This stage of the chemical evolution of tholins, expulsion heteroatoms is also observed in natural carbonaceous materials such as coal or kerogen (Durand, 1980). These study results by infrared spectroscopy show a fairly rapid loss of carbon chains. This loss is classical in the evolution of coals when subjected to increasing maturation: it allows the aliphatic function to restructure the material and polyaromatic units to be gathered in parallel (Bonnet, 2012).

The alkyl groups almost disappear for the residue at 500°C, before this temperature the process for thermal degradation is principal corresponds to the vaporization of moisture, mainly water (<200°C). This hypothesis is confirmed by the result TG-MS.

### **3.5.3 Changes in the structure of the carbon skeleton of tholins**

Raman microscopy used in this work allows us to follow the evolution of polyaromatic units as the temperature for thermal degradation increases. This technique has been widely used to monitor structural natural carbonaceous materials (Tuinstra and Koenig, 1970; Wopenka and Pasteris, 1993; Ferrari and Robertson, 2000; Quirico et al., 2005; Bonal et al.,

2006). In fact, during maturation of carbonaceous materials, expulsion of heteroatoms and loss functions aliphatic polyaromatic units will evolve.

For the amorphous carbon, the G band position increases as the degree of structural order increases and this increase was accompanied by a decrease of its width at mid-height (Ferrari et al., 2003). In the Raman spectra of residues thermal degradation the G band follows exactly this behavior, which reflects an aromatization and/or the polyaromatic units growth for material. Band D also allows us to track the change of polyaromatic skeleton via its intensity variations, in relation to the intensity of the G (Quirico et al., 2005). In the present work, the intensity ratio  $I_D/I_G$  evolves similarly to what has been reported in (Ferrari and Robertson, 2000). According to the (Ferrari and Robertson, 2000) G band position and  $I_D/I_G$  increase with the temperature increases, that means the increasing level of structural order.

### 3.6 Conclusion

In this chapter, a systematic thermal degradation characterization of tholins has been realized. We used many techniques to study the thermal stability of samples and the heating residues.

The TG curves shows that the mass loss percentage for the two sample decomposition, sample 10pc lost more weight and faster than sample 5pc when temperature gets to 800°C, therefore the thermal stability of tholins may be influence by the content of methane used in their synthesis. The thermal degradation of all the samples was divided into three stages: drying stage, main pyrolysis stage and carbonization. Our tholins sample also has a good thermal resistance at high temperature, as they are more stable than HCN-polymer and early-Earth like tholins.

The results of TG-MS revealed the volatile species of thermal decomposition and fragmentation processes for these two samples, the majority of thermal decomposable components in the tholins can release hydrocarbons, such as methane, ethylene, amongst other monomeric components. At the lowest temperatures, the main process of evolution of the Titan's tholins corresponds to the vaporization of moisture, most probably water (<200°C) and then, most of the large fragments are released from the sample at 500°C, including aromatic structures. Beyond 600°C, the residue is shown to be mainly a thermal stable graphitic carbon nitride structure, and the molecules released are small cracking fragments of HCN, C<sub>2</sub>H<sub>4</sub> and C<sub>2</sub>N<sub>2</sub>. Ammonia, which was also detected by the ACP instrument on the



Huygens probe is actually released between 200 and 500°C, not beyond. The ammonia release is actually correlated to the extinction of the amine signature in the thermal residue. The thermal degradation of the material produces small gaseous cracking fragments involving HCN, C<sub>2</sub>H<sub>4</sub> and C<sub>2</sub>N<sub>2</sub> and the residue is no more chemically representative of the initial material, converging towards an amorphous graphitic carbon nitride structure. The shape of the major signals ion intensity curves explains why there are one more peak in the DTG curve of sample 10pc than sample 5pc.

The strongly attached contribution of nitrogen in the tholins structure has been confirmed by the elemental analysis and IR results. The IR spectra for the initial tholins sample and different heating residues show that all of the functional groups changed with the temperature. The elemental analysis shows important nitrogen content in the final residue 800°C.

To conclude this physicochemical evolution of the material during thermal degradation of our experiences, it is possible to say that tholins carbonize gradually, that is to say that those heteroatoms are removed. This loss of nitrogen and hydrogen is accompanied by loss of function aliphatic (alkyls), which will permit polyaromatic units to grow, and also begin to reorganize.

**Chapter 4. The possible chemical  
evolution of the aerosols on the surface  
of Titan**

In the two previous chapters, some properties and structure of Titan's tholins have been studied. These results belong to the intrinsic properties of tholins. As the aerosols of Titan deposit on the surface of Titan after they are produced, studying the chemical evolution of the aerosols on the surface is necessary.

A number of geological structures (dunes, lakes, cryogenic streams, fluvial channels mountains volcanic) have been observed by different instruments onboard the Cassini-Huygens probe, as VIMS, RADAR and DISR instruments (Radebaugh et al., 2008, 2007; Stofan et al., 2006; Lopes et al., 2007; Lorenz et al., 2008) . When the aerosols of Titan come in contact with the surface, they may react with materials present in these geological structures, so that chemical processes could take place. One of the important substance present on the surface of Titan is the water molecule in the solid state or, occasionally, liquid. The presence of water ice on the surface of Titan was already proposed in several articles (Coustenis and Bézard, 1995; Griffith et al., 2003; Lorenz and Lunine, 2005). (Rodriguez et al., 2006) had reached the same conclusion by studying VIMS data.

This is the reason why we propose here to study the potential reaction of Titan's tholins produced with the PAMPRE experiment and liquid water.

Recently, in light of new data obtained by Cassini RADAR, (Lopes et al., 2013) reexamined candidate cryovolcanic features using morphological evidence to infer the origin of features. The evidence was presented to support the cryovolcanic origin of features in the region formerly known as Sotra Facula including the deepest pit so far found on Titan (now known as Sotra Patera), flow-like features (Mohini Fluctus), and some of the highest mountains on Titan (Doom and Erebor Montes). They interpreted this region to be a cryovolcanic complex of multiple cones, craters, and flows (Lopes et al., 2013).

So the objective of this chapter is to test different extraction techniques and detect the maximum compounds of exobiological interest.

## **4.1 The fate of aerosols at the surface of Titan**

The possibilities of chemical reactions that can occur between aerosols and water present at the surface of Titan, however, have a limit to the observed water surface temperature of 90 K is still solid (ice), and the rate for chemical reaction with this solid phase is very low in comparison with those of the liquid phase.

It is however possible that water can exist episodic in liquid form on the surface of Titan. The presence of liquid water would be associated with the melting of ice water under the impact of comets and other celestial bodies, either because the impact would melt water ice on the surface of Titan, or because of the nature of these bodies. Unlike Earth, where most impact body is rocky nature, those arriving on Titan (comets and debris from the body from outside of our system Solar) are further composed of water ice. Thompson and Sagan (1992) estimated at 1% of the total volume of the crater, the volume having melted the impact (or melt percent) but according to recent simulations, this percentage would be largely underestimated. (Brien, et al., 2005) has made an estimation of the lifetime of a liquid environment in an impact crater on Titan: from the case of craters 15 km in diameter and 150 m depth, with a percentage of 2-5% iron (Artemieva and Lunine, 2003), liquid environment can last for  $10^2$ - $10^3$  years before being completely frozen in the effect of low temperatures on the surface of Titan. Starting from the craters of 150 km in diameter and 1.5 km deep, with a percentage of 5-10% melting (Artemieva and Lunine, 2003), this same environment may persist in liquid form for  $10^3$ - $10^4$  years.

#### **4.1.1 Chemical reaction in contact with liquid water: acidic hydrolysis by tholins**

(Khare et al., 1986) was the first to study the chemical evolution of aerosols in contact with liquid water. They also used the acidic pH conditions (HCl 6N) to catalyze the occurring reactions. In this paper, the authors describe hydrolysis experiments carried out in particular of proteins under acidic conditions, and replicate on Titan tholins synthesized in the laboratory. To do this, they use the following procedure:

1. Tholins were suffered acid treatment by hydrochloric acid (HCl) 6N release organic products including amino acids ( $\text{NH}_2\text{-CH(R)-COOH}$ ).

2. Esterification of amino acids by addition of isopropyl alcohol acidified ( $(\text{CH}_3)_2\text{-CHOH} + \text{HCl}$ ) at  $100^\circ\text{C}$  for 3 hours, which produces isopropyl ester hydrochloride ( $\text{Cl-NH}_3^+\text{-CH(R)-COOCH(CH}_3)_2 + \text{H}_2\text{O}$ ).

3. The isopropyl alcohol and unreacted water were removed by evaporation under nitrogen atmosphere.

4. Acylation derivatization isopropyl ester hydrochloride ( $\text{Cl-NH}_3^+\text{-CH(R)-COOCH(CH}_3)_2$ ) synthesized in the previous step with Trifluoroacetic anhydride (TFAA) ( $(\text{CF}_3\text{CO})_2\text{O}$ )

in the presence of dichloromethane ( $\text{CH}_2\text{Cl}_2$ )(solvent) to form N trifluoroacetyl isopropyl esters ( $\text{CF}_3\text{CO-NH-CH (R)-COOCH (CH}_3)_2$ ) which volatile and analyzed by GC-MS.

The products of these reactions were then injected and analyzed in a GC-MS system with a chiral capillary column Chirasil-Valine. The result obtained by Khare et al. is shown in the below **Table 4-1**.

Table 4-1. Amino Acids and Urea identified in acid-treated tholins (Khare et al., 1986).

	mg/g
Glycine	5.30
Alanine	0.70
$\alpha$ -Amino-n-butyric acid	0.10
Valine	t
Threonine	t
Aspartic acid	1.10
Glutamic acid	0.40
$\beta$ -Alanine	1.20
$\beta$ -Amino-n-butyric acid	0.20
$\beta$ -Aminoisobutyric acid	0.13
$\gamma$ -Amino-n-butyric acid	0.30
$\alpha$ -Aminoisobutyric acid	0.06
$\alpha$ -Methyl- $\alpha$ -amino-n-butyric acid (Isovaline)	t
$\alpha,\beta$ -Diaminopropionic acid	0.10
$\alpha,\gamma$ -Diamino-n-butyric acid	0.02
N-Methylglycine	0.18
Urea	10.30
Amino acids	9.79
Urea	10.30

This study was important because it was the first time to study hydrolysis reaction of tholins. Titan produces organic molecules of biological interest, and in this case it can produce amino acids. Amino acids were abundant on the early Earth. Their precursors are partly produced in the primitive atmosphere or in hydrothermal systems sailors. The import of amino acids should also be an extraterrestrial important contribution, as suggested by micrometeorite collection and simulation experiments conducted in the laboratory and in space (Brack, 2007). The possible presence of amino acids on Titan's surface shows that their

formation is possible elsewhere than on Earth, and brings new key questions addressed by the exobiology.

#### **4.1.2 Organic macromolecules tholins in cold aqueous solutions**

In order to measure the rate of the hydrolysis of complex tholins in cold aqueous solutions, (Neish et al., 2008) used the AC electrical discharge under slow flow at a temperature of 195K to produce the sample. The initial gaseous mixture is 0.95N<sub>2</sub>/ 0.05CH<sub>4</sub>. Then, the sample tholins were dissolved in water at four different temperatures and using electrospray ionization coupled with high-resolution Fourier transform ion-cyclotron resonance mass spectrometry to monitor the changes of oxygenated and non-oxygenated species in the mass spectra at different times. The results of this study is that the tholins samples can produce oxygenated species via hydrolysis reactions with activation energies of  $\sim 60 \pm 10 \text{ KJ mol}^{-1}$  after they were placed in liquid water. The half-lives are between 0.3 and 17 days at 273K for this reaction. On the basis of these results, they concluded that oxygen incorporation into organic macromolecules is very fast when compared to planetary timescales for the places where the liquid water exist. This study can be used to infer the prebiotic chemistry on the early Earth and Titan.

#### **4.1.3 Low temperature hydrolysis of laboratory tholins in ammonia-water solutions**

After studying the rates of tholins react with water, (Neish et al., 2009) also researched the tholins react with ammonia-water solutions at low temperature. In this work, tholins were synthesized from a 0.98 N<sub>2</sub>/ 0.02 CH<sub>4</sub> initial gaseous mixtures in a high voltage AC flow discharge reactor, and then dissolved in a 13 wt% ammonia-water solution. In order to elucidate the role ammonia and water play in the reaction, the <sup>15</sup>N labelled ammonia-water and <sup>18</sup>O labelled water were also studied. The results of this work present that the half-lives for the reaction of tholins with ammonia-water is between 0.3 and 14 days at 253K, and yield products with more than one percentage oxygen by mass. The incorporation of oxygen into the tholins is faster in the presence of ammonia. The rate increases could be due to the increased pH of the solution or the presence of ammonia provide a new reaction way. They also confirmed that water is the source of the oxygen incorporates into the oxygen containing products.

#### **4.1.4 Formation of amino acids via low-temperature hydrolysis of tholins**

The study of tholins evolution under conditions thought to be similar to those found in impact melt pools and cryolavas on Titan was carried out in (Neish et al., 2010). The tholins produced by a mixture of 2% CH<sub>4</sub> and 98% N<sub>2</sub> was exposed to an electrical discharge under slow flow at a temperature of 195K. Then the tholins samples were hydrolyzed in 13wt% ammonia water at two different low temperatures (253 and 293K) in a long time. Four amino acids were identified in a tholins sample by using a combination of high-resolution mass spectroscopy and tandem mass spectroscopy fragmentation analysis method. These four amino acids are asparagine, aspartic acid, glutamine, and glutamic acid.

#### **4.1.5 Interaction of aerosols with aqueous ammonia on Titan**

(Ramírez et al., 2010) synthesized laboratory analogues of Titan's aerosols from an N<sub>2</sub>:CH<sub>4</sub> (98:2) mixture irradiated at low temperatures under a continuous flow regime by a cold plasma discharge of 180 W. The analogues were recovered, and placed inside different ammonia concentrations during 10 weeks at temperatures as low as those reported for Titan's surface. After a derivatization process performed to the aerosols' refractory phase with MTBSTFA in DMF, the products were identified and quantified using a GC-MS system. They found derived residues related to amino acids as well as urea. The simplest amino acids glycine and alanine as well as urea, are found regardless of the ammonia concentration and temperature value to which the aerosol analogues were exposed. Their results have important astrobiological implications to Titan's environment particularly if the existence of the suggested subsurface water-ammonia mixture and its deposition on the satellite's surface is validated.

#### **4.1.6 Production yields of organics of astrobiological interest from H<sub>2</sub>O-NH<sub>3</sub> hydrolysis of Titan's tholins**

(Ramírez et al., 2010) performed an analysis on the solid bulk obtained after evolution of tholins-ammonia mixtures. (Poch et al., 2012) focused their analysis on the solutes from the liquid solution. Tholins were found to be very reactive toward an oxygen source. Urea was identified as the main product of Titan's tholins hydrolysis in ammonia-water solutions, with a production yield in mass, ranging from 6 to 12% at 279 K after 10 weeks. Several amino acids -alanine, glycine and aspartic acid- and perhaps the uracil nucleobase were also produced with yields from 0.001 to 0.4%.

All of the above 4.1.6 and 4.1.7 studies used the tholins sample synthesized in the laboratory LISA, with the device named PLASMA, from a high-purity gas mixture of 2% methane ( $\text{CH}_4$ ) and 98% nitrogen ( $\text{N}_2$ ) irradiated in a low-temperature continuous-flow regime by a DC cold plasma discharge.

The difference between the two experiments lies in the fact that tholins produced by PLASMA are synthesized directly on the walls of the reactor whereas tholins produced by PAMPRE are synthesized in the bulk under a “levitation” effect and thus eliminate any “wall effect”. The advantage of PLASMA is that it can operate under low temperatures close to the real atmospheric conditions of Titan (Nguyen et al., 2008).

In my study, we analyzed five different tholins samples, produced by PAMPRE method. Different methane content percentages were used in the initial gaseous mixture in order to research if the methane content percentage in the initial gaseous mixture can affect the compounds that are obtained after GC-MS analysis method. We also used three different extraction methods to treat these five samples to investigate differences among these three methods. We carried out a direct derivatization for the raw tholins without any extraction, and simulate the environment conditions on the surface of Titan when the tholins deposit on the surface of Titan to react with water, and last study if the acidic hydrolysis tholins can produce amino acids and other organics.

## 4.2 Experimental method and procedures

### 4.2.1 The sample synthesis and prepare the sample before GC-MS analysis

In this chapter, all the samples were synthesized by the method PAMPRE. The conditions for synthesizing these samples are the same except the initial methane percentage in the reactant gas. Detailed information about the PAMPRE experiment has been introduced in Chapter 1. **Table 4-2** is the list of analyzed samples in this study.

Table 4-2. Five tholins samples were synthesized using different initial gaseous mixture.

Sample	1	2	3	4	5
$\text{N}_2$ (%)	91	92	93	94	96
$\text{CH}_4$ (%)	9	8	7	6	4



Before injecting the samples into GC-MS instrument they undergo some treatments.

We used three methods to extract organic matter and prepare each sample. For every method the sample mass was approximately 2 mg.

1. The first experiment was to add MTBSTFA (80 $\mu$ l) and DMF (30 $\mu$ l) to the solid sample. Then we heated it at 75°C for 15min. This was done to have a direct analysis of the molecules bearing a labile hydrogen atom in the tholins.
2. The second experiment was to add 300 $\mu$ L of water to the solid sample, then to heat at 100°C for 24 hours, and finally to dry the solution under N<sub>2</sub> atmosphere until the liquid is completely evaporated. The goal was to evaluate the possibility for a neutral hydrolysis of the compounds present in the tholins.
3. The third experiment was to add 300 $\mu$ L HCl (hydrochloric acid) to the solid sample, then to heat at 100°C for 24 hours, and finally to dry the solution under N<sub>2</sub> atmosphere until the liquid is completely evaporated. The goal was to evaluate the influence of an acidic hydrolysis on the tholins.

For methods 2 and 3, molecules obtained after the samples treatments cannot be directly injected because of their high boiling point that prevents them from being volatilized. It is necessary to use a derivatization step which allows decreasing the polarity of the labile organic compounds. We thus, as the experiment 1, have to proceed to an additional step to derive products that can be volatilized. The method 2 and 3 after evaporating the liquid completely, MTBSTFA (30 $\mu$ l) and DMF (10 $\mu$ l) were added into the sample and heated at 75°C for 15min.

Volatility of sample is a requirement for GC analysis. Derivatization will make highly polar materials to be sufficiently volatile so that they can be eluted at reasonable temperatures without thermal decomposition (Knapp, 1979) or molecular rearrangement (Kühnel et al., 2007; Blau and King 1978). Understanding the chemistry of the analytes, derivatizing reagents used in sample preparation, and the detailed functionality of Gas Chromatography are important to get reliable results. For GC analysis, compounds containing functional groups with active hydrogen such as -SH, -OH, -NH and -COOH are of primary concern, because of the tendency of these functional groups to form intermolecular hydrogen bonds (Halket and Zaikin, 2003). These intermolecular hydrogen bonds affect the inherent volatility

of compounds containing them, their tendency to interact with column packing materials and their thermal stability (Sobolevsky et al., 2003). Since GC is used to separate volatile organic compounds, modification of the functional group of a molecule by derivatization enables the analysis of compounds that otherwise cannot be readily monitored by GC. Derivatization process either increases or decreases the volatility of the compound of interest. It also reduces analyte adsorption in the GC system and improves detector response, peak separations and peak symmetry.

There are several types of derivatization: silylation, acylation, alkylation and chiral derivatization. In this study, we use the silylation derivatization, which is the most practical and the most commonly used. Various reagents exist in the case of derivatization by silylation, of which we chose the MTBSTFA (N-tert-butyltrimethylsilyl-N methyltrifluoroacetimid) and DMF as the reagent because the rate of derivatization agent with almost 100%, and it resists undesirable hydrolysis reactions. The derivatization reaction with MTBSTFA is as follows: The principle consists in substitution of a carbonyl group, ether or amine by a silyl group such as presented in the **Figure 4-1**.

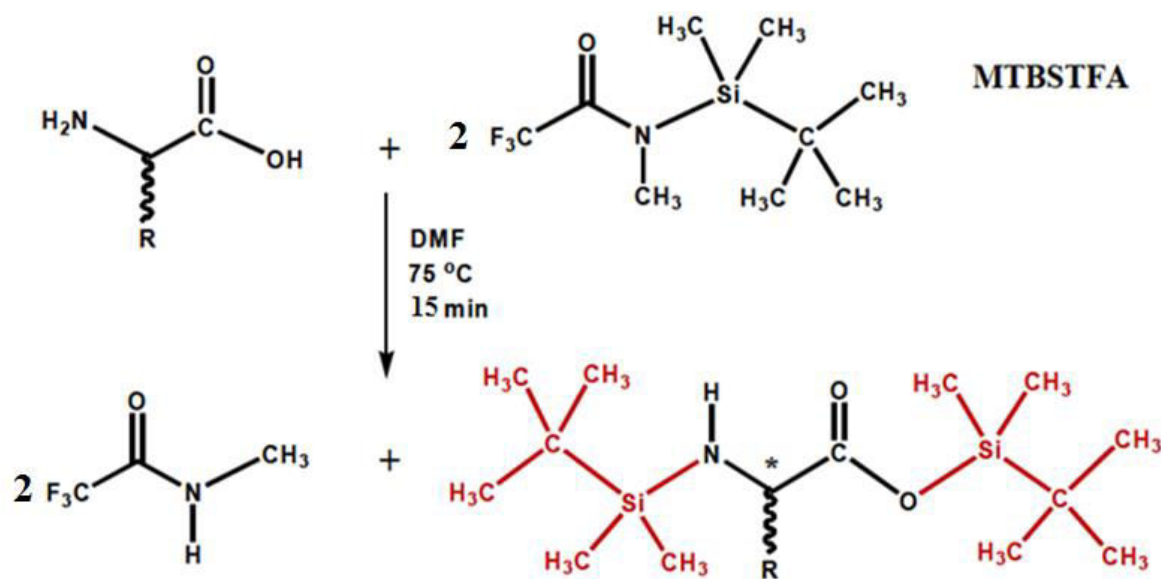


Figure 4-1. Principle of MTBSTFA derivatization: amine and hydroxyl groups are substituted by a silyl group which renders the molecule volatile then can be analyzed by GC-MS.

#### 4.2.2 GC-MS analysis (Gas chromatography and Mass spectrometry)

The Gas Chromatography/Mass Spectrometry (GC/MS) instrument separates chemical mixtures (the GC component) and identifies the components at a molecular level (the MS component). The GC works on the principle that a mixture of gaseous species will be separated into its individual components. The heated gases are carried through a column with an inert gas (such as helium). As the separated substances elute from the column outlet, they flow into the MS. Mass spectrometry identifies compounds by the mass of the analyte molecule, and its products of fragmentation. A “library” of known mass spectra, covering several thousand compounds, is stored along with the software.

Tholins extracts were analyzed with a Thermo Scientific GC-Trace and a Thermo Scientific DSQ II Mass spectrometer operated in the quadrupole detection mode. The ionization mode was electronic impact at 70 eV, and the mass range detection was 10-550m/z. The column used for the separation was Restek Rtx®-5Sil MS (Fused Silica) with 5-meter Integra-Guard MS 30m long, 0.25 mm internal diameter, and 0.25µm film thickness (df) (Equivalent selectivity of Cross bond® 5% diphenyl/95% dimethyl polysiloxane) stable up to 360°C. The column temperature was set with a temperature gradient of 4°C/min from 50°C hold for 3min to 280°C, and then kept at 280°C for 5 more minutes. Helium was used as the carrier gas at a constant flow of 1 mLmin<sup>-1</sup>. The injector was an Optic 3 thermal desorber used in the split mode (1/20) at 250°C. The temperature of the detector was set at 200°C.

Before the sample injection, a blank was performed using the same analytical conditions. This was done to clearly identify potential contaminant species, and to discriminate them from chemical species produced by the hydrolysis reaction.

The chromatograms obtained after injection into the GC-MS analysis of hydrolyzed tholins are provided by the Xcalibur software. These spectra for the oxygen-bearing molecules are analyzed in the following procedures: the masses 73 and 147 are directly sought in specific mass using the software. These are the corresponding masses of fragments found consistently with those of derivatized molecules with a silylation agent such as MTBSTFA (Mai-Julie NGUYEN, 2007).



Figure 4-2. (a) Structural formula corresponding to the ratio of  $m/z = 147$  fragments and its presence is due to the parasitic reaction occurring between an agent MTBSTFA derivatizing molecule and a water molecule. The hydrolysis and derivatization protocol includes a drying step to remove most of the water present, it can, however, never be complete. (b) Structural formula corresponding to the ratio of  $m/z = 73$  fragment, it is the recombination of a silicon with three methyl groups (Mai-Julie NGUYEN, 2007).

The mass fragment 73 corresponds to a degradation product of MTBSTFA,  $\text{Si}(\text{CH}_3)_3$ , while the mass fragment 147 corresponds to the addition of two molecules of  $\text{Si}(\text{CH}_3)_3$  with a water molecule was not removed during the evaporation phase. The evaporation of water can never be total, and MTBSTFA is highly reactive, it degrades rapidly into fragments are routinely found in the mass spectra of the derivatized MTBSTFA.

The first data process is looking directly all chromatographic peaks with the mass fragments 73 and 147. The software allows for the first sorting.

Once the chromatographic peaks containing these masses have been identified, further analysis is performed on these peaks, especially on other masses forming the mass spectra of these peaks.

An example is given below with the spectrum of derivatized alanine using the NIST library.

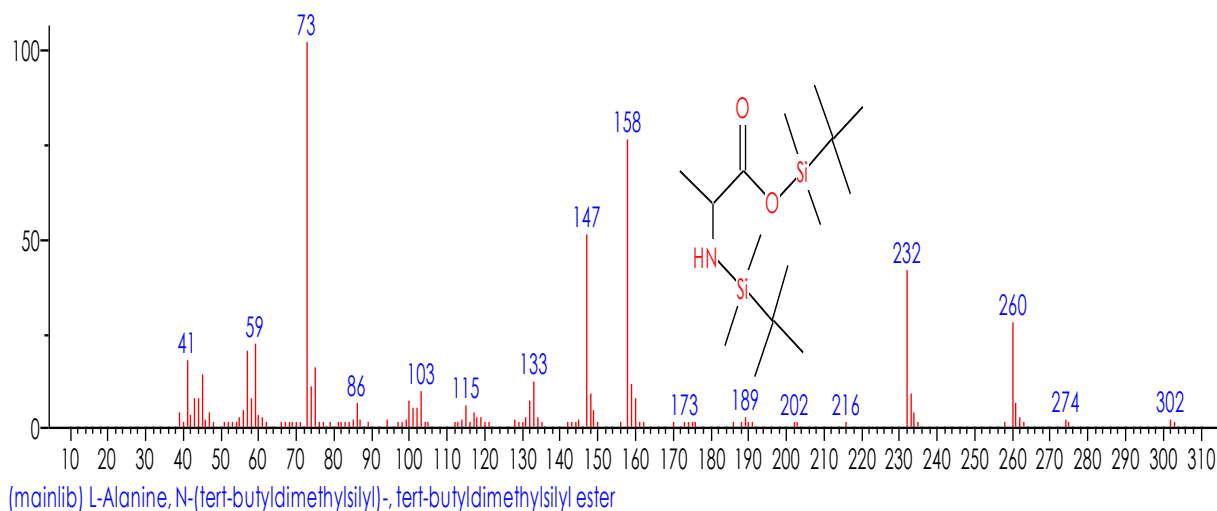


Figure 4-3. Mass spectrum obtained by silylated alanine fragmentation (from the NIST library) and diagram showing the different masses obtained after fragmentation. The masses observed 158, 232, 260 and 302, and the relative peak heights are specific for silylated alanine.

The further analysis of other majority masses present (here 158, 232, 260 and 302) which allows identification of alanine. This "further analysis" is performed by comparing the mass spectra obtained with reference spectra from NIST library.

This analysis also involves the theoretical study of the fragmentation of a molecule that may be causing the observed mass spectrum.

The mass spectra to be compared are obtained after subtraction of the raw spectra (possibly refined by further data treatment removing masses parasites), and the "noise." This noise corresponds to the mass spectrum observed at the baseline of the chromatogram, apart from the output of a peak chromatography. The exploitation and analysis of chromatograms therefore pass through many steps of data processing before identification.

This method enables the detection and identification of many compounds after tholins hydrolysis, in particular amino acids.

The others compounds for example the nitrogenous compounds, we can obtained through analyze the spectra directly.

### 4.2.3 The direct derivatization for non-hydrolyzed samples

In this method, we added MTBSTFA 80 $\mu$ l and DMF 30 $\mu$ l directly into the vial which contains ~2mg solid sample. The experimental conditions and the program for GC-MS have been mentioned in detail in 4.2.1.

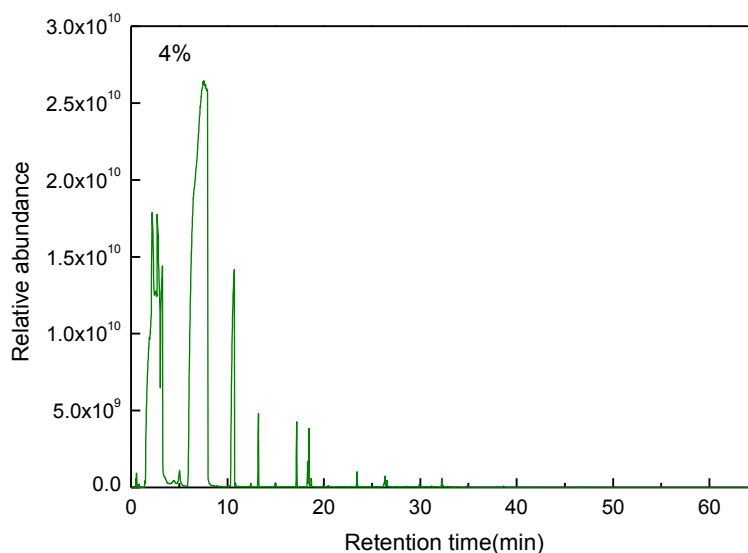


Figure 4-4. Chromatogram reconstructed from mass spectra obtained by injecting a direct derivatization sample of tholins (4%). Chromatographic conditions: column: Restek Rtx®-5Sil MS (Fused Silica) with 5-meter Integra-Guard MS 30m long, 0.25mm ID, 0.25 $\mu$ m df carrier flow(He) 1.0ml/min; temperature programming: isothermal at 50 $^{\circ}$ C for 3min, 4 $^{\circ}$ C min $^{-1}$  up to 280 $^{\circ}$ C isothermal at 280 $^{\circ}$ C for 5min; split: 1/20; temperature of injector 250 $^{\circ}$ C detector: mass spectrometer using 70eV EI.

**Figure 4-4** shows the chromatogram reconstructed from mass spectra obtained by injecting a direct derivatization sample of tholins (4%). The first part of the chromatogram between the start of acquisition and 15 min revealed main peaks due to the presence of pollutants (MTBSTFA degradation). But light compounds can be detected as well. The last part starting after 30 minutes until the end of the acquisition shows that the peaks are mainly due to the "bleeding" of the column. This phenomenon appears when the oven temperature is high and reached the maximum temperature of the column. However, it is necessary to reach a temperature sufficiently high to separate the heaviest (least volatile and) compounds and clean the column from heavier compounds. The acquisition time is also playing a role, so here we used a programming temperature isothermal at 50 $^{\circ}$ C for 3min, 4 $^{\circ}$ C min $^{-1}$  up to 280 $^{\circ}$ C

isothermal at 280°C for 5min to separate the maximum possible while limiting the compounds analysis time.

Same method has been used to analyze the results of all five samples. The complete analysis of the chromatograms **Figure 4-4** shows a large amount of peaks. Among all the peaks a major part of them are not in the NIST library. Then, only a little part of these peaks has been identified. This fact proves that the majority of the tholins compounds are not very common and very specific of the Titan chemistry.

The details of the chromatograms for the five samples are shown in **Figure 4-5**. Positions of the chromatographic peaks of compounds identified by NIST library are shown on the figure. There are also some peaks unidentified. **Figure 4-5** shows that all of the five chromatograms look similar. The same peaks are observed at the similar retention time and only the intensity of some of them differs among the chromatograms. **Table 4-3** together the molecules identified from the chromatograms.

Table 4-3. The compounds have been identified from the chromatographic peaks of Figure 4-5. Only has qualitative analysis. The retention time showed here for sample 4%, these identified compounds for others samples have the similar retention time.

Compounds	Formula	Retention time (min)	Peak number
3-(cyclopropylamino) propionitrile	C <sub>6</sub> H <sub>10</sub> N <sub>2</sub>	5.02	1
Methanimine,1-(1,4,4-trimethyl-2-tetrazenyl)-	C <sub>4</sub> H <sub>11</sub> N <sub>5</sub>	10.85	2
4H-indenol(2,1-d)thiazol-2-amine	C <sub>4</sub> H <sub>11</sub> N <sub>5</sub>	13.21	3
1H-pyrido(4,3-β)indol,2,3,4,5-tetrahydro-1,1,3,3-tetramethyl-	C <sub>15</sub> H <sub>20</sub> N <sub>2</sub>	18.45	4
2-Hydroxyethanoic acid	C <sub>2</sub> H <sub>4</sub> O <sub>3</sub>	22.20	5
Ethanedioic acid	C <sub>2</sub> H <sub>2</sub> O <sub>4</sub>	23.44	6
Urea	CH <sub>4</sub> ON <sub>2</sub>	26.34	7
Octadecanoic acid-bis[(trimethylsilyl-oxy] methyl ester	C <sub>25</sub> H <sub>54</sub> O <sub>4</sub> Si <sub>2</sub>	26.68	8

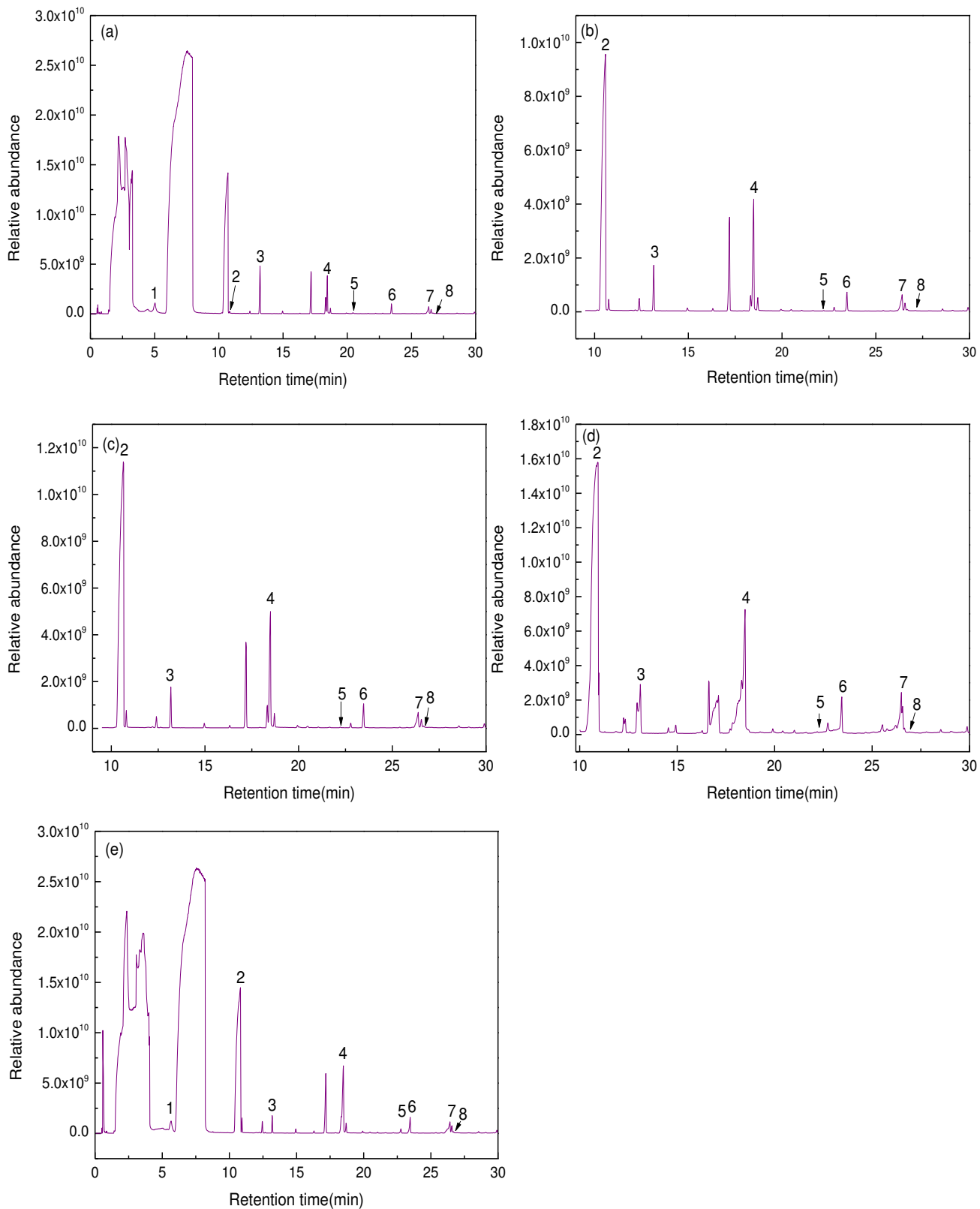


Figure 4-5. The detail chromatograms for five samples with different methane content percentage (a) 4%, (b) 6%, (c) 7%, (d) 8%, (e) 9%.



Throughout an analysis of the mass spectrum corresponding to each chromatographic peak, it can be noticed that there are some compounds can be identified after a direct derivatization for the non-hydrolyzed sample. The content of methane in the initial gaseous mixture does not have an obvious effect on the species of compounds which were identified. Oxygen is missing from the initial gas mixture ( $N_2/CH_4$ ) producing the tholins sample. However the chromatograms reveal the presence of large amounts of urea, when sample is subject to water or HCl hydrolysis, urea is a well-known compounds in tholins. It is certainly due to the oxygen contamination. Other oxygenated compounds have been detected such as ethanedioic and hydroxyl acetic acid. These compounds are oxygen-bearing molecules. The presence of these compounds in the raw aerosol analogues, not subjected to hydrolysis, was unexpected. So there exists an oxygen contaminant during a step of the sample treatment or/and the process for synthesizing the sample. Although this contamination is unintended, it offers interesting clues about aerosols analogues reactivity (Poch et al., 2012).

#### 4.2.4 Tholins hydrolysis in a neutral environment $H_2O$

The chromatograms in **Figure 4-6** present the results obtained after hydrolysis tholins in distilled water at neutral pH. **Table 4-4** together the molecules identified from the chromatograms. This table shows that more molecules are identified than with the direct derivatization. More nitrogenous compounds have been identified, but lots of other nitrogen compounds have not been identified because the NIST library does not contain them and/or there are not soluble in aqueous phase.

Some compounds are still identified after hydrolyzing tholins in pure water. This result indicates that even in hydrolysis reactions are somewhat less effective, tholins can also be hydrolyzed to form molecules include carboxylic acid, and also amino acid: here alanine and glycine. From these results we can observe that glycine, alanine and urea are present in samples exposed to water hydrolysis conditions but glycine, alanine are not present in samples which not expose to hydrolysis. We can also find that the compounds obtained for these five samples are the same so we can have the same conclusion with the first sample treatment method (direct derivatization with raw tholins). The content of methane in the initial gaseous mixture does not affect the quality of the compounds, but may have an influence on the quantity of these compounds. The quantification study has not been further studied in the present work.

Table 4-4. The compounds have been identified from the chromatographic peaks of Figure 4-6. Only has qualitative analysis. The retention time showed here for sample 4%, these identified compounds for others samples have the similar retention time.

Compound	Formula	Retention Time (min)	Main masses	Peak Number
<b>Carboxylic Acid</b>				
Ethanedioic acid	C <sub>2</sub> H <sub>2</sub> O <sub>4</sub>	23.49	73, 147, 261	8
2-Methylsuccinic acid	C <sub>5</sub> H <sub>8</sub> O <sub>4</sub>	29.08	73, 147, 303	12
<b>Hydroxy-Carboxylic Acid</b>				
2-Hydroxy propionic acid	C <sub>5</sub> H <sub>8</sub> O <sub>3</sub>	24.28	73, 147, 172	10
2-Hydroxyethanoic acid	C <sub>2</sub> H <sub>4</sub> O <sub>3</sub>	22.03	73, 147, 189, 247	6
<b>Amino Acid</b>				
Alanine	C <sub>3</sub> H <sub>7</sub> NO <sub>2</sub>	22.75	73, 158, 232, 260	7
Glycine	C <sub>2</sub> H <sub>5</sub> NO <sub>2</sub>	23.6	73, 147, 218, 246	9
<b>Others</b>				
Urea	CH <sub>4</sub> N <sub>2</sub> O	26.25	147, 231	11
1H,9-Pyrazolo[1,2-a]indazole 1,3(2H)-dione	C <sub>10</sub> H <sub>8</sub> N <sub>2</sub> O <sub>2</sub>	13.6		2
<b>Nitrogen compounds</b>				
Methanimine	C <sub>4</sub> H <sub>11</sub> N <sub>5</sub>	11.19		1
N-[3-[4-diethylamino-1-methylbutylamino] propyl] aziridine	C <sub>14</sub> H <sub>31</sub> N <sub>3</sub>	14.62		3
Imidazole	C <sub>3</sub> H <sub>4</sub> N <sub>2</sub>	16.44		4
1-H-Pyrido(4,3-b)indole,2,3,4,5-tetrahydro-1,1,3,3-tetramethyl-	C <sub>15</sub> H <sub>20</sub> N <sub>2</sub>	18.45		5

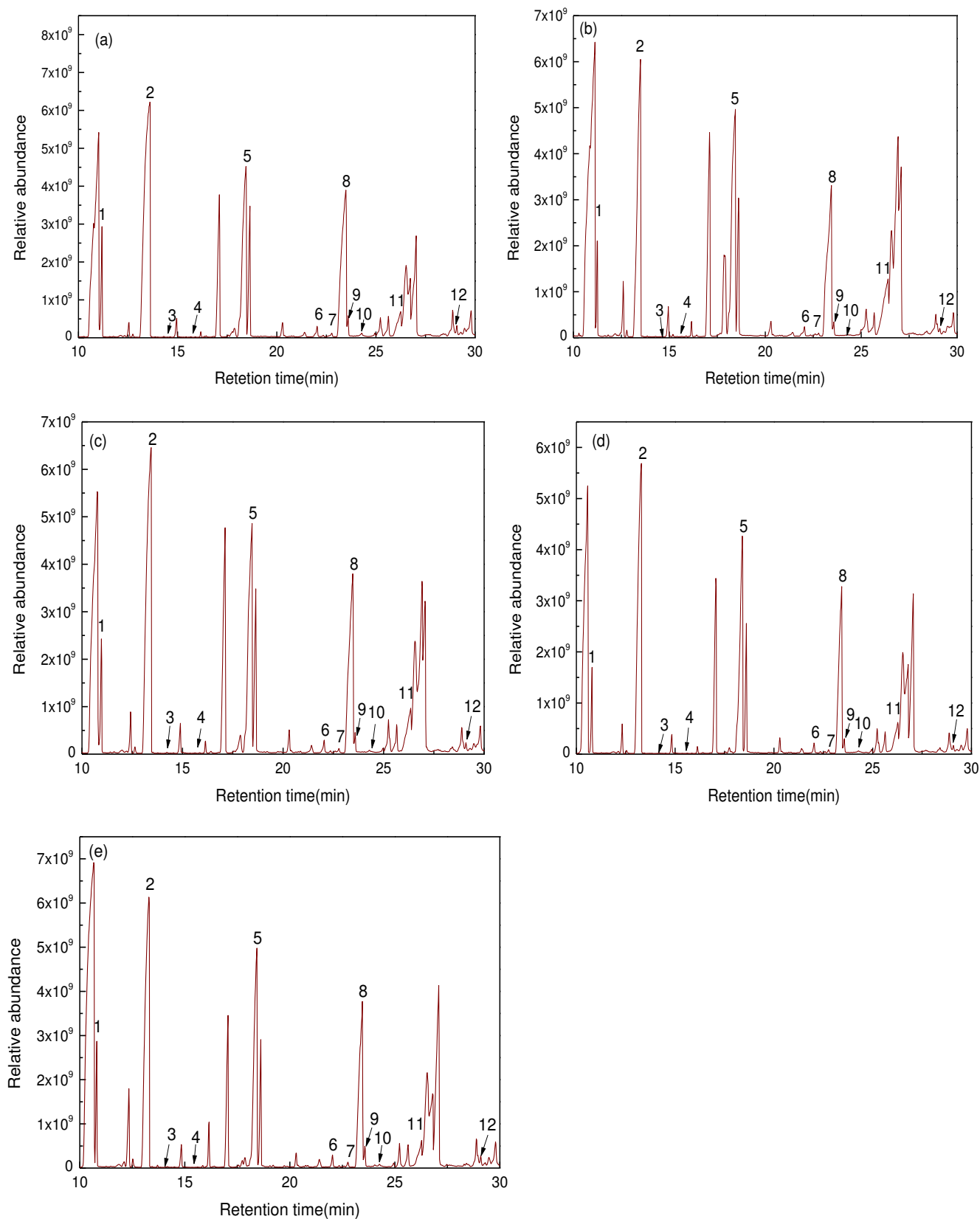


Figure 4-6. The gas chromatograms obtained after tholins hydrolysis in distilled water. The signal of the time range between 20 and 30 min. (a) 4%, (b) 6%, (c) 7%, (d) 8%, (e) 9%.

Extrapolating this result to the aerosols of Titan, these molecules could be present on the surface of Titan under conditions of hydrolysis in contact with water at neutral pH. This finding is particularly interesting and useful; because the possible presence of amino acids on the surface of Titan brings us back to the exobiology theory those amino acids can be formed on other planet not only on Earth.

#### **4.2.5 Tholins hydrolysis in acid environment HCl**

**Table 4-5** presents the identification of each chromatographic peaks obtained after hydrolysis using HCl for every samples. The corresponding peaks are showed on the chromatogram in **Figure 4-7** which is a restriction to time-range between 20 and 30 minutes (for the same reasons as with the case of chromatograms obtained after direct derivatization).

Table 4-5. The compounds have been identified from chromatographic peaks of Figure 4-7. Only has qualitative analysis. The retention time showed here for sample 4%, these compounds for others samples have the similar retention time.

Compound	Formula	Retention Time (min)	Main masses	Peak Number
<b>Carboxylic Acid</b>				
Ethanedioic acid	C <sub>2</sub> H <sub>2</sub> O <sub>4</sub>	23.41	73, 147, 261	3
Malonic acid	C <sub>3</sub> H <sub>4</sub> O <sub>4</sub>	25.84	73, 147, 189, 275	4
2-methylpropanedioic acid	C <sub>4</sub> H <sub>6</sub> O <sub>4</sub>	26.15	73, 147, 289	5
Butanedioic acid(Succinic acid)	C <sub>4</sub> H <sub>6</sub> O <sub>4</sub>	28.93	73, 147, 289	6
2-Methylsuccinic acid	C <sub>5</sub> H <sub>8</sub> O <sub>4</sub>	29.10	73, 147, 303	7
(E)-Butenedioic acid(Fumaric acid)	C <sub>4</sub> H <sub>4</sub> O <sub>4</sub>	29.70	73, 147, 287	8
3-Methyl-pentanedioic acid	C <sub>6</sub> H <sub>10</sub> O <sub>4</sub>	30.72	73, 147, 317	9
pentanedioic acid(Glutaric acid)	C <sub>5</sub> H <sub>8</sub> O <sub>4</sub>	31.26	73, 147, 303	10
<b>Hydroxy-Carboxylic Acid</b>				
2-Hydroxy propionic acid	C <sub>3</sub> H <sub>6</sub> O <sub>3</sub>	21.44	73, 147, 189, 233, 261	1
2-Hydroxyethanoic acid	C <sub>2</sub> H <sub>4</sub> O <sub>3</sub>	22.07	73, 147, 189, 247	2
<b>Amino Acid</b>				
Alanine	C <sub>3</sub> H <sub>7</sub> NO <sub>2</sub>	22.82	73, 147, 218, 260	11(6%, 7%)
<b>Others</b>				
Urea	CH <sub>4</sub> N <sub>2</sub> O	27.04	147, 231	12(6%)
1H,9-Pyrazolo[1,2-a]indazole1,3(2H)-dione	C <sub>10</sub> H <sub>8</sub> N <sub>2</sub> O <sub>2</sub>	13.82		
<b>Nitrogenous Compounds</b>				
Dimethylamine	C <sub>2</sub> H <sub>7</sub> N	0.52		
Methanimine 1-(1.4.4-trimethyl-2-tetrazenyl)-	C <sub>4</sub> H <sub>11</sub> N <sub>5</sub>	11.12		
Cyclizine	C <sub>18</sub> H <sub>22</sub> N <sub>2</sub>	17.80		
1H-Pyrido (4,3-β)indole,2,3,4,5-tetrahydro-1,1,3,3-tetramethyl-	C <sub>15</sub> H <sub>20</sub> N <sub>2</sub>	18.30		

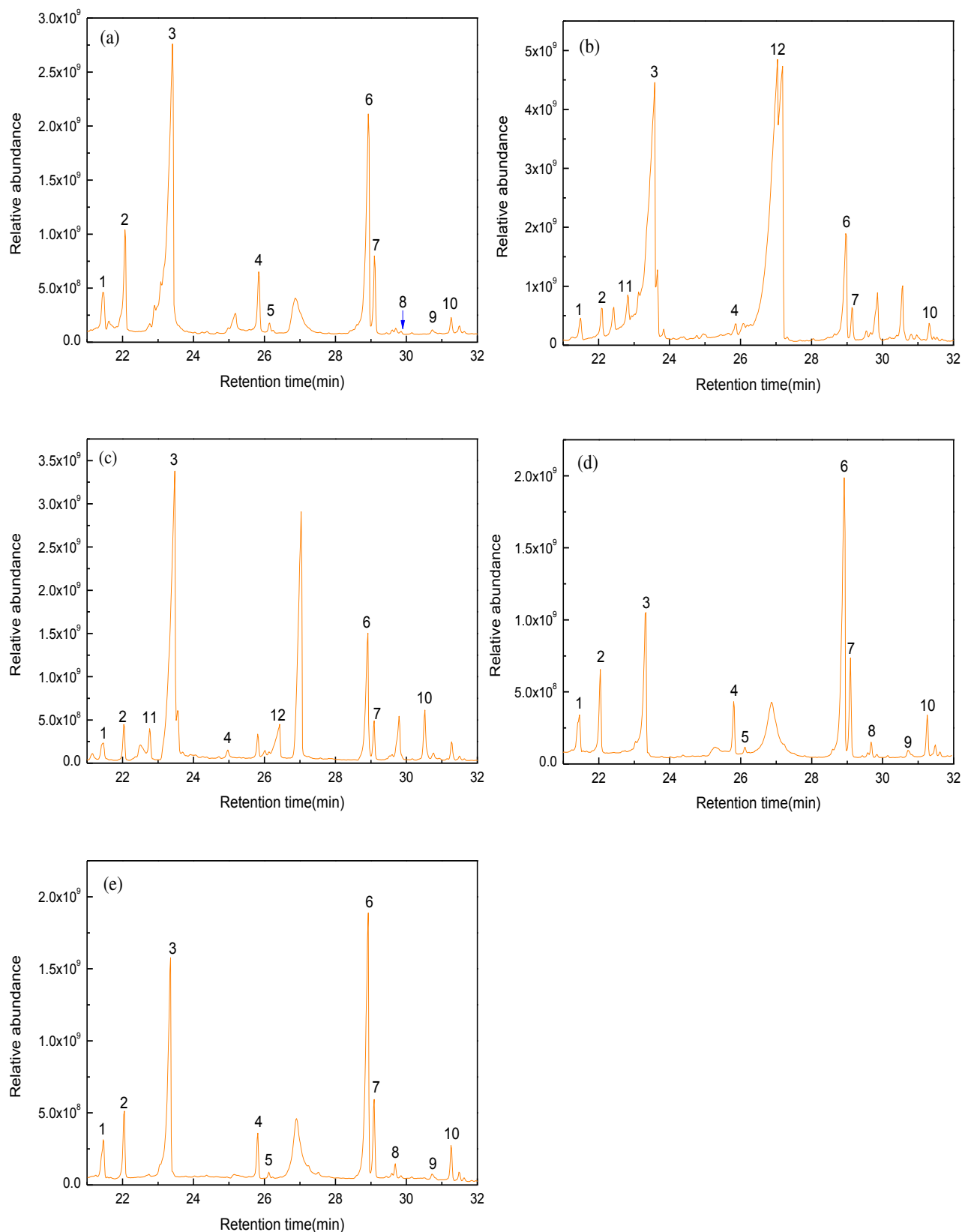


Figure 4-7. Chromatogram obtained after hydrolysis of tholins sample under condition of HCl (a) 4%, (b) 6%, (c) 7%, (d) 8%, (e) 9%.

From a general point of view, the chromatograms obtained by this hydrolysis method generate more peaks than that obtained after hydrolysis only with H<sub>2</sub>O. However the nitrogenous compounds detected are quite similar with the compounds obtained with the other extraction procedure. That means that water or acid hydrolysis does not improve the nitrogenous compounds.

Only one amino acid is identified, against only two in the H<sub>2</sub>O hydrolysis. The glycine acid disappears and the identified amino acid alanine only appears for sample 6% and 7%. The others treated samples did not contain this amino acid. However, a higher number of carboxylic acids were observed after hydrolysis by HCl. On the basis of these results, we can possible have the hypothesis that when the hydrolysis conditions more acids, amino acids could be further degraded into carboxylic acids. The following reaction pathway can be used to explain this hypothesis. These results have already been underlined by Brault et al., 2013 when they studied the influence of the acidic treatment for meteoritic sample. They found a range of degradation of 5 to 20% after hydrolysis treatment on pure amino acids.

### **4.3 The products of chemical evolution of Titan's tholins and how they may form**

First of all even if we have detected some nitrogenous compounds such as dimethylamine or methanimine 1-(1.4.4-trimethyl-2-tetrazenyl)-, few N-compounds have been identified. Two major reasons could explain that fact.

- the number of unidentified peak is important. Most of these peaks seem to be related with N-compounds but the NIST library does not contain these organic products meaning they are atypical.
- the extraction procedure is more favorable to solubilize compounds soluble in water. But most of nitrogenous compounds are poorly soluble in water.

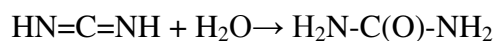
We have shown that the direct derivatization of raw tholins produces urea, which were unexpected because of the oxygen element is not including in the initial gas mixture. It means that there is an oxygen contaminant during a step of the experiment. The incorporation of oxygen may result from the following processes.

The H<sub>2</sub>O and O<sub>2</sub> coming from the laboratory atmosphere can contaminate the sample during the sample synthesis, as the samples are exposed to air during their collection after

their synthesis. The sample can absorb H<sub>2</sub>O vapor leading to a partial hydrolysis of the samples. Maybe this procedure can also happen during the storage of the samples.

A chromatographic peak corresponding to the derivatization product of water was detected in all of our samples. This presence of water can be attributed to the hygroscopic character of tholins during the derivatization process, adsorbing atmospheric water as soon as it is in contact with water. Moreover the MTBSTFA and the DMF contain some trace of water which can explain why we have detected derivatized water in our entire sample.

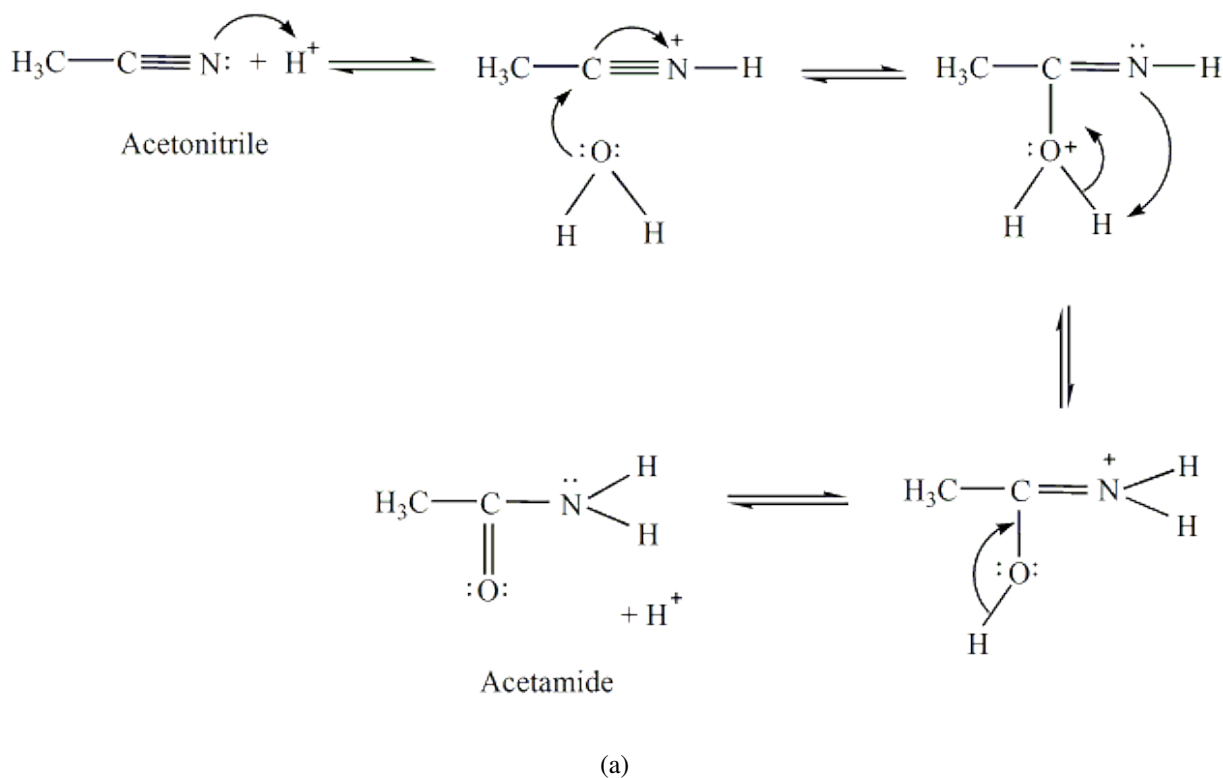
For explaining the production of the identified compounds during the hydrolysis of the samples, their chemical nature can be taken into account. For example, high urea production could be explained by the presence of carbodiimide groups (-N=C=N-) actually suspected or cyanamides (NH<sub>2</sub>-C≡N), very reactive towards a nucleophilic attack such as that of a water molecule (Poch et al., 2012):



Furthermore, the formation of amino acids and carboxylic acid can be explained through classical chemical organic pathway, mainly basic hydrolysis. The study of reaction pathways leading to the hydrolysis products can be explained by nitrile molecules present in the solution. Reaction mechanisms presented here are made from the theoretical study of hydrolysis in organic chemistry by Vollhardt and Schore (Vollhardt et al., 1995; Mai-Julie NGUYEN, 2007) .

**Figure 4-8** shows the chemical pathway to form carboxylic acid from simple nitrile. The pathway followed is the same for training more complex carboxylic acids identified in the hydrolysis products. This reaction pathway contains two major procedures. Firstly, the amide intermediate form and then convert to the carboxylic acid in the further hydrolysis reaction.





Step 1: An acid reaction. The nucleophile activate the nitrile, protonation makes it more electrophilic.

Step 2: The water O functions as the nucleophile attacking the electrophilic C in the  $C\equiv N$ , with the electrons moving towards the positive center.

Step 3: An acid reaction. Deprotonate the oxygen that came from the water molecule. The remaining task is a tautomerization at N and O centers.

Step 4: An acid reaction. Protonate the N gives us the  $-NH_2$  we need.

Step 5: Use the electrons of an adjacent O to neutralise the positive at the N and form the  $\pi$  bond in the  $C=O$ .

Step 6: An acid reaction. Deprotonation of the oxonium ion reveals the carbonyl in the amide intermediate.

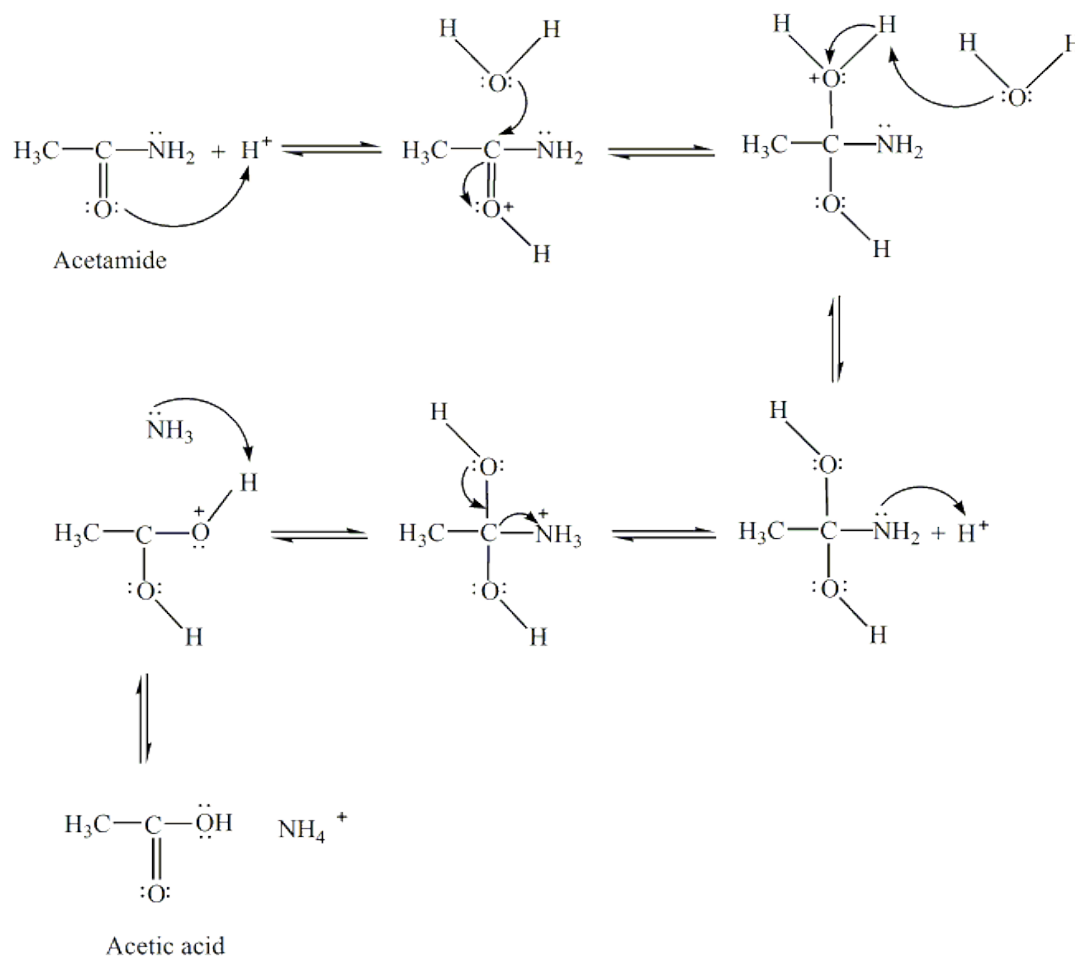


Figure 4-8. Reaction pathway for the hydrolysis of the acetonitrile in the presence of water to form acetic acid (a) from acetonitrile to acetamide (b) from acetamide to acetic acid.

**Step 1:** An acid reaction. Since we only have a weak nucleophile and a poor electrophile we need to activate the ester. Protonation of the amide carbonyl makes it more electrophilic.

**Step 2:** The water O functions as the nucleophile attacking the electrophilic C in the C=O, with the electrons moving towards the oxonium ion, creating the tetrahedral intermediate.

**Step 3:** An acid reaction. Deprotonate the oxygen that came from the water molecule.

**Step 4:** An acid reaction. Need to make the  $\text{-NH}_2$  leave, but need to convert it into a good leaving group first by protonation.

**Step 5:** Use the electrons of adjacent oxygen to help "push out" the leaving group, a neutral ammonia molecule.

**Step 6:** An acid reaction. Deprotonation of the oxonium ion reveals the carbonyl in the carboxylic acid product and regenerates the acid catalyst.

Nitriles are also present in the way of chemical reactions leading to the formation of amino acids as shown in **Figure 4-9** below.

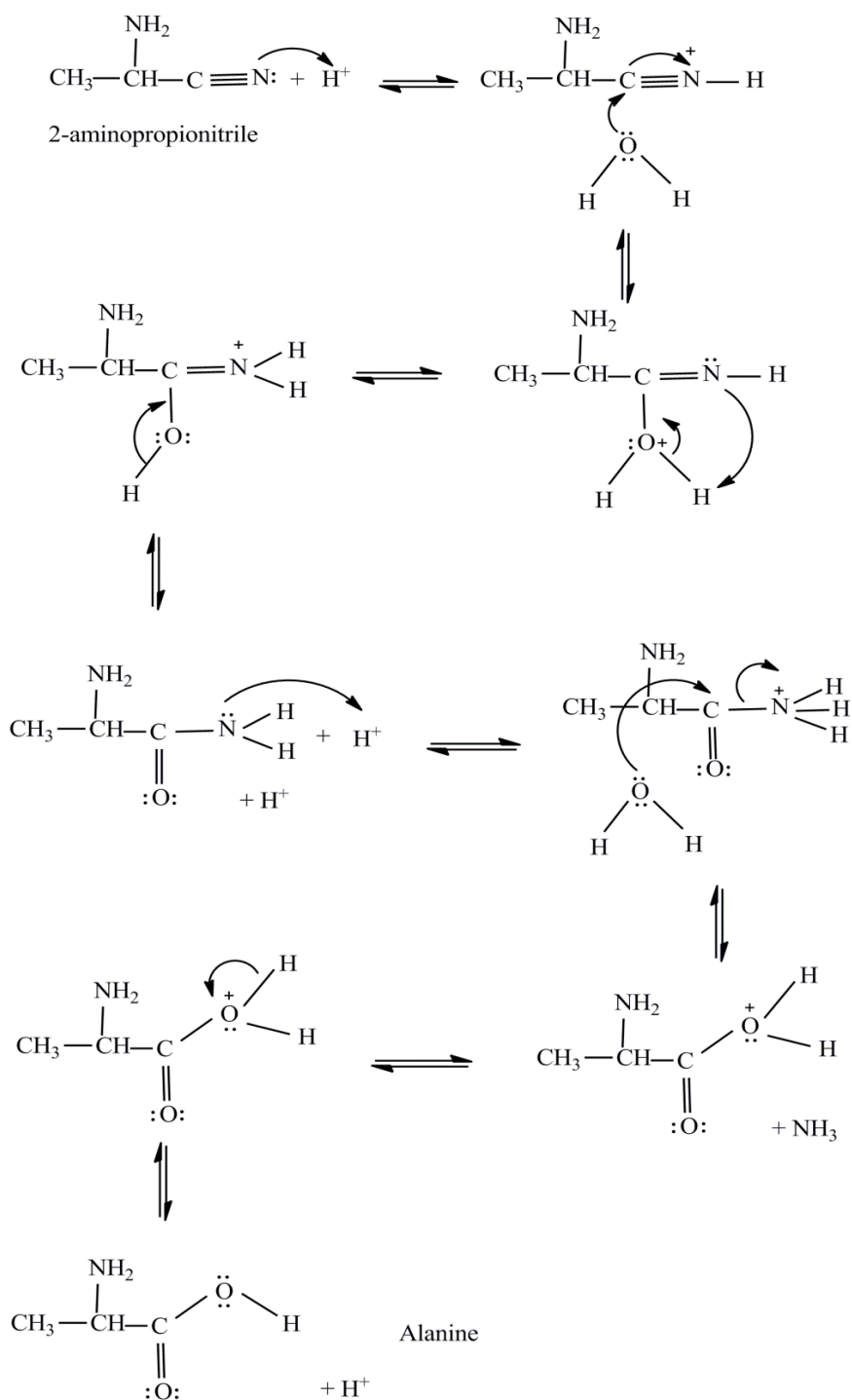


Figure 4-9. Reaction pathway leading to the formation of alanine from the hydrolysis of 2-aminopropionitrile (Mai-Julie NGUYEN, 2007).

The study of this pathway can be extended by further reaction in a particularly strong hydrolysis (see **Figure 4-10** below).

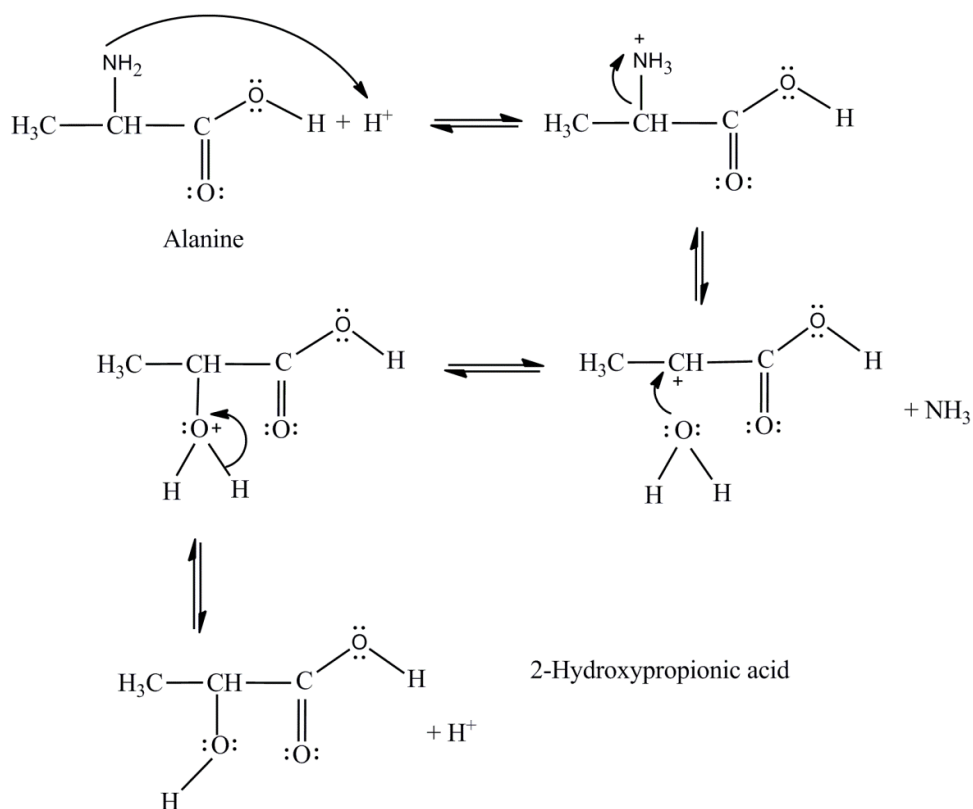


Figure 4-10. Hydrolysis of alanine under very acidic pH leads to the formation a hydroxyl-carboxylic acid (Mai-Julie NGUYEN, 2007).

The sum of the protons on alanine and glycine affects its hydrolysis with the substitution of the amine function with an alcohol. The observation of this additional step would explain the phenomenon that the disappearance of amino acids during the hydrolysis with HCl. A hypothesis had previously been proposed in front part that amino acids could have been degraded into other molecules in stronger hydrolysis conditions and that this could explain the lower number in observed amino acids after hydrolysis with HCl to the number observed after hydrolysis with H<sub>2</sub>O. This allows us to see that alanine in particular can be degraded into 2-hydroxy propionic acid, a molecule actually identified as peak 1 on the chromatogram of **Figure 4-7**. This peak is also one of the majority peaks in the chromatogram. Similarly, glycine can degrade alike and form acetic 2-hydroxyethanoic acid, which is also detected during the analysis. It is therefore quite possible that glycine and alanine also involved their degradation products in the chromatograms. It is interesting to note that the two alcohol-carboxylic acids, identified during hydrolysis can be explained by the degradation of two identified amino acids. The amine functions are involved in the process that amino acids

converse to carboxylic acids: they were attacked in the strong hydrolysis conditions such as those conducted with HCl.

Urea is present in direct derivatization of raw tholins and tholins after hydrolysis using distilled H<sub>2</sub>O. In the hydrolysis using HCl method, urea appeared only in the 6% methane tholins sample. It is known that on Earth, urea is one of the main compounds found in metabolism processes such as the oxidation of amino acids or nitrogenous compounds. In (Ramírez et al., 2010) study, they found that the quantity of urea shows a relationship with the quantity of amino acids, for example alanine and glycine. When urea yields increase, those of alanine and glycine decrease. So they concluded that urea has an important role in the interactions among the hydrolysis products as the smallest of all the synthesized compounds. Urea is one of the by-products of amino acid further oxidation.

The study of hydrolysis pathway allows explaining the absence of urea when HCl is present in very large quantities.

The degradation reaction of the urea is shown in **Figure 4-11**. The degradation pathway of the urea leads to the formation of carbon dioxide molecule.

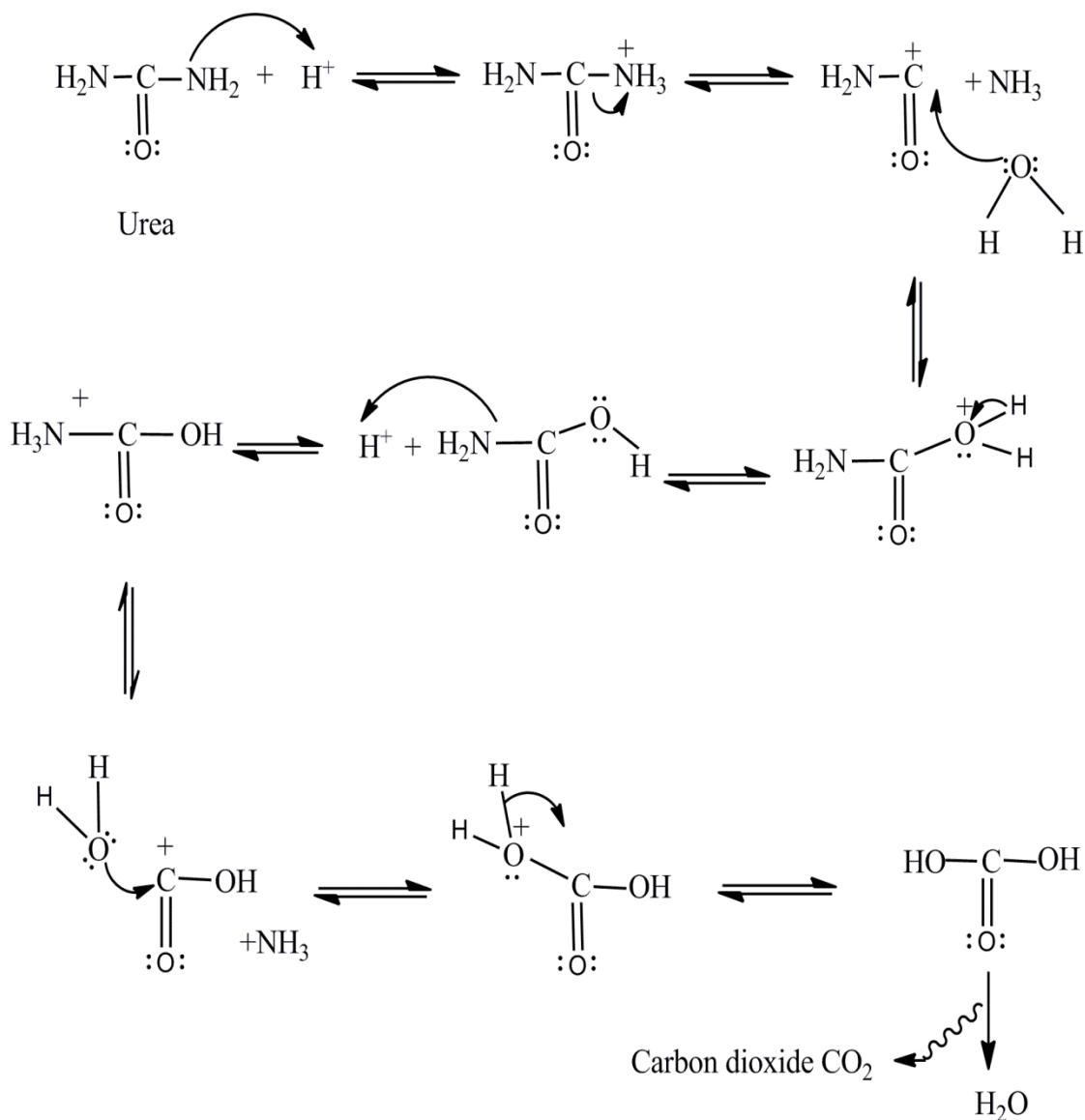


Figure 4-11. Degradation pathway Urea by protonation of the amine functions (Mai-Julie NGUYEN, 2007) .

Through using these reaction pathways to study the identified molecules after tholins suffered the  $\text{H}_2\text{O}$  and  $\text{HCl}$  hydrolysis treatment, the primary products may be present in the soluble phase of tholins that lead to the formation of these identified molecules were obtained and summarized in **Table 4-6**.

Final Product			Intermediate or primary product		
Name	Formula	Structural Formula	Name	Formula	Structural Formula
<b>Amino Acid</b>					
Alanine	C <sub>3</sub> H <sub>7</sub> NO <sub>2</sub>	CH <sub>3</sub> -CH(NH <sub>2</sub> )-COOH	2-aminopropionitrile	C <sub>3</sub> H <sub>6</sub> N <sub>2</sub>	CH <sub>3</sub> -CH(NH <sub>2</sub> )-CN
Glycine	C <sub>2</sub> H <sub>5</sub> NO <sub>2</sub>	CH <sub>2</sub> (NH <sub>2</sub> )-COOH	Cyanamide	CH <sub>2</sub> N <sub>2</sub>	NH <sub>2</sub> -CN
2-Amio-2-methylpropionic	C <sub>4</sub> H <sub>9</sub> NO <sub>2</sub>	(CH <sub>3</sub> ) <sub>2</sub> C(NH <sub>2</sub> )-COOH	2-amino-2-methylpropanenitrile	C <sub>4</sub> H <sub>8</sub> N <sub>2</sub>	(CH <sub>3</sub> ) <sub>2</sub> -C(NH <sub>2</sub> )-CN
<b>Carboxylic Acid</b>					
Ethanedioic acid	C <sub>2</sub> H <sub>2</sub> O <sub>4</sub>	COOH-COOH	Ethanedinitrile(Cyanogen)	C <sub>2</sub> N <sub>2</sub>	NC-CN
Malonic acid	C <sub>3</sub> H <sub>4</sub> O <sub>4</sub>	COOH-CH <sub>2</sub> -COOH	Propanedinitrile(Malononitrile)	C <sub>3</sub> H <sub>2</sub> N <sub>2</sub>	NC-CH <sub>2</sub> -CN
2-Methylpropanedioic acid	C <sub>4</sub> H <sub>6</sub> O <sub>4</sub>	COOH-CH(CH <sub>3</sub> )-COOH	2-methyl-Malononitrile	C <sub>4</sub> H <sub>4</sub> N <sub>2</sub>	NC-CH(CH <sub>3</sub> )-CN
Butanedioic acid(Succinic acid)	C <sub>4</sub> H <sub>6</sub> O <sub>4</sub>	COOH-CH <sub>2</sub> -CH <sub>2</sub> -COOH	Butanedinitrile	C <sub>4</sub> H <sub>4</sub> N <sub>2</sub>	NC-CH <sub>2</sub> -CH <sub>2</sub> -CN
2-Methylsuccinic acid	C <sub>5</sub> H <sub>8</sub> O <sub>4</sub>	COOH-CH <sub>2</sub> -CH(CH <sub>3</sub> )-COOH	Methyl-butanenitrile	C <sub>5</sub> H <sub>6</sub> N <sub>2</sub>	NC-CH <sub>2</sub> -CH(CH <sub>3</sub> )-CN
(E)-Butenedioic acid(Fumaric acid)	C <sub>4</sub> H <sub>4</sub> O <sub>4</sub>	COOH-CH=CH-COOH	(2Z)-2-Butenedinitrile	C <sub>4</sub> H <sub>2</sub> N <sub>2</sub>	NC-CH=CH-CN
3-Methyl-pentanedioic acid	C <sub>6</sub> H <sub>10</sub> O <sub>4</sub>	COOH-CH <sub>2</sub> -CH(CH <sub>3</sub> )-CH <sub>2</sub> -COOH	3-Methyl-Pentanedinitrile	C <sub>6</sub> H <sub>8</sub> N <sub>2</sub>	NC-CH <sub>2</sub> -CH(CH <sub>3</sub> )-CH <sub>2</sub> -CN
Pentanedioic acid(Glutaric acid)	C <sub>5</sub> H <sub>8</sub> O <sub>4</sub>	COOH-CH <sub>2</sub> -CH <sub>2</sub> -CH <sub>2</sub> -COOH	Pentanedinitrile	C <sub>5</sub> H <sub>6</sub> N <sub>2</sub>	NC-CH <sub>2</sub> -CH <sub>2</sub> -CH <sub>2</sub> -CN
<b>Carboxylic Acid, Alcohol</b>					
2-Hydroxy propionic acid	C <sub>3</sub> H <sub>6</sub> O <sub>3</sub>	CH <sub>3</sub> -CH(OH)-COOH	Alanine	C <sub>3</sub> H <sub>7</sub> NO <sub>2</sub>	CH <sub>3</sub> -CH(NH <sub>2</sub> )-COOH
2-Hydroxyethanoic acid	C <sub>2</sub> H <sub>4</sub> O <sub>3</sub>	CH <sub>2</sub> (OH)-COOH	Glycine	C <sub>2</sub> H <sub>5</sub> NO <sub>2</sub>	CH <sub>2</sub> (NH <sub>2</sub> )-COOH
<b>Others</b>					
Urea	CH <sub>4</sub> N <sub>2</sub> O	NH <sub>2</sub> -CO-NH <sub>2</sub>	Cyanamid	CH <sub>2</sub> N <sub>2</sub>	NH <sub>2</sub> -CN

Table 4-6. Summary of the primary products which can lead to the formation of molecules identified after hydrolysis in HCl, distilled water.

Because there also exist other reaction pathways could be implicated the formation of the identified molecules. This analysis and all reaction pathways described above should be taken with caution.

## 4.4 Conclusion

In this chapter, three different treatment methods were applied to Titan's tholins, and the products were analyzed by GC-MS. Through these experiments, we can conclude that:

1. The study of the hydrolysis of tholins under the closest environmental conditions of Titan has been carried out. The soluble part of the aerosols on Titan contain chemical functions (amines, nitriles) which have been detected and, which can react with water and form new molecules comprising amino acids, carboxylic acids with or without alcoholic function, and urea. This study showed that aerosols could evolve chemically after sedimenting on the surface of Titan, even in inefficient hydrolysis conditions (at neutral pH), and form new molecules which include amino acids and urea. The study also showed that these amino acids could in turn develop and produce other molecules containing carboxylic acids and alcohol groups.

2. The oxygen bearing compounds detected in the raw tholins without hydrolysis reveals that the oxygen incorporation may happen during synthesis, collection, storage or derivatization. This oxygen incorporation infers that Titan's tholins are highly reactive in any source of oxygen. Traces of CO, CO<sub>2</sub>, and H<sub>2</sub>O detected in Titan's atmosphere might play a role in the incorporation of oxygen in Titan's aerosol (Poch et al., 2012).

3. When using the HCl hydrolysis method, less amino acid were obtained than expected (even no amino acids). It has been shown that these amino acids had probably been degraded into other molecules containing acid functions carboxylic acid and alcohol. We could detect amino acids only in the methane content percentage 6% and 7% tholins samples. This overview should be pursued by a quantitative study that would extrapolate computing the amount of products that may have accumulated. In a further study, if we want to closer simulate the surface conditions on Titan, there are also some processes which can be studied: for example if the tholins can react with ice water and what compounds can be obtained after this treatment.



Further study is required in order to better understand the difference between the chemical processes inducing tholins formation with the PLASMA and PAMPRE simulations. Other future works should be to quantify the species detected with an internal standard.

---

## Conclusions and perspectives

In this thesis, The PAMPRE simulation experience allows conducting a systematic study of the physicochemical properties of Titan aerosols analogue (tholins), for example their chemical composition, their thermal characterization, chemical structure and their evolution on the surface of Titan. Tholins produced using different simulated techniques are fundamentally different in terms of physical and chemical properties. Based on this thesis work, the conclusions that we can acquire are summarized in the following:

### Conclusions

Tholins chemical properties study can benefit from application of techniques already developed for the study of polymers and macromolecules on Earth. Tholins are kerogen-like in structure and have similar refractive indices. These materials may be kerogen-like in structure containing a variety of functionalities extensively cross-linked. Pyrolysis appears to break covalent bonds liberating smaller, volatile and semi-volatile compounds that can be separated by GC and characterized by MS.

So in the first part of this thesis, we used Pyr-GC-MS technique to study tholins produced with 5pc and 10pc of CH<sub>4</sub>. The number of pyrolysates increase with the temperature increases most of them are nitrogen compounds, while pyrolysis temperature 600°C is a turning point. Only a few differences have been found out between tholins 5pc and tholins 10pc. Pyrrole and its isomers appear at lower temperature for sample 10pc. The benzene and toluene emerge behavior is also different for these two samples. As they are heated, tholins are chemically altered. The evolution of HCN and acetonitrile can be explained through a mechanism similar to the one by which polyacrylonitrile thermally degrades, involving cyclization and aromatization.

The presence of both NH<sub>3</sub> and HCN can demonstrate that nitrogen can be incorporate into Titan's aerosol in different ways, and the general presence of nitrogen in the aerosol suggest that the aerosol acts as an important sink for atmospheric nitrogen (Israël et al., 2005). After comparing with the result of ACP experiment, confirm that the aerosol analogues produced in PAMPRE set-up capable to simulate Titan's aerosols, as found in Coll et al., 2012.

The thermal degradation research showed that sample 10pc lost more weight and faster than sample 5pc when temperature get to 800°C, therefore the thermal stability of tholins may be influence by the content of methane used in their synthesis. The thermal degradation of all the samples was divided into three stages: drying stage, main pyrolysis stage and carbonization. The results of TG-MS revealed the volatile species of thermal decomposition and fragmentation processes for these two samples. The majority of thermal decomposable components in the tholins releases hydrocarbons, such as methane, ethylene, amongst other monomeric components. The thermal degradation of the material produces small gaseous cracking fragments involving HCN, C<sub>2</sub>H<sub>4</sub> and C<sub>2</sub>N<sub>2</sub> and the residue is no more chemically representative of the initial material, converging towards an amorphous graphitic carbon nitride structure. The shape of the major signals ion intensity curves explains why there are one more peak in the DTG curve of sample 10pc than sample 5pc.

Through the further study for the residues at different temperatures, we found that the functional structure (infrared spectroscopy), the elemental percentage (elemental analysis), the position and intensity of the D and G, change with the temperature. The strongly attached contribution of nitrogen in the tholins structure has been confirmed by the elemental analysis and IR results. The IR spectra for the initial tholins sample and different heating residues show that all the functional groups changed with the temperature. The elemental analysis shows important nitrogen content in the final residue 800°C.

To conclude about the physicochemical evolution of the material during thermal degradation in our experiences, it is possible to say that tholins carbonize gradually, with a removal of the heteroatoms. This loss of nitrogen and hydrogen is accompanied by loss of function aliphatic (alkyls), which will permit polyaromatic units to grow, and the carbon chain to reorganize.

After studying the intrinsic properties of tholins, the chemical evolution behavior about the tholins deposit on the surface of Titan was also carried out in the chapter 4. The previous studies showed that aerosols could chemically evolve in a highly acidic environment. In this study we confirm that tholins produced by the PAMPRE experiment could evolve chemically after sediment on the surface of Titan, even in the inefficient hydrolysis conditions (at neutral pH), and form new molecules which include amino acids and urea. The study also showed that these amino acids could continue to develop and produce other molecules containing carboxylic acids and alcohol groups in the acidic environment. But the compounds

including oxygen detected in the raw tholins without hydrolyzation reveals that the oxygen incorporation may have happened during synthesis, collection, storage or derivatization steps. This oxygen incorporation infers that Titan's tholins are highly reactive with any source of oxygen traces. CO, CO<sub>2</sub>, and H<sub>2</sub>O detected in Titan's atmosphere might play a role in the incorporation of oxygen in Titan's aerosol as the result in (Poch et al., 2012).

In Titan's atmosphere, the biologically relevant molecules may be produced in the gas phase, the results in our study indicate that tholins can generate biological precursors when exposed to liquid water. Therefore, we can deduce as a conclusion that, chemistry important to life may be happening on the surface of Titan where liquid water might exist (such as cryovolcanic flows or impact-generated melt pools). However, the temperature on Titan is so low that if life on Titan exists, it would likely be very different from life on earth (or very rare) due to the chemical and physical constraints of subsisting at such low temperatures (Cable et al., 2012).

### **Perspectives**

Results of the Pyr-GC-MS analysis showed interesting results but we need some time to find the problem that prohibits accomplishing the second set of experiments, and try to finish this series experiment. The result for this experiment is also interest for us. Other future works should be to quantify the species detected with the use of an internal standard.

The study of the hydrolysis of tholins in closer conditions than those on Titan showed that aerosols could chemically change when deposited on the surface of Titan, even in contact with water at neutral pH, and form many molecules such as two amino acids (glycine and alanine). But on the base of the qualitative results that we have obtained, this overview should be pursued by a quantitative study that would extrapolate the computing of the amount of products that may have accumulated. In a further study, if we want to simulate closer to the surface conditions on Titan, there are also some processes that can be improved, for example if the tholins can reacted with the ice water and what compounds can be obtained after this treatment.

Further study is required to better understand the difference between the chemical processes inducing tholins formation with the different simulation methods.

Although we have realized a series of simulation method to overcome the difficult for studying the aerosols of Titan, we must also keep in mind that the simulation conditions in the laboratory on Earth are also limited and different from the real Titan. Tholins are also complex chemical material, there is not a complete profile of their composition and structure yet. The new and adequate sample analysis techniques are also needed to accomplish this goal. So in order to prepare the best instrument package for the next in situ mission to Titan, we need to discover the most appropriate analysis technique on Earth.

---

## References

- Alcouffe, G., Cavarroc, M., Cernogora, G., Ouni, F., Jolly, a, Boufendi, L., & Szopa, C. (2010). Capacitively coupled plasma used to simulate Titan's atmospheric chemistry. *Plasma Sources Science and Technology*, *19*(1), 015008.
- A. Brault, A. Buch, C. Freissinet (2013). Influence of hydrolysis on amino acid degradation, submitted, 2013.
- Anderson, C. M., & Samuelson, R. E. (2011). Titan's aerosol and stratospheric ice opacities between 18 and 500 $\mu$ m: Vertical and spectral characteristics from Cassini CIRS. *Icarus*, *212*(2), 762–778.
- Artemieva, N., & Lunine, J. (2003). Cratering on Titan: impact melt, ejecta, and the fate of surface organics. *Icarus*, *164*(2), 471–480.
- Bar-Nun, A., Kleinfeld, I., & Ganor, E. (1988). Shape and optical properties of aerosols formed by photolysis of acetylene, ethylene, and hydrogen cyanide. *J. Geophys. Res.*, *93*(D7), 8383–8387.
- Bernard, J., Quirico, E., Brissaud, O., Montagnac, G., Reynard, B., Mcmillan, P., Coll, P., et al. (2006). Reflectance spectra and chemical structure of Titan's tholins: Application to the analysis of Cassini–Huygens observations. *Icarus*, *185*(1), 301–307.
- Bernard, J.-M., Coll, P., Coustenis, A., & Raulin, F. (2003). Experimental simulation of Titan's atmosphere: Detection of ammonia and ethylene oxide. *Planetary and Space Science*, *51*(14-15), 1003–1011.
- Blau, K., & King, G. S. (1978). *Handbook of derivatives for chromatography*. Heyden.
- Bonal, L., Quirico, E., Bourot-Denise, M., & Montagnac, G. (2006). Determination of the petrologic type of CV3 chondrites by Raman spectroscopy of included organic matter. *Geochimica et Cosmochimica Acta*, *70*(7), 1849–1863.

- Bonnet, J.-Y. (2012). L'azote comme élément mineur dans les macromolécules organiques chondritiques et cométaires: simulations expérimentales contraintes par les cosmomatériaux. Ph.D. thesis. Université de Grenoble, France.
- Borucki, W. J., Giver, L. P., McKay, C. P., Scattergood, T., & Parris, J. E. (1988). Lightning production of hydrocarbons and HCN on Titan: Laboratory measurements. *Icarus*, 76(1), 125–134.
- Brack, A. (2007). From Interstellar Amino Acids to Prebiotic Catalytic Peptides: A Review. *Chemistry & Biodiversity*, 4(4), 665–679.
- Brown, R. H., Baines, K. H., Bellucci, G., Bibring, J.-P., Buratti, B. J., Capaccioni, F., Cerroni, P., et al. (2004). The Cassini Visual And Infrared Mapping Spectrometer (Vims) Investigation. *Space Science Reviews*, 115(1-4), 111–168.
- Brown, R., Lebreton, J., & Waite, J. (2009). *Titan from Cassini-Huygens*.
- Cable, M. L., Hörst, S. M., Hodyss, R., Beauchamp, P. M., Smith, M. a., & Willis, P. a. (2012). Titan tholins: simulating Titan organic chemistry in the Cassini-Huygens era. *Chemical reviews*, 112(3), 1882–1909.
- Cabane M, Rannou P, Chassefi ere E, Israel G (1993). Fractal aggregates in Titan's atmosphere. *Planetary and Space Science*, 41:257–267
- Cardona, M., & Guntherodt, G. (1982). *Light scattering in solids III. Topics in Applied Physics* (Vol. 51).
- Carrasco, N, Alcaraz, C., Dutuit, O., Plessis, S., Thissen, R., Vuitton, V., Yelle, R., et al. (2008). Sensitivity of a Titan ionospheric model to the ion-molecule reaction parameters. *Planetary and Space Science*, 56(12), 1644–1657.
- Carrasco, N, Schmitz-Afonso, I., Bonnet, J.-Y., Quirico, E., Thissen, R., Dutuit, O., Bagag, a, et al. (2009). Chemical characterization of Titan's tholins: solubility, morphology and molecular structure revisited. *The journal of physical chemistry. A*, 113(42), 11195–203.
- Carrasco, Nathalie, Gautier, T., Es-sebbar, E., Pernot, P., & Cernogora, G. (2012). Volatile products controlling Titan's tholins production. *Icarus*, 219(1), 230–240.

- Cavarroc, M. (2007). Nucléation , croissance et comportement de poussières dans les plasmas réactifs radiofréquence basse pression: Des nanocristaux aux grains submicroniques polycristallins. Ph.D. thesis. Université d'Orléans, France.
- Clarke, D., & Ferris, J. (1997). Chemical evolution on Titan: comparisons to the prebiotic Earth. *Origins of Life and Evolution of the Biosphere*, 27, 225–248.
- Coates, A.J., Crary, F.J., Lewis, G.R., Young, D.T., Waite, J.H., Sittler, E.C., 2007. Discovery of heavy negative ions in Titan's ionosphere. *Geophysical Research Letters* 34, L22103.
- Coll, P, Coscia, D., & Gazeau, M. (1998). Review and latest results of laboratory investigations of Titan's aerosols. *Origins of Life and Evolution of the Biosphere*, 28, 195–213.
- Coll, P, Coscia, D., Smith, N., Gazeau, M., Ramirez, S., Cernogora, G., Israel, G., et al. (1999). Experimental laboratory simulation of Titan's atmosphere: aerosols and gas phase. *Planetary and Space Science*, 47(10-11), 1331–1340.
- Coll, P, Coscia, D., Gazeau, M. C., & Raulin, F. (1997). New planetary atmosphere simulations: application to the organic aerosols of Titan. *Advances in space research: the official journal of the Committee on Space Research (COSPAR)*, 19(7), 1113–9.
- Coll, P, Guillemin, J., Gazeau, M., & Raulin, F. (1999). Report and implications of the first observation of C<sub>4</sub>N<sub>2</sub> in laboratory simulations of Titan's atmosphere. *Planetary and Space Science*, 47, 1433–1440.
- Coll, P., Coscia, D., Gazeau, M. C., De Vanssay, E., Guillemin, J. C., & Raulin, F. (1995). Organic chemistry in Titan's atmosphere: New data from laboratory simulations at low temperature. *Advances in Space Research*, 16(2), 93–103.
- Coll, P., Navarro-González, R., Szopa, C., Poch, O., Ramírez, S. I., Coscia, D., Raulin, F., et al. (2013). Can laboratory tholins mimic the chemistry producing Titan's aerosols? A review in light of ACP experimental results. *Planetary and Space Science*, 77, 91–103.
- Coll, Patrice, & Bernard, J. (2003). Oxirane: An Exotic Oxygenated Organic Compound on Titan? *The Astrophysical Journal*, 598, 700–703.



- Coustenis, A., & Bézard, B. (1995). Titan's atmosphere from Voyager infrared observations IV. Latitudinal variations of temperature and composition. *Icarus*, *115*, 126–140.
- Cruikshank, D. P., Imanaka, H., & Dalle Ore, C. M. (2005). Tholins as coloring agents on outer Solar System bodies. *Advances in Space Research*, *36*(2), 178–183.
- David W. Clarke, Joseph, J. C., & Ferris, J. P. (2000). The Design and Use of a Photochemical Flow Reactor: A Laboratory Study of the Atmospheric Chemistry of Cyanoacetylene on Titan. *Icarus*, *147*(1), 282–291.
- De Kok, R., Irwin, P. G. J., Teanby, N. a., Lellouch, E., Bézard, B., Vinatier, S., Nixon, C. a., et al. (2007). Oxygen compounds in Titan's stratosphere as observed by Cassini CIRS. *Icarus*, *186*(2), 354–363.
- De La Fuente, J. L., Ruiz-Bermejo, M., Menor-Salván, C., & Osuna-Esteban, S. (2011). Thermal characterization of HCN polymers by TG–MS, TG, DTA and DSC methods. *Polymer Degradation and Stability*, *96*(5), 943–948.
- De la Fuente, J. L., Ruiz-Bermejo, M., Menor-Salván, C., & Osuna-Esteban, S. (2013). Pyrolysis study of hydrophobic tholins By TG-MS, TG, DTA and DSC methods. *Journal of Thermal Analysis and Calorimetry*, *111*(3), 1699–1706.
- De Vanssay, E., Gazeau, M. C., Guillemin, J. C., & Raulin, F. (1995). Experimental simulation of Titan's organic chemistry at low temperature. *Planetary and Space Science*, *43*(1-2), 25–31.
- Derenne, S., Coelho, C., Anquetil, C., Szopa, C., Rahman, a. S., McMillan, P. F., Corà, F., et al. (2012). New insights into the structure and chemistry of Titan's tholins via  $^{13}\text{C}$  and  $^{15}\text{N}$  solid state nuclear magnetic resonance spectroscopy. *Icarus*, *221*(2), 844–853.
- Durand, B. (1980). *Kerogen: Insoluble Organic Matter from Sedimentary Rocks*. Editions Technip.
- Ehrenfreund, P., Boon, J. J., Commandeur, J., Sagan, C., Thompson, W. R., & Khare, B. (1995). Analytical pyrolysis experiments of Titan aerosol analogues in preparation for the Cassini Huygens mission. *Advances in space research*, *15*(3), 335–42.

- European Space Agency. (2005). Seeing , touching and smelling the extraordinarily Earth-like world of Titan. *ESA News*, (January 21).
- Ferrari, a., & Robertson, J. (2000). Interpretation of Raman spectra of disordered and amorphous carbon. *Physical Review B*, *61*(20), 14095–14107.
- Ferrari, a., Rodil, S., & Robertson, J. (2003). Interpretation of infrared and Raman spectra of amorphous carbon nitrides. *Physical Review B*, *67*(15), 1–20.
- Ferris, J., Tran, B., Joseph, J., Vuitton, V., Briggs, R., & Force, M. (2005). The role of photochemistry in Titan's atmospheric chemistry. *Advances in Space Research*, *36*(2), 251–257.
- Fulchignoni, M., Aboudan, a., Angrilli, F., Antonello, M., Bastianello, S., Bettanini, C., Bianchini, G., et al. (2004). A stratospheric balloon experiment to test the Huygens atmospheric structure instrument (HASI). *Planetary and Space Science*, *52*(9), 867–880.
- Gautier, T., Carrasco, N., Buch, A., Szopa, C., Sciamma-O'Brien, E., & Cernogora, G. (2011). Nitrile gas chemistry in Titan's atmosphere. *Icarus*, *213*(2), 625–635.
- Gautier, T., Carrasco, N., Mahjoub, A., Vinatier, S., Giuliani, A., Szopa, C., Anderson, C. M., et al. (2012). Mid- and far-infrared absorption spectroscopy of Titan's aerosols analogues. *Icarus*, *221*(1), 320–327.
- Griffith, C. a, Owen, T., Geballe, T. R., Rayner, J., & Rannou, P. (2003). Evidence for the exposure of water ice on Titan's surface. *Science (New York, N.Y.)*, *300*(5619), 628–30.
- Gupta, S., Ochiai, E., & Ponnampereuma, C. (1981). Organic synthesis in the atmosphere of Titan. *Nature*, *293*(5835), 725–727.
- H.Mellottée, & C.Vovelle.(1982). Pyrolyse du polyacrylonitrile-I. *European Polymer Journal*, *18*, 999–1006.
- Hadamcik, E., Renard, J.-B., Alcouffe, G., Cernogora, G., Lévasseur-Regourd, a. C., & Szopa, C.(2009). Laboratory light-scattering measurements with Titan's aerosols analogues produced by a dusty plasma. *Planetary and Space Science*, *57*(13), 1631–1641.

- Halket, J. M., & Zaikin, V. (2003). Derivatization in mass spectrometry--1. Silylation. *Eur J Mass Spectrom (Chichester, Eng)*, 9(1), 1–21.
- Hodyss, R. (2006). Methods for the analysis of organic chemistry on Titan. Ph.D.thesis. California institute of technology. Pasadena, California.
- Imanaka, H., Khare, B., & Elsila, J. (2004). Laboratory experiments of Titan tholin formed in cold plasma at various pressures: implications for nitrogen-containing polycyclic aromatic compounds in Titan haze. *Icarus*, 168(2), 344–366.
- Imanaka, H., & Smith, M. a. (2009). EUV photochemical production of unsaturated hydrocarbons: implications to EUV photochemistry in Titan and Jovian planets. *The journal of physical chemistry. A*, 113(42), 11187–94.
- Imanaka, H., & Smith, M. a. (2010). Formation of nitrogenated organic aerosols in the Titan upper atmosphere. *Proceedings of the National Academy of Sciences of the United States of America*, 107(28), 12423–8.
- Imanaka, H., & Smith, M. A. (2007). Role of photoionization in the formation of complex organic molecules in Titan's upper atmosphere. *Geophysical Research Letters*, 34(2), 2204.
- Israel, G., Cabane, M., Brun, J.-F., Niemann, H., Way, S., Riedler, W., Steller, M., et al. (2002). Huygens probe aerosol collector pyrolyser experiment. *Space Science Reviews*, 104(1-4), 433–468.
- Israel, G., Cabane, M., Raulin, F., Chassefiere, E., & Boon, J. J. (1991). Aerosols in Titan's atmosphere : models, sampling techniques and chemical analysis. *Annales geophysicae*, 9(1), 1–13.
- Israël, G., Szopa, C., Raulin, F., Cabane, M., Niemann, H. B., Atreya, S. K., Bauer, S. J., et al. (2005). Complex organic matter in Titan's atmospheric aerosols from in situ pyrolysis and analysis. *Nature*, 438(7069), 796–799.
- Jacovi, R., Laufer, D., Dimitrov, V., & Bar-Nun, A. (2010). Chemical composition of simulated Titan's mid atmospheric aerosols. *Journal of Geophysical Research: Planets*, 115(E7).

- Khare, B. N., E. L. O. Bakes, H. Imanaka, C. P. McKay, D. P. Cruikshank, and E. T. Arakawa (2002). Analysis of the Time-Dependent Chemical Evolution of Titan Haze Tholin. *Icarus*, 160, pp. 172-182.
- Khare, B N, Sagan, C., Ogino, H., Nagy, B., Er, C., Schram, K. H., & Arakawa, E. T. (1986). Amino acids derived from Titan tholins. *Icarus*, 68(1), 176–84.
- Khare, B. N., Sagan, C., Arakawa, E. T., Suits, F., Callcott, T. A., & Williams, M. W. (1984a). Optical constants of organic tholins produced in a simulated Titanian atmosphere: from soft X-ray to microwave frequencies. *Icarus*, 60(1), 127–137.
- Khare, B N, Sagan, C., Thompson, W. R., Arakawa, E. T., Suits, F., Callcott, T. A., Williams, M. W., et al. (1984b). The organic aerosols of Titan. *Advances in Space Research*, 4(12), 59–68.
- Khare, B.N., Sagan, C., Zumberge, J. E., Sklarew, D. S., & Nagy, B. (1981). Organic solids produced by electrical discharge in reducing atmospheres: Tholin molecular analysis. *Icarus*, 48(2), 290–297.
- Knapp, D. R. (1979). *Handbook of Analytical Derivatization Reactions*. Wiley. Retrieved
- Kühnel, E., Laffan, D. D. P., Lloyd-Jones, G. C., Del Campo, T., Shepperson, I. R., & Slaughter, J. L. (2007). Mechanism of Methyl Esterification of Carboxylic Acids by Trimethylsilyldiazomethane. *Angewandte Chemie International Edition*, 46(37), 7075–7078.
- Larkin, P. (2011). *IR and Raman spectroscopy principals and spectral interpretation*.
- Lavvas, P., Sander, M., Kraft, M., & Imanaka, H. (2011). Surface chemistry and particle shape: processes for the evolution of aerosols in Titan's atmosphere. *The Astrophysical Journal*, 728(2), 80–90.
- Lavvas, Panayotis, Yelle, R. V., & Vuitton, V. (2009). The detached haze layer in Titan's mesosphere. *Icarus*, 201(2), 626–633.
- Liang, M.-C., Yung, Y. L., & Shemansky, D. E. (2007). Photolytically Generated Aerosols in the Mesosphere and Thermosphere of Titan. *The Astrophysical Journal*, 661(2), L199–L202.

- Linder, D. R., et al. (1998), The Cassini CAPS electron spectrometer, in *Measurement Techniques in Space Plasmas: Particles*, AGU Geophys. Monogr. Ser., vol. 102, edited by R. E. Pfaff, J. E. Borovsky, and D. T. Young, pp. 257–262, AGU, Washington, D. C.
- Lin-Vien, D., Colthup, N.B., Fateley, W.G., Grasselli, J. G. (1991). The handbook of infrared and Raman characteristic frequencies of organic molecules. *Academic Press, San Diego*, (503pp).
- Liu, S., Gangopadhyay, S., & Sreenivas, G. (1997). Infrared studies of hydrogenated amorphous carbon (a-C: H) and its alloys (a-C: H, N, F). *Physical Review B*, 55(19), 13020–13024.
- Lopes, R. M. C., Kirk, R. L., Mitchell, K. L., LeGall, a., Barnes, J. W., Hayes, a., Kargel, J., et al. (2013). Cryovolcanism on Titan: New results from Cassini RADAR and VIMS. *Journal of Geophysical Research: Planets*, 118(3), 416–435.
- Lopes, R., Mitchell, K., & Stofan, E. (2007). Cryovolcanic features on Titan’s surface as revealed by the Cassini Titan Radar Mapper. *Icarus*, 186(2), 395–412.
- López-Puertas, M., Dinelli, B. M., Adriani, A., Funke, B., García-Comas, M., Moriconi, M. L., D’Aversa, E., et al. (2013). Large Abundances of Polycyclic Aromatic Hydrocarbons in Titan’S Upper Atmosphere. *The Astrophysical Journal*, 770(2), 132–139.
- Lorenz, R. D., Lopes, R. M., Paganelli, F., Lunine, J. I., Kirk, R. L., Mitchell, K. L., Soderblom, L. a., et al. (2008). Fluvial channels on Titan: Initial Cassini RADAR observations. *Planetary and Space Science*, 56(8), 1132–1144.
- Lorenz, R. D., & Lunine, J. I. (2005). Titan’s surface before Cassini. *Planetary and Space Science*, 53(5), 557–576.
- Mahjoub, a., Carrasco, N., Dahoo, P.-R., Gautier, T., Szopa, C., & Cernogora, G. (2012). Influence of methane concentration on the optical indices of Titan’s aerosols analogues. *Icarus*, 221(2), 670–677.
- Mai-Julie NGUYEN. (2007). Nouvelles contraintes sur la nature physico-chimique des aérosols de Titan: analyse des données de la mission Cassini-Huygens et simulation expérimentale en laboratoire. Ph.D. Thesis. Université Paris XII Val-de-Marne, France.

- Matthews, C. N., & Minard, R. D. (2006). Hydrogen cyanide polymers, comets and the origin of life. *Faraday Discussions*, *133*, 393–401.
- McCord, T.B., Hansen, G. B., Buratti, B. J., Clark, R. N., Cruikshank, D. P., D'Aversa, E., Griffith, C. a., et al. (2006). Composition of Titan's surface from Cassini VIMS. *Planetary and Space Science*, *54*(15), 1524–1539.
- McCord, Thomas B., Hayne, P., Combe, J.-P., Hansen, G. B., Barnes, J. W., Rodriguez, S., Le Mouélic, S., et al. (2008). Titan's surface: Search for spectral diversity and composition using the Cassini VIMS investigation. *Icarus*, *194*(1), 212–242.
- McDonald, G. D., Thompson, W. R., Heinrich, M., Khare, B. N., & Sagan, C. (1994). Chemical investigation of Titan and Triton tholins. *Icarus*, *108*, 137–45.
- McGuigan, M., Waite, J. H., Imanaka, H., & Sacks, R. D. (2006). Analysis of Titan tholin pyrolysis products by comprehensive two-dimensional gas chromatography-time-of-flight mass spectrometry. *Journal of chromatography. A*, *1132*(1-2), 280–8.
- Mckay, C. P. (1996). Elemental composition , solubility , and optical properties of Titan ' s organic haze. *Science*, *44*(8), 741–747.
- McKay, C. P., Pollack, J. B., & Courtin, R. (1989). The thermal structure of Titan's atmosphere. *Icarus*, *80*(1), 23–53.
- Mutsukura, N., & Akita, K. (1999). Infrared absorption spectroscopy measurements of amorphous CN<sub>x</sub> films prepared in CH<sub>4</sub>/N<sub>2</sub> r.f. discharge. *Thin Solid Films*, *349*, 115–119.
- Navarro-González, R., & Ramírez, S. (1997). Corona discharge of Titan's troposphere. *Advances in Space Research*, *19*(7), 1121–1133.
- Neish, C D, Somogyi, a, Imanaka, H., Lunine, J. I., & Smith, M. a. (2008). Rate measurements of the hydrolysis of complex organic macromolecules in cold aqueous solutions: implications for prebiotic chemistry on the early Earth and Titan. *Astrobiology*, *8*(2), 273–87.
- Neish, C., Somogyi, Á., & Smith, M. (2010). Titan's primordial soup: formation of amino acids via low-temperature hydrolysis of tholins. *Astrobiology*, *10*(3), 337–347.

- Neish, Catherine D., Somogyi, Á., Lunine, J. I., & Smith, M. a. (2009). Low temperature hydrolysis of laboratory tholins in ammonia-water solutions: Implications for prebiotic chemistry on Titan. *Icarus*, 201(1), 412–421.
- Nguyen, M., Raulin, F., Coll, P., Derenne, S., Szopa, C., Cernogora, G., Israel, G., et al. (2008). From Titan's tholins to Titan's aerosols: Isotopic study and chemical evolution at Titan's surface. *Advances in Space Research*, 42(1), 48–53.
- Niemann, H. B., Atreya, S. K., Bauer, S. J., Carignan, G. R., Demick, J. E., Frost, R. L., Gautier, D., et al. (2005). The abundances of constituents of Titan's atmosphere from the GCMS instrument on the Huygens probe. *Nature*, 438(7069), 779–84.
- O'Brien, D. P., Lorenz, R. D., & Lunine, J. I. (2005). Numerical calculations of the longevity of impact oases on Titan. *Icarus*, 173(1), 243–253.
- Pernot, P., Carrasco, N., Thissen, R., & Schmitz-Afonso, I. (2010). Tholinomics—Chemical Analysis of Nitrogen-Rich Polymers. *Analytical Chemistry*, 82(4), 1371–1380.
- Pietrogrand, M. C., Coll, P., Sternberg, R., Szopa, C., Navarro-Gonzalez, R., Vidal-Madjar, C., & Dondi, F. (2001). Analysis of complex mixtures recovered from space missions statistical approach to the study of Titan atmosphere analogues (tholins). *Journal of chromatography. A*, 939(1-2), 69–77.
- Poch, O., Coll, P., Buch, a., Ramírez, S. I., & Raulin, F. (2012). Production yields of organics of astrobiological interest from H<sub>2</sub>O–NH<sub>3</sub> hydrolysis of Titan's tholins. *Planetary and Space Science*, 61(1), 114–123.
- Podolak, M., & Giver, L. (1979). On inhomogeneous scattering models of Titan's atmosphere. *Icarus*, 37(37), 361–376.
- Quirico, E., Montagnac, G., Lees, V., McMillan, P. F., Szopa, C., Cernogora, G., Rouzaud, J.-N., et al. (2008). New experimental constraints on the composition and structure of tholins. *Icarus*, 198(1), 218–231.
- Quirico, E., Rouzaud, J.-N., Bonal, L., & Montagnac, G. (2005). Maturation grade of coals as revealed by Raman spectroscopy: progress and problems. *Spectrochimica acta. Part A, Molecular and biomolecular spectroscopy*, 61(10), 2368–77.

- Radebaugh, J., Lorenz, R. D., Lunine, J. I., Wall, S. D., Boubin, G., Reffet, E., Kirk, R. L., et al. (2008). Dunes on Titan observed by Cassini Radar. *Icarus*, *194*(2), 690–703.
- Radebaugh, Jani, Lorenz, R. D., Kirk, R. L., Lunine, J. I., Stofan, E. R., Lopes, R. M. C., & Wall, S. D. (2007). Mountains on Titan observed by Cassini Radar. *Icarus*, *192*(1), 77–91.
- Rages, K., & Pollack, J. B. (1983). Vertical distribution of scattering hazes in Titan's upper atmosphere. *Icarus*, *55*(1), 50–62.
- Ramírez, S. I., Coll, P., Buch, A., Brassé, C., Poch, O., & Raulin, F. (2010). The fate of aerosols on the surface of Titan. *Faraday Discussions*, *147*, 419–427.
- Ramirez, S. I., Navarro-gonz, R., Coll, P., & Raulin, F. (2001). Possible contribution of different energy sources to the production of organics in Titan's atmosphere, *27*(2), 261–270.
- Ramírez, Sandra I., Navarro-González, R., Coll, P., & Raulin, F. (2005). Organic chemistry induced by corona discharges in Titan's troposphere: Laboratory simulations. *Advances in Space Research*, *36*(2), 274–280.
- Rannou, P., Cours, T., Le Mouélic, S., Rodriguez, S., Sotin, C., Drossart, P., & Brown, R. (2010). Titan haze distribution and optical properties retrieved from recent observations. *Icarus*, *208*(2), 850–867.
- Raulin, F., Coll, P., & Coscia, D. (1998). An exobiological view of Titan and the Cassini-Huygens mission. *Advances in Space Research*, *22*(3), 353–362.
- Raulin, F., Dubouloz, N., & Frère, C. (1989). Prebiotic-like organic syntheses in extraterrestrial environments: The case of titan. *Advances in Space Research*, *9*(6), 35–47.
- Rodil, S. E., Ferrari, a. C., Robertson, J., & Milne, W. I. (2001). Raman and infrared modes of hydrogenated amorphous carbon nitride. *Journal of Applied Physics*, *89*(10), 5425.
- Rodriguez, S., Mouélic, S. Le, & Sotin, C. (2006). Cassini/VIMS hyperspectral observations of the HUYGENS landing site on Titan. *Planetary and space science*, *33*(0), 1–40.



- Ruiz-Bermejo, M, Menor-Salván, C., Osuna-Esteban, S., & Veintemillas-Verdaguer, S. (2007). Prebiotic microreactors: a synthesis of purines and dihydroxy compounds in aqueous aerosol. *Origins of life and evolution of the biosphere*, 37(2), 123–142.
- Ruiz-Bermejo, Marta, Menor-Salván, C., De la Fuente, J. L., Mateo-Martí, E., Osuna-Esteban, S., Martín-Gago, J. Á., & Veintemillas-Verdaguer, S. (2009). CH<sub>4</sub>/N<sub>2</sub>/H<sub>2</sub>-spark hydrophobic tholins: A systematic approach to the characterisation of tholins. Part II. *Icarus*, 204(2), 672–680.
- Ruiz-Bermejo, Marta, Menor-Salván, C., Mateo-Martí, E., Osuna-Esteban, S., Martín-Gago, J. Á., & Veintemillas-Verdaguer, S. (2008). CH<sub>4</sub>/N<sub>2</sub>/H<sub>2</sub> spark hydrophilic tholins: A systematic approach to the characterization of tholins. *Icarus*, 198(1), 232–241.
- Sagan C, Khare BN, Thompson WR, McDonald GD, Wing MR, Bada JL, Vo-Dinh T, A. E. (1993). Polycyclic aromatic hydrocarbons in the atmospheres of titan and jupiter. *Astrophysical j*, 414, 399–405.
- Sagan, C., & Khare, B. N. (1979). Tholins: organic chemistry of interstellar grains and gas. *Nature*, 277(5692), 102–107.
- Sagan, C., & Reid Thompson, W. (1984). Production and condensation of organic gases in the atmosphere of Titan. *Icarus*, 59(2), 133–161.
- Sarah Marie Hörst. (2011). *Post-Cassini investigation of Titan atmospheric chemistry*. Ph.D. thesis. The university of Arizona.
- Sarker, N., Somogyi, A., Lunine, J. I., & Smith, M. A. (2003). Titan aerosol analogues: analysis of the nonvolatile tholins. *Astrobiology*, 3(4), 719–726.
- Sazanov, Y. N., & Griбанov, a. V. (2009). Criteria of polymer carbonization. *Russian Journal of Applied Chemistry*, 82(3), 473–482.
- Scattergood, T., Lesser, P., & Owen, T. (1975). Production of organic molecules in the outer solar system by proton irradiation: Laboratory simulations. *Icarus*, 24(4), 465–471.
- Scattergood, T., & Owen, T. (1977). On the sources of ultraviolet absorption in spectra of Titan and the outer planets. *Icarus*, 30(4), 780–788.

- Scattergood, T. W., Lau, E. Y., & Stone, B. M. (1992). Titan's aerosols I. Laboratory investigations of shapes, size distributions, and aggregation of particles produced by UV photolysis of model Titan atmospheres. *Icarus*, *99*(1), 98–105.
- Scattergood, T. W., McKay, C. P., Borucki, W. J., Giver, L. P., Van Ghysseghem, H., Parris, J. E., & Miller, S. L. (1989). Production of organic compounds in plasmas: A comparison among electric sparks, laser-induced plasmas, and UV light. *Icarus*, *81*(2), 413–428.
- Sciamma-O'Brien, E., Carrasco, N., Szopa, C., Buch, a., & Cernogora, G. (2010). Titan's atmosphere: An optimal gas mixture for aerosol production? *Icarus*, *209*(2), 704–714.
- Sekine, Y., S, L., Imanaka, H., Matsui, T., Bakes, E. L. O., Mckay, C., Khare, B. N., et al. (2008). The role of organic haze in Titan's atmospheric chemistry II. Effect of heterogeneous reaction to the hydrogen budget and chemical composition of the atmosphere. *Icarus*, *194*(1), 201–211.
- Shemansky DE, Stewart AIF, West RA, Esposito LW, Hallett JT, Liu XM (2005). The Cassini UVIS stellar probe of the Titan atmosphere. *Science* 308:978–982
- Shemansky D (2006) in Abstracts of 36th COSPAR Scientific Assembly, 2006 July 16–23, Beijing, China (Paris: COSPAR), 2748
- Sobolevsky, T. G., Revelsky, A. I., Miller, B., Oriedo, V., Chernetsova, E. S., & Revelsky, I. A. (2003). Comparison of silylation and esterification/acetylation procedures in GC-MS analysis of amino acids. *Journal of Separation Science*, *26*(17), 1474–1478.
- Somogyi, A., Oh, C.-H., Smith, M. A., & Lunine, J. I. (2005). Organic environments on Saturn's moon, Titan: simulating chemical reactions and analyzing products by FT-ICR and ion-trap mass spectrometry. *Journal of the American Society for Mass Spectrometry*, *16*(6), 850–859.
- Stofan, E R, Elachi, C., Lunine, J. I., Lorenz, R. D., Stiles, B., Mitchell, K. L., Ostro, S., et al. (2007). The lakes of Titan. *Nature*, *445*(7123), 61–64.
- Stofan, E.R., Lunine, J. I., Lopes, R., Paganelli, F., Lorenz, R. D., Wood, C. a., Kirk, R., et al. (2006). Mapping of Titan: Results from the first Titan radar passes. *Icarus*, *185*(2), 443–456.

- Surianarayanan, M., Vijayaraghavan, R., & Raghavan, K. V. (1998). Spectroscopic investigations of polyacrylonitrile thermal degradation. *Journal of Polymer science: part A: polymer chemistry*, 36, 2503–2512.
- Szopa, C., Cernogora, G., Boufendi, L., Correia, J., & Coll, P. (2006). PAMPRE: A dusty plasma experiment for Titan's tholins production and study. *Planetary and Space Science*, 54(4), 394–404.
- Takano, Y., Tsuboi, T., & Kaneko, T. (2004). Pyrolysis of high-molecular-weight complex organics synthesized from a simulated interstellar gas mixture irradiated with 3 MeV proton beam. *Bulletin of the Chemical Society of Japan*, 77, 779–783.
- Thissen, R., & Dutuit, O. (2009). High resolution mass spectrometry of Tholins: comparison with HCN polymers. *European Planetary Science Congress*, 4.
- Thompson, W. R., Henry, T. J., Schwartz, J. M., Khare, B. N., & Sagan, C. (1991). Plasma discharge in  $N_2+CH_4$  at low pressures: experimental results and applications to Titan. *Icarus*, 90, 57–73.
- Thompson W.R. and Sagan C., 1992. Organic chemistry on Titan: surface interactions. *ESA SP-338*, 167–176.
- Tomasko, M G, Archinal, B., Becker, T., Bézard, B., Bushroë, M., Combes, M., Cook, D., et al. (2005). Rain, winds and haze during the Huygens probe's descent to Titan's surface. *Nature*, 438(7069), 765–78.
- Tomasko, M.G., Doose, L., Engel, S., Dafoe, L. E., West, R., Lemmon, M., Karkoschka, E., et al. (2008). A model of Titan's aerosols based on measurements made inside the atmosphere. *Planetary and Space Science*, 56(5), 669–707.
- Tomasko, Martin G, & West, R. A. (2009). *Aerosols in Titan 's Atmosphere* (pp.297–322).
- Trainer, M. G., Pavlov, A. A., DeWitt, H. L., Jimenez, J. L., McKay, C. P., Toon, O. B., & Tolbert, M. A. (2006). Organic haze on Titan and the early Earth. *Proceedings of the National Academy of Sciences of the United States of America*, 103(48), 18035–18042.

- Tran, B., Ferris, J. P., & Chera, J. J. (2003a). The photochemical formation of a titan haze analog. Structural analysis by x-ray photoelectron and infrared spectroscopy. *Icarus*, *162*(1), 114–124.
- Tran, B. N., Joseph, J. C., Ferris, J. P., Persans, P. D., & Chera, J. J. (2003b). Simulation of Titan haze formation using a photochemical flow reactor. *Icarus*, *165*(2), 379–390.
- Tran, B. N., Force, M., Briggs, R. G., Ferris, J. P., Persans, P., & Chera, J. J. (2008). Titan's atmospheric chemistry: Photolysis of gas mixtures containing hydrogen cyanide and carbon monoxide at 185 and 254 nm. *Icarus*, *193*(1), 224–232.
- Tran, B. N., Joseph, J. C., Force, M., Briggs, R. G., Vuitton, V., & Ferris, J. P. (2005). Photochemical processes on Titan: Irradiation of mixtures of gases that simulate Titan's atmosphere. *Icarus*, *177*(1), 106–115.
- Tuinstra, F., & J. L. Koenig. (1970). Raman Spectrum of Graphite. *The Journal of Chemical Physics*, *53*(3), 1126.
- Vinatier, S., Bézard, B., Nixon, C. a., Mamoutkine, A., Carlson, R. C., Jennings, D. E., Guandique, E. a., et al. (2010). Analysis of Cassini/CIRS limb spectra of Titan acquired during the nominal mission. *Icarus*, *205*(2), 559–570.
- Vinatier, S., Rannou, P., Anderson, C. M., Bézard, B., De Kok, R., & Samuelson, R. E. (2012). Optical constants of Titan's stratospheric aerosols in the 70–1500cm<sup>-1</sup> spectral range constrained by Cassini/CIRS observations. *Icarus*, *219*(1), 5–12.
- Vollhardt and Schore, 1995. Organic chemistry. *DeBoeck University Press*, second edition.
- Vuitton, V., Doussin, J., Benilan, Y., Raulin, F., & Gazeau, M. (2006). Experimental and theoretical study of hydrocarbon photochemistry applied to Titan stratosphere. *Icarus*, *185*(1), 287–300.
- Vuitton, V., Lavvas, P., Yelle, R. V., Galand, M., Wellbrock, a., Lewis, G. R., Coates, a. J., et al. (2009a). Negative ion chemistry in Titan's upper atmosphere. *Planetary and Space Science*, *57*(13), 1558–1572.

- Vuitton, Véronique, Tran, B. N., Persans, P. D., & Ferris, J. P. (2009b). Determination of the complex refractive indices of Titan haze analogs using photothermal deflection spectroscopy. *Icarus*, 203(2), 663–671.
- Vuitton, Véronique, Bonnet, J.-Y., Frisari, M., Thissen, R., Quirico, E., Dutuit, O., Schmitt, B., et al. (2010). Very high resolution mass spectrometry of HCN polymers and tholins. *Faraday Discussions*, 147, 495–509.
- Waite, J. H., Young, D. T., Cravens, T. E., Coates, a J., Crary, F. J., Magee, B., & Westlake, J. (2007). The process of tholin formation in Titan's upper atmosphere. *Science (New York, N.Y.)*, 316(5826), 870–875.
- Wilson, E. (2003). Chemical sources of haze formation in Titan's atmosphere. *Planetary and Space Science*, 51(14-15), 1017–1033.
- Wopenka, B., & Pasteris, J. D. (1993). Structural characterization of kerogens to granulite-facies graphite : Applicability of Raman microprobe spectroscopy. *American Mineralogist*, 78, 533–557.
- Xue, T., McKinney, M., & Wilkie, C. (1997). The thermal degradation of polyacrylonitrile. *Polymer Degradation and Stability*, 3910(97), 193–202.
- Yelle, R. V., Vuitton, V., Lavvas, P., Klippenstein, S. J., Smith, M. a., Hörst, S. M., & Cui, J. (2010). Formation of NH<sub>3</sub> and CH<sub>2</sub>NH in Titan's upper atmosphere. *Faraday Discussions*, 147, 31.
- Young, D., Berthelier, J., & Blanc, M. (2004). Cassini plasma spectrometer investigation. *Space Science Reviews*, 114, 1–112.
- Yung, Y., Allen, M., & Pinto, J. (1984). Photochemistry of the atmosphere of Titan- Comparison between model and observations. *The Astrophysical Journal supplement series*, 55,465–506.

---

## Appendix

### Acronyms and Symbols

#### Acronyms

<b>ACP-GCMS</b>	Aerosol Collector and Pyrolyze-Gas Chromatograph and Mass Spectrometer
<b>APPI</b>	Atmospheric Pressure Photo Ionization
<b>BWF</b>	Breigt-Wigner-Fano
<b>CAPS</b>	Cassini Plasma Spectrometer
<b>CIRS</b>	Composite Infrared Spectrometer
<b>DISR</b>	Descent Imager / Spectral Radiometer
<b>DMF</b>	N, N-Dimethylformamide
<b>DSC</b>	Differential Scanning Calorimetry
<b>DTG</b>	Differential thermogravimetric
<b>FTIR</b>	Fourier Transform Infrared Spectroscopy
<b>FWHM</b>	Full Width at Half Maximum
<b>GC-MS</b>	Gas Chromatograph and Mass Spectrometer
<b>HASI</b>	Huygens Atmosphere Structure Instrument
<b>HRTEM</b>	High Resolution Transmission Electron Microscopy
<b>INMS</b>	Ion and Neutral Mass Spectrometer
<b>IR</b>	Infrared Spectroscopy
<b>LATMOS</b>	Laboratoire Atmosphères, Milieux, Observations Spatiales
<b>LISA</b>	Laboratoire Interuniversitaire des Systèmes Atmosphériques
<b>MTBSTFA</b>	N-tert-butyldimethylsilyl-N-methyltrifluoroacetamide
<b>NIST</b>	National Institute of Standards and Technology
<b>NMR</b>	Nuclear Magnetic Resonance
<b>OES</b>	Optical Emission Spectroscopy

---

<b>PAH</b>	Polycyclic aromatic hydrocarbon
<b>PAMPRE</b>	Production d'Aerosols en Microgravite par Plasma Reactifs
<b>Pyr-GCMS</b>	Pyrolysis Gas Chromatograph and Mass Spectrometer
<b>SEM</b>	Scanning Electron Microscopy
<b>TCD</b>	Thermal Conductivity Detector
<b>TGA</b>	Thermo gravimetric analysis
<b>TG-MS</b>	Thermogravimetry Mass Spectrometry
<b>UVIS</b>	Ultraviolet Imaging Spectrograph
<b>VIMS</b>	Visible and Infrared Mapping Spectrometer
<b>XRD</b>	X-ray Diffraction

## Symbols

$a$	polarizability of the molecules
$I_0$	peak intensity
$I_{(D)}/I_{(G)}$	intensity ratio of the D-band and G-band,
$N$	number of scattering molecules in a given state
$Q$	vibrational amplitude
$Q^{-1}$	BWF coupling coefficient
$V$	frequency of the exciting laser
$V_L$	laser excitation frequency
$V_m$	vibrational energy
$\omega_0$	peak position

## List of Figures

- Figure 1-1. Vertical profile of the Titan and Earth atmosphere (cable et al., 2010). ..... 8
- Figure 1-2. Averaged GCMS mass spectrum acquired at the surface showing ion count rates versus mass per charge ( $m/z$ ). Beyond increased methane, compounds found at the surface included firm detection of ethane and tentative detection of cyanogen, benzene, and carbon dioxide (Niemann et al., 2005). ..... 12
- Figure 1-3. Titan's Nile: The radar image on the left taken by the Cassini space probe shows the vast river system as it flows north into the moon's Ligeia Mare sea. The right is a satellite image of the real Nile in Egypt. Image credit: NASA/JPL–Caltech/ASI. .... 13
- Figure 1-4. Processes included in the model. In this example, the PACs provide primary particles which then coagulate to form an aggregate. Eventually the surface chemistry acting on the aggregate provides a new, larger primary particle (Lavvas et al., 2011). ..... 15
- Figure 1-5. This figure shows the variations of single scattering albedo with wavelength at altitudes above 144 km and between 30 and 80 km, as labeled from (Tomasko et al., 2008). The measurements come from different portions of the DISR data set as indicated by the horizontal lines along the bottom of the figure (Note that SA represents the two channels of the DISR solar aureole camera). The error bars approximate one sigma uncertainties in the derived values. The dotted-and- dashed line is the single scattering albedo computed for the haze aggregate particles using 1.5 times the imaginary refractive index reported by (Khare et al., 1984a). The slope toward the blue is in reasonable agreement with the variation of single scattering albedo at high altitudes but does not show the decrease required for the haze aerosols long ward of 900 nm. .... 16
- Figure 1-6. Derived extinction cross-section in the  $610\text{-}1500\text{cm}^{-1}$  spectral range (black) using CIRS observations (present work), in the  $30\text{-}560\text{ cm}^{-1}$  spectral range (blue) using CIRS observations (Anderson and Samuelson, 2011) and in the  $6300\text{-}23,000\text{ cm}^{-1}$  region (red) using DISR observations (Tomasko et al., 2008). The extinction cross section of Titan's aerosol is compared with a theoretical extinction cross-section calculated for a fractal aerosol made of 3000 monomers of  $0.05\text{ }\mu\text{m}$  radius and displaying the tholins optical constants of (Khare et al., 1984a). ..... 17



Figure 1-7. From Liang et al., (2007) Aerosol density (filled circles) derived from the UVIS 1 Sco occultation compared to the CH<sub>4</sub> density (dashed line) scaled by 10<sup>-9</sup> (Shemansky et al., 2005; Shemansky 2006). The increase of the mixing ratio of the UVIS aerosols through the mesosphere to at least 1,000 km implies that the production of aerosols must take place at significant rates throughout the mesosphere and thermosphere. The UVIS-derived temperature profile is shown by the dotted line. Model aerosol profiles computed by Liang et al., (2007) are shown by the thin and thick solid lines (Tomasko and West, 2009). ..... 18

Figure 1-8. Black line represents our tholin 5% spectrum. Titan's aerosols spectra derived from observations with Cassini CIRS (Anderson and Samuelson, 2011; Vinatier et al., 2011) are plotted in red. The blue line represents tholin spectra reconstituted from Khare et al., (1984a) data (from Quirico et al., (2008))..... 19

Figure 1-9. Energy (and mass, converted assuming singly charged ions) spectra at an altitude of 953 km during the T16 encounter. (top) Dotted trace shows total counts, dashed trace shows signal due to ionospheric electrons, and solid trace shows counts due to negative ions only. (bottom) Negative ion density measured in each ELS energy bin. In each case error bars are associated with statistical uncertainties on the counts (Coates et al., 2007). ..... 20

Figure 1-10. Cartoon showing the chemical process leading up to the formation of tholins in Titan's upper atmosphere. The process begins with free energy from solar UV radiation and energetic particles impinging on Titan's atmosphere. The most abundant constituents (CH<sub>4</sub> and N<sub>2</sub>) combine through a number of reaction pathways to form larger organic and nitrile compounds (100 to 350 daltons) that eventually lead to the formation of negatively charged aerosols (20 to 8000 daltons) observed at ~1000 km (Waite et al., 2007). ..... 22

Figure 1-11. The summary of the laboratory teams which interest on Titan's atmospheric chemistry of all over the world. Written next to the energy source used by each team, is the numbered identification of the corresponding reference, where details about the synthesis are provided. n<sup>o</sup>1= Bar-Nun's team, n<sup>o</sup>2= Dodonova's work, n<sup>o</sup>3= Matthews's work, n<sup>o</sup>4= NASA Ames team, n<sup>o</sup>5= Navarro-González's team, n<sup>o</sup>6= Ponnampereena's team, n<sup>o</sup>7= Raulin's team, n<sup>o</sup>8= Sagan's team, n<sup>o</sup>9= Ferris' team, n<sup>o</sup>10= Smith's team, n<sup>o</sup>11= Koike et al., 2003, n<sup>o</sup>12= Centro de Astrobiología, Spain, n<sup>o</sup>13= PAMPRE team; n<sup>o</sup>14= SETUP team (Coll et al., 2012). ..... 24

Figure 1-12. PAMPRE instrument at LATMOS laboratory. .... 25

---

Figure 1-13. Picture for the CH <sub>4</sub> -N <sub>2</sub> plasma in the PAMPRE reactor, the green trace corresponds to the diffusion of powders suspended at 532 nm green laser. ....	26
Figure 1-14. Experimental set-up for PAMPRE. ....	27
Figure 1-15. The cross section of the upper part of the reactor chamber. ....	28
Figure 1-16. Cathode and containment cage. ....	29
Figure 1-17. Diagram of tuning box. ....	30
Figure 2-1. Schematic view of the furnace pyrolyzer <i>Pyrojector II</i> <sup>TM</sup> (S.G.E., Melbourne, Australia). ....	50
Figure 2-2. The tholins sample 5pc pyrolyzed in He at 200°C. ....	53
Figure 2-3. The chromatogram for tholins sample 5pc pyrolyzed at 400°C. ....	54
Figure 2-4. The chromatogram for tholins sample 5pc pyrolyzed at 600°C. ....	55
Figure 2-5. The chromatogram for tholins sample 5pc pyrolyzed at 900°C. ....	57
Figure 2-6. The chromatogram for tholins sample 10pc pyrolyzed at 400°C. ....	58
Figure 2-7. The chromatogram for tholins sample 10pc pyrolyzed at 600°C. ....	59
Figure 2-8. The chromatogram for tholins sample 10pc pyrolyzed at 600°C. ....	60
Figure 2-9. Two-dimensional projection of the tholins sample pyrolyzed in H <sub>2</sub> at 600°C (McGuigan et al., 2006). ....	63
Figure 2-10. Thermal degradation of polyacrylonitrile. X refers to any possible nucleophile, including nitriles (Hodyss, 2006). ....	64
Figure 2-11. The diagram summarizing the detection of HCN, NH <sub>3</sub> and the refractory core for the aerosols of Titan after pyrolysis at 600°C (Mai-Julie NGUYEN, 2007). ....	65
Figure 2-12. Temporal evolution of the intensity of the MS signatures attributed to ammonia for the second aerosol sample pyrolysis by the ACP experiment (Coll et al., 2012). ....	65
Figure 3-1. Molecular motions which change distance between atoms for water and CO <sub>2</sub> . ...	71

---

Figure 3-2. Schematic illustration of Rayleigh scattering as well as Stokes and anti-Stokes Raman scattering. The laser excitation frequency ( $\nu_L$ ) is represented by the upward arrows and is much higher in energy than the molecular vibrations. The frequency of the scattered photon (downward arrows) is unchanged in Rayleigh scattering but is of either lower or higher frequency in Raman scattering. The dashed lines indicate the “virtual state” (Larkin, 2011).....	72
Figure 3-3. The sample to be analyzed is placed in a capsule of Tin for CHNS analysis, a capsule of silver for O analysis. It is compacted in a small pellet form before being introduced into the analyzer to be burn. ....	74
Figure 3-4. The principal schematic of CHNS elemental analysis. ....	74
Figure 3-5. Calibration curves obtained during the calibration of the instrument for elemental analysis. ....	75
Figure 3-6. Thermogravimetric curves for 800°C, 500°C, 400°C, 300°C (a) sample5pc, (b) sample10pc.....	77
Figure 3-7. TG (a) and DTG (b) curves for sample 5pc, the final temperature is 800°C. ....	79
Figure 3-8. DSC and DTG curves for the sample 5pc, heating rate is 10K/min and under the argon atmosphere. ....	80
Figure 3-9. TG (a) and DTG (b) curves for sample 10pc, the final temperature is 800°C. ....	81
Figure 3-10. DSC and DTG curves for the sample 10pc, heating rate is 10K/min and under the argon atmosphere. ....	81
Figure 3-11. Thermogravimetric curves for sample 10pc and sample 5pc at the final temperature 800°C.....	82
Figure 3-12. DTG curves for sample 10pc and sample 5pc, the final temperature is 800°C..	83
Figure 3-13. Ion intensity curves for tholins sample 5pc (a) all of the volatile species (b) ion current intensity for every m/z as a function of temperature. ....	85
Figure 3-14. Ion intensity curves for tholins sample 10pc (a) all of the volatile species (b) ion current intensity for every m/z as a function of temperature. ....	88

---

Figure 3-15. DTG curve (a) and MS principal signal comparison (b) as a function of temperature for sample 5pc (A) and sample 10pc (B). .....	89
Figure 3-16. The infrared spectra for initial sample 5pc and different temperature heating residues. (The range of wave frequencies investigated from 600 to 4000 $\text{cm}^{-1}$ . Each spectrum was obtained by addition of 4 scans with a resolution of 4.0 $\text{cm}^{-1}$ and the baseline is modified automatic by the software of instrument).....	91
Figure 3-17. The infrared spectra for initial sample 10pc and different temperature heating residues.....	93
Figure 3-18. Modes of vibration bands related to Raman spectra of carbonaceous materials. G-band is allocated to the mode symmetry $E_{2g2}$ corresponding to movements of folding of conjugated carbon-carbon bonds are shown in cycles; or in olefin chains. The D band is attributed for its mode of $A_{1g}$ symmetry breathing mode corresponding to the aromatic ring (Ferraris al., 2000). .....	94
Figure 3-19. Typical Raman spectra of all the tholins residues for different temperature. The G-band and D-band are clearly seen. ....	94
Figure 3-20. Raman spectra are fit by a double band profile, band D is adjusted by a Lorentzian and a G band profile Breit-Wigner-Fano to obtain the spectral parameters FWHM-D, FWHM-G, $I_D$ , $I_G$ , $\omega_0D$ , $\omega_0G$ (Bonal et al., 2006). .....	95
Figure 3-21. The parameter change of the G band Raman spectra for residues of heating tholins sample 5pc. Parameters are both very well correlated with each other when the temperature rises. ....	96
Figure 3-22. The change of G band position (a) and FWHM (b) as a function of temperature. ....	97
Figure 3-23. The intensity ratio of the D-band and G-band, $I_{(D)}/I_{(G)}$ , as a function of heating temperature.....	98
Figure 3-24. Elemental composition of initial tholins and the residues as a function of temperature (a) sample 5pc; (b) sample 10pc. ....	99

- Figure 3-25. Variation of elemental compositions (C/N and C/H) as a function of temperature (a) sample 5pc (b) sample 10pc..... 100
- Figure 3-26. Compare thermal properties of Titan's tholins, HCN polymer and other tholins. (A) TG curves of HCN polymer (De La Fuente et al., 2011) and Titan's tholins; (B) mass loss for Titan's tholins, other tholins (Khare et al., 1981; Ruiz-Bermejo et al., 2007), and HCN polymer..... 101
- Figure 4-1. Principle of MTBSTFA derivatization: amine and hydroxyl groups are substituted by a silyl group which renders the molecule volatile then can be analyzed by GC-MS..... 113
- Figure 4-2. (a) Structural formula corresponding to the ratio of  $m/z = 147$  fragments and its presence is due to the parasitic reaction occurring between an agent MTBSTFA derivatizing molecule and a water molecule. The hydrolysis and derivatization protocol includes a drying step to remove most of the water present, it can, however, never be complete. (b) Structural formula corresponding to the ratio of  $m/z = 73$  fragment, it is the recombination of a silicon with three methyl groups (Mai-Julie NGUYEN, 2007)..... 115
- Figure 4-3. Mass spectrum obtained by silylated alanine fragmentation (from the NIST library) and diagram showing the different masses obtained after fragmentation. The masses observed 158, 232, 260 and 302, and the relative peak heights are specific for silylated alanine. .... 116
- Figure 4-4. Chromatogram reconstructed from mass spectra obtained by injecting a direct derivatization sample of tholins (4%). Chromatographic conditions: column: Restek Rtx®-5Sil MS (Fused Silica) with 5-meter Integra-Guard MS 30m long, 0.25mm ID, 0.25 $\mu$ m df) carrier flow(He) 1.0ml/min; temperature programming: isothermal at 50°C for 3min, 4°C min<sup>-1</sup> up to 280°C isothermal at 280°C for 5min; split: 1/20; temperature of injector 250°C detector: mass spectrometer using 70eV EI. .... 117
- Figure 4-5. The detail chromatograms for five samples with different methane content percentage (a) 4%, (b) 6%, (c) 7%, (d) 8%, (e) 9%. .... 119
- Figure 4-6. The gas chromatograms obtained after tholins hydrolysis in distilled water. The signal of the time range between 20 and 30 min. (a) 4%, (b) 6%, (c) 7%, (d) 8%, (e) 9%.... 122
- Figure 4-7. Chromatogram obtained after hydrolysis of tholins sample under condition of HCl (a) 4%, (b) 6%, (c) 7%, (d) 8%, (e) 9%..... 125

---

Figure 4-8. Reaction pathway for the hydrolysis of the acetonitrile in the presence of water to form acetic acid (a) from acetonitrile to acetamide (b) from acetamide to acetic acid.....	129
Figure 4-9. Reaction pathway leading to the formation of alanine from the hydrolysis of 2-aminopropionitrile (Mai-Julie NGUYEN, 2007). .....	130
Figure 4-10. Hydrolysis of alanine under very acidic pH leads to the formation a hydroxyl-carboxylic acid .....	131
Figure 4-11. Degradation pathway Urea by protonation of the amine functions (Mai-Julie NGUYEN, 2007) .....	133



---

## List of Tables

Table 1-1. Titan versus Earth. ....	7
Table 1-2. Summary of previous analysis of PAMPRE tholins, on the basis of the summary in (Sarah Marie Hörst, 2011).....	39
Table 2-1. Molecules identified in PAMPRE tholins from Pyr-GC-MS (Szopa et al., 2006). 47	
Table 2-2. Compounds identified in tholins pyrolysate for sample 5% at temperature 200°C.53	
Table 2-3. Compounds identified in tholins pyrolysate for sample 5pc at temperature 600°C. ....	56
Table 2-4. Compounds identified in tholins pyrolysate for sample 10pc at temperature 400°C. ....	58
Table 2-5. Compounds identified in tholins pyrolysate for sample 10pc at temperature 600°C. ....	60
Table 3-1. The temperature of DTG maximal with corresponding rates of mass loss for sample 10pc, sample 5pc.....	83
Table 3-2. Summary of the possible gaseous organic and inorganic compounds obtained during TG-MS analysis. Heating rate was 10°C/min, final temperature is 800°C, in the argon atmosphere. ....	87
Table 4-1. Amino Acids and Urea identified in acid-treated tholins (Khare et al., 1986). ....	108
Table 4-2. Five tholins samples were synthesized using different initial gaseous mixture. ..	111
Table 4-3. The compounds have been identified from the chromatographic peaks of Figure 4-5. Only has qualitative analysis. The compounds indicated in black color are sure, the compound indicated in green is not sure. The retention time showed here for sample 4%, these compounds for others samples have the similar retention time. ....	118



Table 4-4. The compounds have been identified from the chromatographic peaks of Figure 4-6. Only has qualitative analysis. The retention time showed here for sample 4%, these compounds for others samples have the similar retention time. .... 121

Table 4-5. The compounds have been identified from chromatographic peaks of Figure 4-7. Only has qualitative analysis. The retention time showed here for sample 4%, these compounds for others samples have the similar retention time. .... 124

Table 4-6. Summary of the primary products which can lead to the formation of molecules identified after hydrolysis in HCl, distilled water. .... 134



## **Abstract**

Since the achievement of the first results from the Cassini Huygens mission, Titan's aerosols present an astrobiological interest as their characterization enables to evaluate the prebiotic chemistry that occurred on the primitive Earth. To better understand the physical chemistry of the aerosols of Titan is important for scientists. The laboratory via analyzing the properties of tholins (analogues of Titan's aerosols) overcomes the difficulties for analyzing Titan's aerosols directly. In this thesis work, the research object is tholins produced by the PAMPRE experiment. Pyr-GC-MS analysis technique was used to characterize the composition and structure of tholins. The thermal stability and the properties change with the temperature have been realized by thermal degradation study. Finally, the evolution of organic aerosols after precipitation on the surface of Titan was also investigated through GC-MS analysis of tholins. The results obtained can be used to interpret data collected by observations of Titan from Earth or by the Cassini-Huygens probe, to better characterize the satellite and its evolution.

**Keywords:** Titan, tholins, Pyr-GC-MS, thermal degradation, GC-MS

## **Résumé**

Depuis l'obtention des premiers résultats de la mission Cassini Huygens, les aérosols de Titan présentent un intérêt astrobiologique car leur caractérisation permet d'évaluer la chimie prébiotique qui a eu lieu sur la Terre primitive. Mieux comprendre les propriétés physico-chimiques des aérosols de Titan est important pour les scientifiques. Le laboratoire via l'analyse des propriétés des tholins (l'analogue des aérosols de Titan) permet de surmonter les difficultés d'analyser les aérosols de Titan directement. Dans ce travail de thèse, l'objet de la recherche est l'analyse des tholins produits par l'expérience PAMPRE. La technique d'analyse Pyr-GC-MS a été utilisée pour caractériser la composition et la structure de tholins. La stabilité thermique et le changement des propriétés en fonction de la température ont été réalisés par l'étude de la dégradation thermique. Enfin, l'évolution des aérosols organiques après leur précipitation sur la surface de Titan a également été étudiée selon la méthode GC-MS d'analyse des tholins. Les résultats obtenus peuvent être utilisés pour interpréter les données recueillies par des observations de Titan de la terre ou par la sonde Cassini-Huygens, afin de mieux caractériser le satellite et son évolution.

**Mots Clés :** Titan, tholins, Pyr-GC-MS, dégradation thermique, GC-MS